



An Investigation on the Performance of Hybrid Visible Light and Radio Frequency for Vehicular Communication

By

Gurinder Singh

PhD-17110

under the guidance of

Dr. Anand Srivastava

Professor, IIIT-Delhi

&

Dr. Vivek Ashok Bohara

Professor, IIIT-Delhi

Indraprastha Institute of Information Technology, Delhi

December, 2023

©Indraprastha Institute of Information Technology (IIITD), New Delhi



An Investigation on the Performance of Hybrid Visible Light and Radio Frequency for Vehicular Communication

By

Gurinder Singh

PhD-17110

under the guidance of

Dr. Anand Srivastava

Professor, IIIT-Delhi

&

Dr. Vivek Ashok Bohara

Professor, IIIT-Delhi

submitted

**in partial fulfillment of the requirements for the degree of
Doctor of Philosophy**

to

Indraprastha Institute of Information Technology, Delhi

Decemeber, 2023

Certificate

This is to certify that the thesis titled "*An Investigation on the Performance of Hybrid Visible Light and Radio Frequency for Vehicular Communication*" is being submitted by **Gurinder Singh** to the *Indraprastha Institute of Information Technology-Delhi*, for the award of the degree of *Doctor of Philosophy*, is an original research work carried out by him under my supervision. In my opinion, the thesis has reached the standards fulfilling the requirements of the regulations relating to the degree. The results contained in this thesis have not been submitted in part or full to any other university or institute for the award of any degree/diploma.



Prof. Anand Srivastava,

Department of Electronics and Communication Engineering,
Indraprastha Institute of Information Technology-Delhi
New Delhi-110020



Prof. Vivek Ashok Bohara,

Department of Electronics and Communication Engineering,
Indraprastha Institute of Information Technology-Delhi
New Delhi-110020

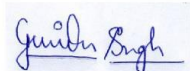
Dedicated to my parents ...

Acknowledgements

Foremost, I would like to express my sincere gratitude to my supervisors, Prof. Anand Srivastava and Prof. Vivek Ashok Bohara for their invaluable guidance and continuous support during my Ph.D research. Their wide knowledge, strong research enthusiasm, meticulous scrutiny, scholarly advice, and hard-working attitude have admired me during all my PhD period, and will have a profound effect on my future career. I find myself extremely lucky to have such a nice supervisors and mentors for my Ph.D research.

I would like to thank all my collaborators: Dr. Zilong Liu, Dr. Md Noor-A-Rahim, Dr. Gourab Ghatak and Prof. Dirk Pesch for their helpful suggestions and comments on my research. This research work was financially supported by the Visvesvaraya Ph.D. Scheme of Ministry of Electronics and Information Technology (MEITY), Government of India, implemented by Digital India Corporation.

I am extremely thankful to my colleagues particularly Anand Singh, Mohd Hamza Naim Sheikh, Dilnashin Anwar, and Rizwana Ahmed for providing me necessary technical advice and constructive suggestions on my research works and directions. Last and the most importantly, I would like to express my deepest gratitude to my beloved family, especially my parents, who always unconditionally support me at any time.



Gurinder Singh

PhD17110

Abstract

With the advent of connected autonomous vehicles, we are expecting to witness a new era of unprecedented user experiences, improved road safety, a wide range of compelling transportation applications, etc. A large number of disruptive communication technologies are emerging for the sixth generation (6G) wireless network aiming to support advanced use cases for intelligent transportation systems (ITS). An example of such a disruptive technology is constituted by hybrid Visible Light Communication (VLC) and Radio Frequency (RF) systems, which can play a major role in advanced ITS.

The first part of this dissertation highlights the potential benefit of employing vehicular-VLC (V-VLC) along with conventional vehicular-RF (V-RF) for enhanced vehicular message dissemination at road intersection. Further, we propose two practical deployment strategies namely hybrid RF-VLC with relaying and V-RF with Reconfigurable Intelligent Surface (RIS) which may serve as a preferred alternative for future ITS to meet ultra-high reliable and ultra-low latency communication for 6G vehicular networks.

In order to provide vehicles with reliable, ubiquitous, and massive connectivity, an appropriate multiple access (MA) scheme should be adopted. An appealing MA scheme referred to as non-orthogonal multiple access (NOMA) has been gaining significant research attention in vehicular networks among academia and industry. To this end, the proposed framework also aim to present a comprehensive qualitative and quantitative analysis on the performance of Optical Power Domain-NOMA (OPD-NOMA) enabled V-VLC systems. In addition to above, we propose a novel cooperative NOMA (C-NOMA) assisted hybrid visible light and radio frequency communication for improving safety message dissemination at road intersection.

Recently, RIS is also emerging as a disruptive communication technology for enhancing the signal quality and transmission coverage in wireless vehicular networks. Despite the widespread interest in applying RISs in various wireless vehicular environments, there is a paucity of intensive research efforts on exploring optical-RIS (O-RIS) for vehicular communication. It is anticipated that 6G-ITS applications viz. autonomous driving, platooning and cooperative

driving shall witness the proliferation of such O-RIS and hybrid RF-VLC technologies, while fulfilling stringent 6G key performance indicators (KPIs) requirements. Motivated by the above insights, the proposed work also aim to highlight the advantageous amalgamation of O-RIS and hybrid RF-VLC technologies for enhanced vehicular message dissemination particularly at road intersection. The proposed analytical framework developed in this dissertation allows us to answer several important questions pertaining to transportation networks, smart infrastructure planning, and personnel deployment.

Table of contents

Abstract	xi
List of figures	xv
List of tables	xix
List of Symbols	xxiv
1 Introduction	1
1.1 Objectives	3
1.2 Contributions and Research Outcomes	3
1.3 Organization	5
2 Background and Related Works	7
2.1 Hybrid RF-VLC V2X Systems	7
2.1.1 V2X Communication Technologies	9
2.2 Non-Orthogonal Multiple Access (NOMA)	12
2.2.1 NOMA for VLC	12
2.3 Reconfigurable Intelligent Surfaces	13
2.3.1 Related Works	13
3 Reliable Packet Transmission for V2X Networks	17
3.1 Overview of Part I	17
3.2 Preliminaries and assumptions	19
3.2.1 Network Model	19
3.2.2 Channel Model for V-VLC and V-RF	20
3.2.3 MAC Protocols	22

3.2.4	Intensity of Interfering PPP	22
3.3	Performance Evaluation	23
3.3.1	Outage Probability	23
3.3.2	Throughput	28
3.3.3	Data Oriented Characterization: DOR and IOR	28
3.4	Numerical Results and Discussion	29
3.5	Concluding remarks	35
3.6	Overview of Part II	36
3.6.1	Motivation and Contributions	36
3.7	Network model and preliminaries	38
3.7.1	Scenario Description	38
3.8	Performance Evaluation	41
3.8.1	Outage Probability for V-RF with relaying	41
3.8.2	Outage Probability for hybrid VLC-RF with relaying	44
3.8.3	Outage Probability for V-RF with RIS	46
3.9	Numerical Results and analysis	48
3.10	Concluding remarks	51
4	OPD NOMA for Vehicular Communication	53
4.1	OPD NOMA for Vehicular Networks	53
4.2	System Model and Preliminaries	54
4.2.1	System Model	54
4.2.2	Practical Challenges	55
4.3	Performance Analysis	57
4.3.1	NOMA Outage Expression for V-VLC	58
4.3.2	NOMA Outage Expression for V-RF	62
4.3.3	Average Achievable Rate for V-VLC	65
4.3.4	Average Achievable Rate for V-RF	66
4.4	Numerical Results	67
4.5	Concluding Remarks	72
4.6	Overview of Part II	73
4.7	System Model and Assumptions	74
4.7.1	Network Scenario	74
4.8	Performance Analysis	78
4.8.1	Outage Probability for V-VLC	78
4.8.2	Outage Probability for V-RF	81
4.9	Average Achievable Rate	86

4.10	Numerical Results	88
4.11	Concluding Remarks	93
5	Optical RIS for Vehicular Network	95
5.1	Introduction	95
5.2	System Overview	96
5.3	Performance Analysis	96
5.3.1	Outage Probability	96
5.3.2	System Goodput Analysis	99
5.3.3	Delay Outage Analysis	100
5.4	Results and Discussions	100
5.5	Concluding Remarks	102
6	Impact of Weather Conditions and Interference	103
6.1	Introduction	103
6.1.1	Contribution	103
6.2	System Model	104
6.2.1	Cumulative distribution function (CDF) of Interference	106
6.3	Probability of successful transmission	108
6.3.1	No channel fading with path loss exponent, $\alpha=2$	109
6.3.2	Rayleigh fading case	109
6.4	Simulation Results and Discussion	110
6.5	Concluding Remarks	113
6.6	Overview of Part II	114
6.7	Case Study: Hybrid RF-VLC V2X Systems	114
6.8	Concluding Remarks	117
7	Conclusion and Future Work	119
7.1	Summary	119
7.2	Future Directions	120
7.2.1	Reconfigurable Intelligent Surfaces (RIS) Enabled Hybrid RF-VLC V2X Systems	120
7.2.2	ML-assisted System Design	121
7.2.3	Deployment Issues	122
7.2.4	Coexistence of mmWave, THz and VLC	123
7.2.5	NOMA and its variants	123
7.2.6	Standardization Activities	124

Appendix A Author's Publications

125

References

127

List of figures

2.1	Performance trade-offs of conventional VLC and RF based V2X communication systems.	8
2.2	Illustration of a generic hybrid RF-VLC communication in a vehicular network.	9
3.1	Illustration of safety message dissemination in a vehicular network at road intersection. A desired vehicle can communicate with RSU via VLC shown by zig-zag or RF link shown by red transmission signal.	19
3.2	Abstraction used for modeling. The desired vehicle is marked in green circle, while RSU is marked in triangle, is assumed to be located at the center of road intersection. All links can either be V-VLC or V-RF link.	20
3.3	(a) Illustration of critical distance, d_c . Here, $d_c=h/\tan(\Psi_{FOV})$ (b)Transition diagram of hybrid V-VLC/V-RF network configuration. Here, β and ζ denote the SINR threshold for standalone V-VLC and V-RF networks, respectively.	21
3.4	Comparison of analytical (solid line) and simulation (dashed line) results for outage probability, P_{out} versus distance for V-VLC links only (blue), V-RF links only (red) and hybrid V-VLC/V-RF Links (green) with slotted ALOHA protocol.	31
3.5	Comparison of analytical (solid line) and simulation (dashed line) results for outage probability, P_{out} versus distance for V-VLC link only (blue), V-RF link only (red) and hybrid V-VLC/V-RF link (green) with CSMA CA protocol.	31
3.6	Outage probability, P_{out} and throughput, T as a function of access probability, ρ for standalone V-VLC link, V-RF link and hybrid V-VLC/VRF link when distance between the desired vehicle and RSU, R is 150 m.	32
3.7	Delay outage performance of V-VLC Link only, V-RF Link only and hybrid V-VLC/V-RF Link for CSMA case for two different distance between the desired vehicle and RSU. Here, access probability, ρ is 0.01.	33

3.8	Information Outage Rate of V-VLC Link only, V-RF Link only and hybrid V-VLC/V-RF Link for slotted ALOHA case for two different distance between the desired vehicle and RSU. Here, access probability, ρ is 0.01.	34
3.9	Illustration of road intersection scenario where vehicles in blocked line-of-sight (solid red line) can communicate via Hybrid V-VLC/V-RF with relaying (solid green line) and V-RF with RIS (solid black line).	37
3.10	Abstraction system model for vehicular communications involving a source S , relay R /RIS and a destination D in presence of one dimensional Poisson field of interference.	38
3.11	Illustration of proposed V2X deployment strategies: (a) Hybrid V-VLC/V-RF scheme and (b) V-RF with RIS scheme.	39
3.12	Analytical (solid line) and simulation (markers) results for outage probability, \mathcal{P}_{out} versus distance from intersection, i.e $\ S - R\ = \ R - D\ $ for conventional V-RF, proposed hybrid V-VLC/V-RF and RIS aided V-RF communication. . .	48
3.13	Outage probability, \mathcal{P}_{out} and throughput, \mathcal{T} variation with access probability, ρ for two different distances between the source and destination, $d_0 \in (50m, 150m)$	49
3.14	Delay outage performance of Conventional V-RF with relaying, hybrid VLC-RF with relaying, and RIS aided V-RF ($N = 30, 80$) for two different distance between the source and destination, $d_0 \in (50m, 150m)$	50
3.15	Delay outage rate variation with increasing value of RIS elements, N for two different distances between the source and destination, $d_0 \in (50m, 150m)$. . .	51
4.1	Typical I2V and V2V-VLC scenario.	55
4.2	OPD NOMA based V2X system model.	55
4.3	Abstraction used for modelling. The desired vehicles are marked in triangle, while interferers are marked in cross marks. Here, L and h denotes the inter lane distance and height of traffic lamp respectively.	56
4.4	Outage Probability, $\mathcal{P}_{out,VLC}$ as a function of vehicular density, λ : (a) V-VLC, and (b) V-RF. Impact of power allocation coefficient, ξ_1 : (c) V-VLC, and (d) V-RF.	69
4.5	Comparison of analytical (solid line) and simulation (dashed line) results for outage probability, \mathcal{P}_{out} versus distance of far-off NOMA user for OPD NOMA based V-VLC link (red) and NOMA based V-RF link (magenta)	70
4.6	Average achievable rate, \mathcal{R} variation with vehicular density, λ : (a) V-VLC, and (b) V-RF.	71

4.7	Average achievable rate, \mathcal{R} of V-RF as a function of power allocation coefficient, ξ_1 : (a) V-VLC, and (b) V-RF.	72
4.8	Real life application scenario: At road intersection, vehicles in blocked LOS (dashed red line) can communicate via C-NOMA supported hybrid V-VLC/V-RF systems. The SR link can either be V-VLC (red color line) or V-RF (solid magenta line) link, while $RD_{1,2}$ link is a V-RF link.	74
4.9	Abstraction model of the considered scenario. The source vehicle is marked with red triangle, destination vehicles are marked with yellow squares, and interfering vehicles with black circles. The desired link is represented by red dotted line and the interference link is represented by black dotted line. H denotes the height of the traffic light.	75
4.10	Illustration of cooperative NOMA aided hybrid VLC-RF based V2X with relaying.	76
4.11	Outage probability as a function of vehicular density λ : (a) Hybrid transmission without MRC, and (b) Hybrid transmission with MRC.	88
4.12	Outage probability as a function of power allocation coefficient a_1 : (a) Hybrid transmission without MRC, (b) Hybrid transmission with MRC.	89
4.13	Outage probability, Pout and throughput, T as a function of access probability, ρ for standalone V-VLC link, V-RF link and hybrid V-VLC/VRF link when distance between the desired vehicle and RSU, R is 150 m.	91
4.14	(a) Outage probability as a function of vehicular density λ for Lambertian and empirical model (b) Average achievable rate as a function of vehicular density λ for Lambertian and empirical model. Here, $\rho=0.01$, $\alpha=2$ and $a_1=0.8$	92
4.15	Impact of vehicular speed: (a) Outage probability, and (b) average achievable rate.	93
5.1	Real life application scenario: At road intersection, the vehicles in blocked LOS can communicate via O-RIS (dashed red line) or V-RF links (solid green line) in presence of interference from adjacent lane vehicles (dashed yellow line).	96
5.2	3D coordinate system model: O-RIS can be deployed at road intersection to relax the line-of-sight (LOS) requirement between source and destination vehicles in a V-VLC systems.	97
5.3	Comparison of analytical (solid line) and simulation (markers) results of outage performance for various configuration with varying vehicular density, λ . Here, $d_o = 50m$	100
5.4	(a) 3D outage plots and (b) Impact of vehicle's speed on outage performance. Here, $d_o = 50m$	101

5.5	(a) System goodput versus number of training bits (b_T) for $R \in \{3, 5\}$ and (b) Impact of delay threshold (t_{th}) on DOR.	102
6.1	System model. Here, vehicle C and vehicle D act as interferers (denoted by green solid line) for the dedicated communication link (denoted by red solid line) between vehicle A and vehicle B.	105
6.2	OEM headlamp optical illumination pattern with receiver height of 0.7 m. The values in the plots represent the received optical power and are in dBm. . . .	105
6.3	Simplified geometrical layout. Vehicle A is assumed to be located at the origin O . Here, D denotes distance between legitimate vehicle and receiver.	106
6.4	Reference scenario illustrating coverage and interference region using VLC attocells. Here, r and D denotes radius of VLC attocell under coverage region of desired vehicle and communication-range respectively.	106
6.5	Probability of successful transmission over a range of threshold power (a) sparse traffic scenario when $s=50$ m, (b) medium traffic scenario when $s=20$ m, and (c) dense traffic scenario when $s=12.5$ m.	111
6.6	OEM headlamp optical radiation pattern with receiver height of 0.7 m with interference when space headway between interferers is 20 m under (a) light fog ($V=0.1$ Km), (b) dense fog ($V=0.05$ Km) and (c) dry snow condition (Snow rate= 10 mm/hr).	112
6.7	Illustration of a generic hybrid RF-VLC communication in a vehicular network.	114
6.8	PRP at RSU for pure V-RF, pure V-VLC and LA hybrid RF-VLC V2X communication system under rain, fog and dry snow conditions.	115
6.9	Delay outage performance for pure V-RF, pure V-VLC and LA hybrid RF-VLC V2X communication system as a function of delay threshold, T_{th}	116
6.10	Achievable data rate for different network configuration for different values of distance between RSU and desired vehicle.	117
7.1	O-RIS/metasurface can be deployed on RSU/buildings at road intersection to relax the LOS requirement between source and destination vehicles in hybrid RF-VLC V2X systems.	121

List of tables

2.1	Comparison of DSRC/IEEE 802.11p, C-V2X, VLC, LTE and 5G NR V2X . . .	10
2.2	Summary of RIS-VLC proposed performance enhancement schemes	14
3.1	V-VLC and V-RF system parameters	30
4.1	System Model Parameters	68
6.1	Average received optical power for V-VLC in presence of interference when space headway between interferer is 20 m under different environmental deterrents at a distance of 100 m from transmitter.	113

List of Abbreviations

CAV	Connected and automated vehicular
ITS	Intelligent transportation systems
V2X	Vehicle-to-everything
C-V2X	Cellular-V2X
DSRC	Dedicated short-range communication
5G NR	5G New Radio
VLC	Visible light communication
V-VLC	Vehicular-VLC
NOMA	Non orthogonal multiple Access
OPD NOMA	Optical power domain NOMA
C-NOMA	Cooperative NOMA
CSI	Channel state information
RIS	Reconfigurable intelligent surfaces
O-RIS	Optical-RIS
BSMs	Basic safety messages
FeMBB	Further enhanced Mobile Broadband
MBLL	Mobile BroadBand and Low-Latency
mLLMT	massive Low-Latency Machine-Type communication
SNR	Signal-to-noise ratio
MRC	Maximal ratio combining
SC	Selection combining
VANETs	Vehicular adhoc networks
ISI	Inter-symbol interference
UAV	Unmanned aerial vehicle
LED	Light emitting diode
LOS	Line-of-sight
LTE	Long term evaluation
LTE-A	Long term evaluation advanced

IMR	Intelligent metasurface reflector
IMA	Intelligent mirror array
PDF	Probability density function
CDF	Cumulative distribution function
MGF	Moment generating function
QoS	Quality of service
RSUs	Road side units
V-RF	Vehicular-Radio frequency
EE	Energy Efficiency
DOR	Delay outage rate
IOR	Information outage rate
MAC	Medium access control
CSMA CA	Carrier sense multiple access with collision avoidance

Introduction

Connected and automated vehicular (CAV) technologies are expected to support improved road safety and driving comfort in future intelligent transportation systems (ITS). To fully support CAV, next generation vehicles will be equipped with a wide range of sensors and thus there is a strong demand for reliable near-real-time exchange of sensing and control data. Such a demand will be filled by vehicle-to-everything (V2X) communication which comprises a wide range of communication technologies such as vehicle-to-vehicle (V2V) and vehicle-to-infrastructure (V2I) communications[1]. The most salient V2X communication technologies are dedicated short-range communication (DSRC)-aided V2X and cellular-V2X (C-V2X). While DSRC-V2X represents a mature cost-efficient V2X technology, C-V2X has attracted much attention in recent years due to its significantly improved coverage, throughput, and latency. Thanks to sophisticated cellular infrastructure, C-V2X outperforms due to centralized resource allocation as well as enhanced communication/sensing capabilities. Several 3GPP V2X initiatives (such as LTE-V2X and 5G New Radio (NR)-V2X) have contributed to the prominence of C-V2X. With an abundance of both advanced sensors and communication devices, however, new challenges arise for the emerging next generation V2X networks[2]. More explicitly, stringent system reliability ($\sim 99.999\%$), end-to-end latency (<5 ms), coverage-quality, spectral efficiency, energy rating, networking, and privacy/security specifications should be met to support various C-V2X use case requirements [3]. Although the current C-V2X technology (such as 5G-NR-V2X) offers substantial performance gains over its predecessor, the improved performance is achieved at the cost of requiring additional spectral/hardware resources, while utilizing LTE-based system architectures and mechanisms. Thus, V2X networks based on 5G NR may not be able to meet the above-mentioned rigorous requirements and use cases of the emerging intelligent autonomous vehicles. A paradigm shift from conventional communication networks in favor of more flexible and diversified approaches is necessary. In fact, this transformation is

beginning to take shape with the intensifying research into 6G wireless communication networks aiming for incorporating disruptive concepts[4]. In addition to intelligent and ubiquitous V2X systems, 6G is expected to provide significant data rate increases (e.g., up to Tbps), extremely fast wireless access (e.g., in the range of sub-milliseconds) and massive increase in wireless connections (e.g., billions of connected devices) as well as more extensive, more energy-efficient, and more environmentally friendly three-dimensional (3D) communications.

To realize the above vision of 6G-V2X, this research work advocates the intrinsic amalgamation of Radio frequency (RF) and Visible Light Communication (VLC) solutions, which are complementary to each other due to their respective benefits and trade-offs. Autonomous driving requires close monitoring of the surrounding area around the vehicle by deploying various sensors such as LIDAR, RADAR, camera, ultrasonic sensor, etc. In particular, a camera can not only allow the vehicle to recognize its surrounding objects, it can also be used as a receiver for VLC. Such a camera can then communicate via VLC with a large number of devices because of its spatial separation feature, thereby facilitating object recognition around the vehicle, obstacle location estimation, and even communication. By intelligently combining VLCaided V2X communications with classic RF-based communications, our objective is to increase the data rates, reduce the transmission latency, improve reliability, reduce power consumption, and enhance safety. However, one of major challenges for vehicular-VLC (V-VLC) arises from its outdoor operation. Meteorological phenomenon such as fog, rain, snow etc influences the reliability as well as range of V-VLC. In terms of commercialization progress, there has been renewed industry interest in implementing and commercializing VLC technology to create new value chains, and in the meantime several pilot projects have been launched to promote research in this new field. For instance, pureLiFi is the global leader in bringing to market the world's first commercial light antennas making LiFi possible—for all kinds of applications, from industrial to consumer, and from smart cars to smartphones¹. Besides, various globally recognized LiFi companies like Oldecomm, VLNComm, Panasonic corporation, Signify, and Lucibel also primarily focus on bringing next-generation VLC front-end products to commercial markets². In particular, Oledcomm is a French telecommunications company that began its research into LiFi systems that can be used extensively in the automotive sector.

¹<https://www.purelifi.com/taking-lifi-mainstream/>

²<https://lifi.co/lifi-companies/>

1.1 Objectives

The main aim of this dissertation is to provide analytical framework for evaluating performance of hybrid visible light and radio frequency for vehicular communication systems. Specifically, the objectives of this dissertation are as follows.

- To highlight the potential benefit of employing heterogeneous visible light and radio frequency for enhanced vehicular message dissemination at road intersection. We make use of various analytical tools of stochastic geometry to characterize the performance of various network configurations, i.e., standalone V-VLC, stand-alone V-RF and hybrid V-VLC/V-RF network.
- To investigate the performance of Optical Power Domain Non Orthogonal Multiple Access (OPD-NOMA) enabled vehicular-VLC (V-VLC) systems. In addition to above, we evaluate analytically the performance of cooperative NOMA (C-NOMA) assisted hybrid visible light and radio frequency communication for improving safety message dissemination at road intersection.
- To explore the advantageous amalgamation of optical reconfigurable intelligent surface (O-RIS) and hybrid RF-VLC technologies for enhanced vehicular message dissemination particularly at road intersection.
- To study the impact of interference and meteorological phenomenon on the performance of hybrid V-VLC/V-RF system.

1.2 Contributions and Research Outcomes

The main contributions of this dissertation are summarized below along with relevant publications.

- We analyzed the impact of interference and meteorological phenomenon on the performance of hybrid V-VLC/V-RF system. Specifically, we showed that regardless of any meteorological impact, a properly configured link-aggregated hybrid V-VLC/V-RF system is capable of meeting stringent ultra high reliability ($\geq 99.999\%$) and ultra-low latency (< 3 ms) requirements, making it a promising candidate for 6G Vehicle-to-Everything (V2X) Communications.
 - **G. Singh**, A. Srivastava, and V. Bohara, “On Feasibility of VLC Based Car-to-Car Communication under Solar Irradiance and Fog Conditions,” in Proc. *ACM 1st Int.*

- Workshop Commun. Comput. Connected Veh. Platooning, ACM MobiCom*, Oct. 2018, pp. 1–7.
- **G. Singh**, A. Srivastava, and V. A. Bohara, “Impact of Weather Conditions and Interference on the Performance of VLC based V2V Communication,” in *Proc. IEEE 21st International Conference on Transparent Optical Network (ICTON)*, Angers, France, July, 2019, pp. 1–4.
 - K. Joshi, N. Roy, **G.Singh**, V.A.Bohara and A. Srivastava, “Experimental Observations on the Feasibility of VLC-Based V2X Communications under various Environmental Deterrents”, *IEEE International Conference on Advanced Networks and Telecommunications Systems (ANTS)*, Dec 2019 BITS Goa, India.
 - **G.Singh**, A. Srivastava, and V.A.Bohara, “Stochastic Geometry Based Interference Characterization for RF and VLC Based Vehicular Communication System”, *IEEE System Journal*, vol. 15, no. 2, pp. 2035-2045, Sept. 2020.
 - **G. Singh**, A. Srivastava, V. A. Bohara, M.N. Rahim, Zilong L., and Pesch D., “Towards 6G-V2X: Aggregated RF-VLC for Ultra-Reliable and Low-Latency Autonomous Driving Under Meteorological Impact”, submitted to *IEEE Communication Standards Magazine*, Jan, 2023. Available online: <https://arxiv.org/abs/2208.06287>
- We explored the potential benefits and practical challenges associated with implementation of OPD-NOMA scheme for VLC based vehicle-to-everything (V2X) networks with a major aim of providing vehicles with reliable, ubiquitous, and massive connectivity. Additionally, we propose a novel C-NOMA assisted hybrid visible light and radio frequency communication for improving safety message dissemination at road intersection.
 - **G.Singh**, A. Srivastava, V.A.Bohara, and Zilong L. “Comparison of PD-NOMA for RF and VLC based Vehicular Communication Under Various Weather Conditions”, *Wireless World Research Forum Meeting 44*, Copenhagen, Denmark, June, 2020.
 - **G.Singh**, A. Srivastava, V.A.Bohara, and Zilong L. “Downlink Performance of Optical Power Domain NOMA for Beyond 5G Enabled V2X Networks”, *IEEE Open Journal of Vehicular Technology*, vol. 2, pp. 235-248, May 2021.
 - **G. Singh**, D. Gupta, A. Srivastava, V. A. Bohara, and Zilong L., “Exploring Cooperative NOMA Assisted Hybrid Visible Light and Radio Frequency for Enhanced Vehicular Message Dissemination at Road Intersections”, *Elsevier Physical Communication*, Sept., 2022.
 - We investigated the use of V-VLC for basic safety messages (BSMs) dissemination in lieu of conventional V-RF communication in road intersection applications, where the

reception performance is affected by interference from the concurrent transmissions of other vehicles. In addition, we proposed two practical deployment strategies namely hybrid RF-VLC with relaying and V-RF with Reconfigurable Intelligent Surface (RIS) which may serve as a preferred alternative for future ITS.

- **G.Singh**, A. Srivastava, V.A.Bohara, Zilong L., M.N. Rahim, and G. Ghatak, “Heterogeneous Visible Light and Radio Communication for Improving Safety Message Dissemination at Road Intersection”, *IEEE Transactions on Intelligent Transportation Systems*, Feb, 2022.
- **G. Singh**, A. Srivastava and V. A. Bohara, “Visible Light and Reconfigurable Intelligent Surfaces for Beyond 5G V2X Communication Networks at Road Intersections”, *IEEE Transactions on Vehicular Technology*, Apr., 2022.
- The proposed framework highlighted the advantageous amalgamation of O-RIS and hybrid RF-VLC technologies for enhanced vehicular message dissemination particularly at road intersection.
 - T. Pal, **G.Singh**, A. Srivastava, and V.A.Bohara “On Performance of Optical-RIS Aided Vehicular Communication Systems”, *Wireless World Research Forum Meeting 47*, Bristol, UK, June 2022.
 - **G. Singh**, T.Pal, A. Srivastava and V. A. Bohara, “Optical RIS Enabled Hybrid RF-VLC V2X Communication Network: A Promising New Frontier for 6G-ITS”, *IEEE International Conference on Advanced Networks and Telecommunications Systems (ANTS)*”, MNIT Jaipur, Dec, 2023. Accepted for publication.

1.3 Organization

The remainder of this dissertation has been organized as follows. In chapter 2, the background and related work of this dissertation has been outlined. This chapter also introduces the concept of NOMA and RIS in context to vehicular communication. The reliability of packet transmission at road intersection for hybrid vehicular-VLC and V-RF communication system has been investigated in chapter 3 in terms of outage probability, throughput and latency using various analytical tools of stochastic geometry. We investigate the applicability of downlink OPD NOMA enabled V2X network for typical infrastructure-to-vehicle (I2V) communication in presence of interference caused from concurrent vehicle-to-vehicle (V2V) transmissions in chapter 4. Further, this Chapter also propose a novel cooperative non orthogonal multiple access (NOMA) enabled hybrid vehicular visible light communication (V-VLC)/V-RF communication

for improving safety message dissemination and enabling massive connectivity among vehicles for road intersection scenarios. In chapter 5, we unlocked the potential benefit of employing optical-RIS (O-RIS) enabled hybrid RFVLC V2X communication for enhanced vehicular message dissemination at road intersection. The impact of interference and meteorological phenomenon on the performance of hybrid V-VLC/V-RF system has been analyzed in Chapter 6. Finally, we summarize our contributions and discuss potential future works in chapter 7.

Background and Related Works

In this chapter, we provide a brief overview of hybrid RF-VLC V2X communication systems. This chapter also introduces the concept of non orthogonal multiple access (NOMA) and reconfigurable intelligent surfaces (RIS) in context to vehicular network.

2.1 Hybrid RF-VLC V2X Systems

Pure RF links may suffer from excessive RF interference in scenarios of high road-traffic density, which increases the communication latency owing to packet delivery failures and aggressive ARQ retransmission attempts. This in turn increases the spectrum congestion in dynamic vehicular environments. As a possible solution, the non-interfering unlicensed VLC band may be harnessed in unison with the RF band for improved V2X communications, while supporting enhanced security[5]. Furthermore, a VLC-enabled V2X system will need minimal setup costs as VLC-based V2X can use light emitting diodes (LEDs) or laser diodes (LDs) that are already present in the vehicular head- and tail-lights or in street/traffic lights. Despite the above benefits, standalone VLC networks also have their drawbacks, including their limited coverage distance, sensitivity to background light and line-of-sight (LOS) blockage. These impediments are conveniently circumvented by the classic RF wireless networks, which exhibit wider coverage and higher transmission integrity in the absence of LOS. 6G-V2X is envisioned to play a pivotal role on attaining the ambitious goals for internet of vehicles by satisfying the more rigorous key performance indicators (KPIs) that were partially fulfilled by 5G for vehicle communications. Indeed, it is expected that 5G use cases categories will evolve to Further enhanced Mobile Broadband (FeMBB), Mobile BroadBand and Low-Latency (MBLL), ultramassive Machine-Type Communication (umMTC), and massive Low-Latency Machine-Type communication (mLLMT) with extreme requirements such as data rates over 1

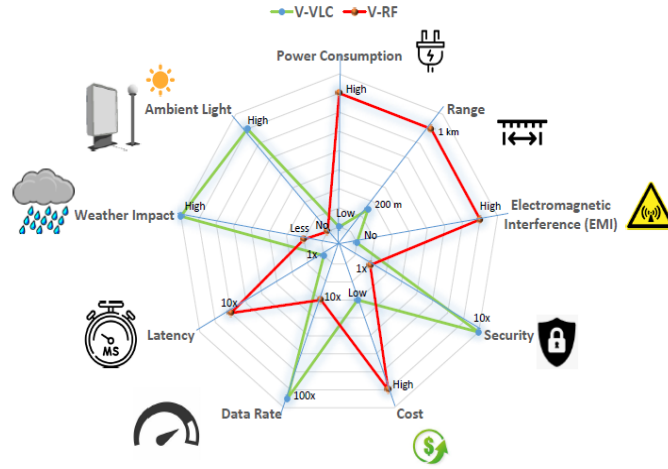


Figure 2.1: Performance trade-offs of conventional VLC and RF based V2X communication systems.

Tbps, end-to-end delays lower than 1 ms, network availability and reliability beyond 99.999%, extreme connection density of over 10^7 devices/ km^2 , and spectrum efficiency over 5 times that of 5G while supporting extreme mobility. By intelligently combining, we show that the integration of VLC and RF improves the overall system performance to meet the stringent KPI requirements of 6G-V2X networks. As depicted in Fig. 2.1, hybrid RF-VLC based V2X systems have the potential to deliver significantly improved vehicular message disseminations by exploiting the complementary advantages of standalone VLC and RF systems. There are two main categories of hybrid RF-VLC based vehicular communication systems[6]:

a. **Link-Aggregated (LA) Hybrid RF-VLC V2X systems:** In order to improve the achievable data rate and connection reliability, the vehicular nodes employ both VLC and RF links simultaneously.

b. **Non-Link Aggregated (non-LA) Hybrid RF-VLC V2X systems:** In this case, the vehicular nodes utilize either VLC or RF technology at a given time instant to optimize the network parameters.

As shown in Fig. 2.2, there are five primary scenarios in which VLC can complement and strengthen RF communication in V2X networks: (1) V2V communications via front lights or back lights, (2) U2V (UAV-to-Vehicle) communication, (3) V2V communication via Re-configurable Intelligent Surfaces (RIS¹), (4) V2X communications via traffic lights, and (5) V2X communications via street lights. The latter may be viewed as a second layer of ubiquitous small-cell VLC BSs. In addition to increasing data rates, VLC has the potential to

¹RIS refers to reconfigurable metasurfaces consisting of numerous passive antenna-elements having adjustable phases. In fact, in advance RISs, one can effectively control not only the phase, but potentially even the frequency, amplitude and the polarization of the incident wireless signals to overcome the deleterious effects of natural wireless propagation[2].

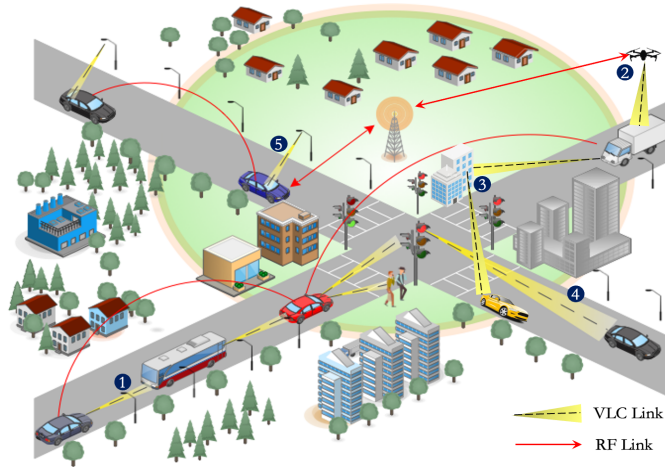


Figure 2.2: Illustration of a generic hybrid RF-VLC communication in a vehicular network.

address some of the limitations of traditional V2X communication based on RF. For example, in the left bottom corner of Fig. 2.2, the RF-based V2V communication of two cars separated by a large bus may suffer from severe packet loss due to the shadowing effect. In this case, the transmitting car may use VLC to communicate with the bus; subsequently, the bus could forward the messages to the receiving car in the shadowed region. Moreover, the data packets can also be relayed using traffic/street lights at urban intersections, allowing vehicles to interact across perpendicular streets, where traditional RF-based solution is often plagued by severe packet loss. Further, the use of optical-RIS (O-RIS)² can further combat packet loss, enhancing signal quality and providing wider coverage in a VLC aided V2X systems. Apart from the above, VLC enabled unmanned aerial vehicle (UAV) based U2V communication[8] can be utilized for smart traffic monitoring system to monitor, track and control allowed speed, other traffic violations and suspicious behavior of vehicles moving on the road. Although RF-based relaying in context of vehicular communication has been widely explored in the literature, resultant interference has to be mitigated in high-density vehicular environments.

2.1.1 V2X Communication Technologies

To fully support connected and automated vehicle (CAV), there is a growing demand for ultrareliable and near-real-time exchange of sensing and control data collected by many on-board sensors and communication devices. Such a demand is believed to be met by the next generation vehicle-to-everything (V2X) communication technologies in the form of, for example, vehicle-to-vehicle (V2V) and vehicle-to-infrastructure (V2I) communications.

²O-RIS can be envisioned as an extension of RIS for THz optical wireless signals and eventually for VLC[7].

There are two major V2X streams: dedicated short-range communication (DSRC)-aided V2X and cellular-V2X (C-V2X) [9, 10]. While DSRC represents a mature cost-efficient V2X technology, CV2X has attracted much attention in recent years because of its significantly improved coverage, throughput, and latency. The latter is due to the improved physical layer, centralized resource allocation, as well as sophisticated cellular infrastructure. Several 3GPP

Table 2.1: Comparison of DSRC/IEEE 802.11p, C-V2X, VLC, LTE and 5G NR V2X

Features	DSRC/IEEE 802.11p	C-V2X	VLC	LTE	5G NR
Standard	IEEE 802.11p	IEEE 802.11	IEEE 802.15.7	3GPP Rel-10/11/12	3GPP Rel-15/16
Frequency Band(s)	5.86-5.92 GHz	2.4 GHz, 5.2 GHz	300-800 THz	450 MHz-4.99 GHz	700 MHz-100 GHz
Channel width	10 MHz	20 MHz	NA	upto 100 MHz	NA
Bit Rate	3-27 Mbps	6.54 Mbps	11.67 Kbps-96 Mbps THz	upto 1 Gbps	upto 20 Gbps
Range	upto 1 km	100-500 m	<200 m	tens of meters to 30 km	Ubiquitous
Mobility support	upto 60 km/h	Low	Low	upto 350 km/h	upto 500 km/h
V2V support	Yes:Ad hoc	Yes:Ad hoc	Yes	Yes:via D2D	Yes
V2I support	Yes	Yes	Yes	Yes	Yes
Deployment	RSU	Hotspot, Access Point	Available Road Lights	May use the available eNodes B	NSA and SA mode
Market Penetration	Low	High	Low	Potentially high	NA

V2X initiatives (such as LTE-V2X and 5G New Radio (NR)-V2X) have contributed to the prominence of C-V2X. With an abundance of both advanced sensors and communication devices, however, new challenges arise for the emerging next generation V2X networks. More explicitly, stringent system reliability (99.999%), end-to-end latency (<1 ms), coverage-quality, spectral efficiency, energy rating, networking, and privacy/security specifications should be met to support various C-V2X use case requirements. Although the current C-V2X technology (such as 5G-NR-V2X) offers substantial performance gains over its predecessor, the improved performance is achieved at the cost of requiring additional spectral/hardware resources, while

utilizing LTEbased system architectures and mechanisms. In the essence, 6G-V2X will be a prominent supporter for the evolution towards a truly Intelligent Transportation System (ITS) and the realization of the emerging CAV by fulfilling the limitations of V2X based 5G NR, once vehicular networks are becoming highly dynamic and complex with stringent requirements on ultra-low latency, high reliability, and massive connections.

With the vehicular density increases, the above mentioned technologies tends to suffer from higher interference, lower packet delivery rates and longer communication delay due to channel congestion (for e.g. in challenging platooning scenarios[11]) [12–14]. Compounding the issue further is the limited available RF spectrum which may not be able to suffice the growing demands for future ITS [15]. The high latency issues associated with DSRC have been discussed in [16]. In particular, at highly dense traffic scenarios, DSRC is affected by severe packet collisions, resulting in more frequent re-transmissions and high latency. Against this background, VLC can be considered as complementary solution to the existing DSRC and an economically viable candidate for B5G V2X network. Vehicular networking applications can take advantage of the LED-equipped lighting modules and transportation infrastructure to implement V-VLC[17]. Table 2.1 compares various V2X communication technologies. Besides supporting high data rate communications [18–20], the V-VLC technology posses inherent advantages over DSRC technology such as lower cost, lower power consumption, less complex transceiver design, enhanced security, improved link quality, less delay and anti-electromagnetic interference [21]. Despite all the aforementioned V-VLC advantages, V-VLC also suffers from the fact that most of its applications require direct line-of-sight (LOS) communication which could increase probability of connectivity loss for long range communication. Further, the performance of V-VLC systems deteriorates in presence of adverse weather conditions and interference caused by artificial and natural light sources[22]. Therefore, recent literature has explored the feasibility of integrating V-VLC with the existing DSRC to improve the overall performance of V2X networks. V-RF can address V-VLC’s shortcomings, such as low communication range and inability to propagate through opaque objects and V-VLC can offer high data transmission rates with very low interference in LOS scenarios. Such hybrid V-VLC and V-RF concepts have been proposed in literature[23, 24]. In [23], the authors proposed a radio and visible light hybrid protocol for improving the reliability of control message used in autonomous platooning systems. The authors in [24] proposed an IEEE 802.11p and VLC based hybrid security protocol for vehicular platooning applications. In addition, few reports on experimental demonstration of such hybrid V-VLC/V-RF networks are also documented in the literature [25, 26]. *Masini et al.* showed packet delivery rate improvement by considering vehicles equipped with both DSRC and VLC interfaces as compared to standalone technologies

[25]. In [26], the authors investigated experimentally that complementary usage of 5G and VLC can achieve ultra-low latency upto 12 *ms* for vehicular communication.

2.2 Non-Orthogonal Multiple Access (NOMA)

The next generation vehicular network will also require reliable massive connectivity and reduced resource collision, hence a suitable multiple access (MA) scheme should be adopted that can cater for these requirements. Recently, Non-Orthogonal Multiple Access (NOMA) scheme has emerged as favourable multiple access scheme for next generation cellular networks. Compared to other multiple access techniques, NOMA provides higher spectral efficiency, better connectivity, user fairness, reduced latency and enhanced data rates which also makes it a strong contender for future development of vehicular networks[27]. NOMA allows multiple users to share the same channel resource via power domain or code domain multiplexing.

2.2.1 NOMA for VLC

There are a number of impressive advantages to VLC, but it also has some serious drawbacks. In particular, the relatively limited modulation bandwidth of LED is a critical concern when it comes to the design of high-data-rate VLC systems. While VLC enables numerous users to access the network at once, conventional OMA techniques do not promote efficient resource usage. As a result, NOMA, and more specifically, PD- NOMA, can be viewed as a suitable multiple access strategy that provides adequate bandwidth for a typical VLC systems. To efficiently meet 6G-V2X requirements, the integration of VLC and NOMA is emerging as a disruptive technique for advanced use cases in connected autonomous vehicles[12]. The power-domain non-orthogonal multiple access (NOMA) [28] scheme has been extensively studied in recent years by allowing several users to access the same resource with distinctive power levels, thus increasing the spectral efficiency of the system. Additionally, it offers enlarged number of connectivity, lower access latency, and reduced resource collision. In comparison to orthogonal multiple access (OMA), NOMA achieves enhanced sum rates by utilizing successive interference cancellation (SIC) decoding at the receiver. The performance of optical power domain-NOMA (OPD-NOMA) in VLC based systems have recently attracted considerable research attention [29–36]. In order to improve quality-of-service (QoS) requirement, the cooperative techniques can be applied into NOMA networks. Cooperative technique is an effective solution to extend the coverage and overcome channel impairments such as fading, pathloss and shadowing. Depending on the cooperation types, there exists two main categories of cooperative NOMA (C-NOMA) techniques with user cooperation and dedicated relaying

cooperation, respectively [37]. NOMA users collaborate as relays in the former, while in the latter category, dedicated relay nodes are distributed in the network. Several C-NOMA schemes have been discussed in the literature from various perspectives [37–39]. It is anticipated that the integration of cooperative techniques, NOMA, V-VLC, and V-RF systems can be exploited to improve the performance of V2X communication system with wider communication coverage, higher data rate, reduced transmission latency and increased spectral efficiency [40, 41].

2.3 Reconfigurable Intelligent Surfaces

Recently, RIS has also been recognized as one promising technology for the B5G ecosystem [12, 42]. The efficient integration of RISs into vehicular network brings both new opportunities as well as challenges, which deserve a dedicated investigation. RIS is specifically a reconfigurable array of reflecting elements, wherein each element can independently alter the phase and/or attenuation of the incident signal [43]. Further, RISs are both energy as well as cost-efficient since they are composed of semi-passive elements and can be installed on existing infrastructure, like, building and walls. In optical domain, O-RIS are categorized as: intelligent metasurface reflector (IMR) and intelligent mirror array (IMA) [44]. It is anticipated that 6G-ITS applications viz. autonomous driving, platooning and cooperative driving shall witness proliferation of such O-RIS and hybrid RF-VLC technologies, while fulfilling stringent 6G key performance indicators (KPIs) requirements.

2.3.1 Related Works

An RIS-enabled vehicular communication has attracted widespread attention in enhancing wireless transmission [45–47]. In [45], the authors studied efficient resource allocation scheme for intelligent reflecting surface aided vehicular communications based on large-scale slowly varying channel statistics instead of instantaneous channel state information (CSI). Given the blockage and vehicle density in practical road conditions, the authors in [46] proposed to use RIS to improve the coverage and outage performance in vehicular network. An RIS enabled vehicular network is considered in [47] to improve the physical layer security. Specifically, two RIS-based vehicular network system models are proposed. One model with an RIS based access point (AP) and another model with an RIS based relay. Numerous use case scenarios for such RIS aided vehicular communication have been discussed in [48]. In particular, the authors in [48] explored potential benefits of employing reconfigurable meta-surfaces on prominent vehicular use cases, such as cooperative driving and vulnerable road users (VRUs) detection. To efficiently integrate with next generation V2X communication scenarios, RIS still needs to

address fundamental challenges such as reflection optimization, optimal placement, and channel estimation in a highly dynamic vehicular environment[12]. Despite the widespread interest in

Table 2.2: Summary of RIS-VLC proposed performance enhancement schemes

Ref.	Mian Contribution	Key VLC issues	Proposed Technique(s)
[49]	Date rate maximization for RIS aided VLC systems	Link Blockages Device orientation User orientation	A sine-cosine metaheuristic is used to obtain optimal configuration of RIS mirror arrays
[50]	Energy efficiency maximization for RIS aided VLC systems	Link Blockages	A typical interior point method is used to obtain optimal time allocation, DC offset distribution and power control, A one dimensional search method is used to obtain sub-optimal phase shift solution
[51]	Secrecy rate maximization for RIS aided VLC systems	Security	A modified particle swarm optimization algorithm is used to obtain optimal mirror RIS configuration
[52]	Sum rate rate maximization for RIS aided VLC systems	Link Blockages	A greedy algorithm is used to associate LEDs with RIS elements.
[53]	Spectral efficiency maximization for RIS aided VLC systems	Link Blockages	A frozen variable method is used to solve RIS-LEDs association problem. A minorization-maximization algorithm is used to solve RIS-LED association/LED power control problems.
[54]	Illumination and data rate enhancements for RIS aided VLC systems	Illumination	A two stage heuristic approach is used to optimize RIS mirror placements, LEDs' transmit power, and LED user assignment problem.

applying RISs in various wireless vehicular environment, there is paucity of intensive research efforts on exploring RIS assisted VLC (also referred to as optical-RIS (O-RIS)) for vehicular communication. In fact, a promising solution to relax the LoS constraint in V2XVLC networks is represented by O-RIS. Very recently, the authors in [55] considered a parallel vehicle-to-vehicle (V2V)- VLC system and investigated the signal-to-noise-ratio (SNR) versus the distance between adjacent RIS units. There have been many research activities on optimizing

the configuration of intelligent mirror array (IMA) and intelligent metasurface resonator (IMR) RISs in VLC systems (see Table 2.2), few attempts have been made to investigate the RIS element to AP/user assignment design problem and the RIS array positioning design problem.

Reliable Packet Transmission for V2X Networks

This chapter investigates the reliability of packet transmission at a road intersection. In particular, in part-I, we investigate the potential benefit of employing V-VLC along with conventional V-RF for enhanced vehicular message dissemination at road intersections, while in part II, we discuss two practical deployment strategies which may serve as a preferred alternative for future ITS to meet ultra-high reliable and ultra-low latency communication for beyond 5G (B5G) vehicular networks.

Part I

3.1 Overview of Part I

Visible light communication (VLC) has recently emerged as an affordable and scalable technology supporting very high data rates for short range vehicle-to-vehicle (V2V) communication. In this work, we advocate the use of vehicular- VLC (V-VLC) for basic safety messages (BSMs) dissemination in lieu of conventional vehicular radio frequency (V-RF) communication in road intersection applications, where the reception performance is affected by interference from the concurrent transmissions of other vehicles. We make use of stochastic geometry to characterize the interference from the same lane as well as the perpendicular lane for various network configurations, i.e., standalone V-VLC, stand-alone V-RF and hybrid V-VLC/V-RF network. Specifically, by modeling the interfering vehicles' locations as a spatial Poisson point process (PPP), we are able to capture a static two-dimensional road geometry as well as the impact of interference due to vehicles clustering in the vicinity of road intersection in terms of

outage probability and throughput. In addition to the above, the performance of spatial ALOHA and carrier sense multiple access with collision avoidance medium access control (CSMA/CA MAC) protocol for standalone V-VLC, standalone V-RF and hybrid V-VLC/V-RF network configuration for relaying BSMs at road intersections is also compared. The performance metrics such as delay outage rate (DOR) and information outage rate (IOR) is utilized to investigate the impact of latency associated with various network configurations.

A primary objective of this work is to showcase the potential benefit of employing V-VLC along with conventional V-RF by improving the relaying performance of BSMs at road intersections. Specifically, the major contributions of this work are summarized below:

- We explore the co-deployment of V-VLC and V-RF communication systems for relaying BSMs at a road intersection. We consider data transmission using either V-VLC link or V-RF link at a certain time instances. The parallel combination of V-VLC and V-RF links leads to improved outage performance, throughput, and reliability of the overall system. We compare the performance of the proposed hybrid V-VLC/V-RF network with the standalone V-VLC and standalone V-RF network using various analytical tools of stochastic geometry.
- We show the limitation of standalone V-VLC over V-RF when the distance between the desired vehicle and RSU is less than the critical distance referred to as “*dead zone*” region, which exists due to restricted field-of-view (FOV) of receiver.
- We compare the performance of spatial ALOHA and CSMA/CA MAC protocol based standalone V-VLC, standalone V-RF and hybrid V-VLC/V-RF network configuration for relaying BSMs at road intersection.
- We propose to use DOR and IOR as performance metrics to investigate the impact of latency on various network configurations. In practice, a large latency is intolerable for many safety/warning-related messages. These data-oriented characterization can be applied to develop an upper bound on queuing performance over point-to-point vehicular communication links.

Numerical results illustrate that the implementation of MAC protocol-based hybrid V-VLC/V-RF network leads to considerable improvement in outage performance, throughput and low latency as compared to stand-alone V-VLC or stand-alone V-RF network.

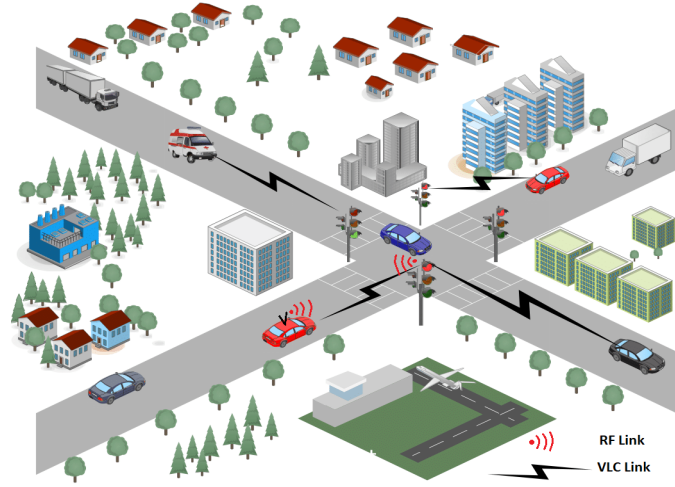


Figure 3.1: Illustration of safety message dissemination in a vehicular network at road intersection. A desired vehicle can communicate with RSU via VLC shown by zig-zag or RF link shown by red transmission signal.

3.2 Preliminaries and assumptions

3.2.1 Network Model

We consider an intersection scenario with two perpendicular roads, as shown in Fig. 3.1. For ease of analysis, it is assumed that each road carries a stream of interfering vehicles modeled as one-dimensional homogeneous PPPs. The intensities of interfering vehicles on H -road (located behind desired vehicle) and V -road are denoted by λ_H and λ_V respectively, and the PPPs describing the locations of the vehicles on the two roads are represented by $\phi_H \sim \text{PPP}(\lambda_H)$ and $\phi_V \sim \text{PPP}(\lambda_V)$ respectively. Each vehicle periodically generates a packet containing some information collected on board, such as the vehicle position, speed, acceleration and flow of direction. The desired vehicle close to intersection is assumed to carry critical road information which needs to be immediately communicated to RSU. Both VLC and IEEE 802.11p transceivers are assumed integrated on board and can be used separately (also called standalone V-VLC or V-RF network) or jointly (also called Hybrid V-VLC/V-RF network). The RSU is assumed to be positioned at the crossroads; RSUs for 802.11p are already installed, while RSUs for VLC can be considered integrated in the road lamps or traffic lights. When V-VLC is addressed, the communication between the vehicle and RSU happen through the head or rear LED headlamp, while the reception at RSU is carried out through photodetectors.

Fig. 3.2 portrays a generalized and simplified abstraction model of the proposed scenario. All links can either be VLC link (standalone V-VLC network) or RF link (standalone V-RF network). Both VLC as well as RF link are assumed to be available for hybrid V-VLC/V-RF

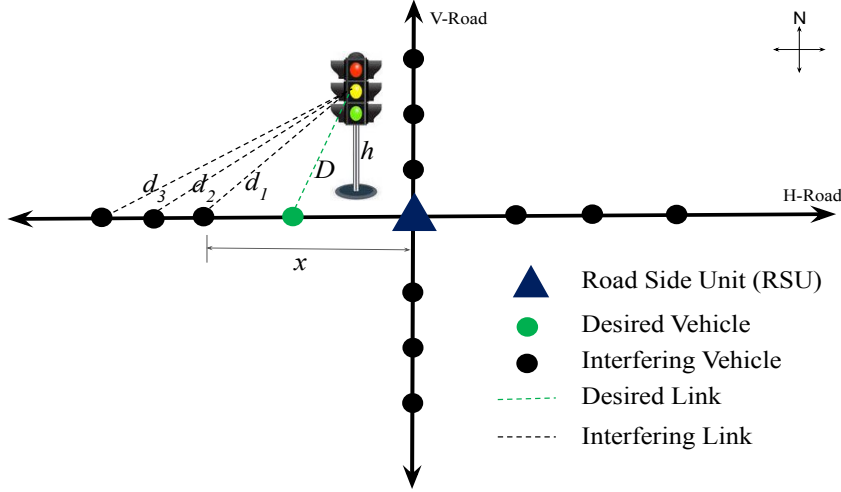


Figure 3.2: Abstraction used for modeling. The desired vehicle is marked in green circle, while RSU is marked in triangle, is assumed to be located at the center of road intersection. All links can either be V-VLC or V-RF link.

network configuration. Vehicles on horizontal road H and vertical road V , represented by black circle, transmit concurrently and cause interference. Interestingly, unlike V-RF communication, based on practical receiver implementation, V-VLC suffers interference from vehicles on the same lane. As shown in Fig. 3.3 (a), there also exists a critical distance, d_c , below which V-VLC may become un-operational (referred to as “dead zone” region for V-VLC). In such case, V-RF communication is the only feasible means of communication between the desired vehicle and RSU.

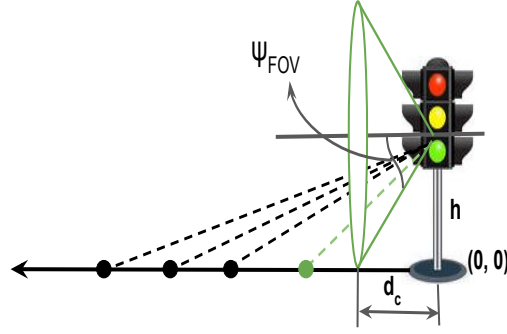
Fig. 3.3 (b) shows transition diagram of hard switching based hybrid V-VLC/V-RF network configuration. An outage occurs when both V-VLC and V-RF links fall into outage. Re-initialization is decided depending upon the distance between the desired vehicle and RSU. In general, unlike V-RF, V-VLC network is a reliable option for low communication range.

3.2.2 Channel Model for V-VLC and V-RF

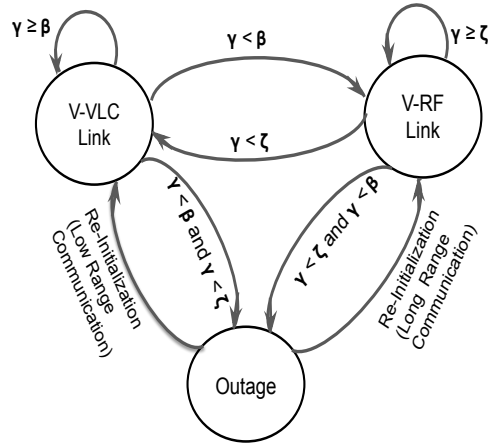
For a V-VLC system, the channel DC gain between k -th user and RSU can be modeled using Lambertian emission model as follows [56]

$$h_k = \frac{(m+1)A_R}{2\pi d_k^2} \cos^m(\phi_k) \cos(\Psi_k) T_s(\Psi_k) G(\Psi_k), \quad (3.1)$$

where, A_R , d_k , ϕ_k , and Ψ_k denote the area of PD, the Euclidean distance between the k^{th} vehicle and RSU, the angle of irradiance and the angle of arrival (AoA) respectively. $T_s(\Psi_k)$ denotes



(a)



(b)

Figure 3.3: (a) Illustration of critical distance, d_c . Here, $d_c = h/\tan(\Psi_{FOV})$ (b) Transition diagram of hybrid V-VLC/V-RF network configuration. Here, β and ζ denote the SINR threshold for standalone V-VLC and V-RF networks, respectively.

the gain of the optical filter at the receiver; In above, m is the order of the Lambertian model which is given by $m = -\frac{\ln(2)}{\ln(\cos(\phi_{\frac{1}{2}}))}$. $G(\Psi_k)$ denotes the gain of optical concentrator at the receiver front-end which is given as

$$G(\Psi_k) = \begin{cases} \frac{n^2}{\sin^2 \Psi_{FOV}}; & \text{if } 0 \leq \phi_k \leq \Psi_{FOV}, \\ 0; & \text{if } \phi_k > \Psi_{FOV}, \end{cases} \quad (3.2)$$

where n denotes the refractive index of the optical concentrator. Based on simple geometrical illustration shown in Fig. 3.2, one can observe that $\cos(\phi_k) = \cos(\psi_k) = \frac{x_k}{\sqrt{(h^2 + x_k^2)}}$ where, h

denotes the height of RSU. (3.1) can be rewritten as:

$$h_k = \frac{(m+1)A_R}{2\pi} \frac{x_k^{(m+1)}}{(h^2 + x_k^2)^{\frac{(m+3)}{2}}} T_s(\Psi_k) G(\Psi_k), \quad (3.3)$$

The channel power can be obtained as: $Z_k^{V-VLC} = (h_k)^2$. In case of V-RF communication, we assume that the received signal amplitude in RF based V2V channel follows Rayleigh probability distribution function (PDF). Since Rayleigh fading is considered, fading gain (h_x) is an exponential random variable of unit mean.

3.2.3 MAC Protocols

In this section, we provide a brief introduction on MAC protocols such as slotted ALOHA, and CSMA/CA which have been well studied in literature [57–60]. The MAC protocol governs when a particular user can access the channel, and helps to reduce the overwhelming amount of interference from other users in a network. The two most common MAC protocols used for ad-hoc networks are slotted ALOHA and CSMA/CA. Besides, several MAC protocols have been proposed for VANET safety applications[57–59]. In slotted ALOHA, nodes that have a packet to send, access the channel during a time slot with a transmission probability $\rho \in [0, 1]$. In contrary, in CSMA, before sending a packet, a node verifies that whether the channel is free by listening to the channel. Only if the channel is free, the node transmits the packet. If the channel is busy, the node is forced to wait a random back-off time before it can try again [60]. In this work, we compare performance of spatial ALOHA and CSMA based MAC protocols which has not been investigated in context of V-VLC communication.

3.2.4 Intensity of Interfering PPP

The interference's intensity λ_{MAC} typically depends on the type of MAC that is being utilized. We compare the performance of the proposed scenario between two cases: slotted ALOHA with transmission probability, $\rho \in [0, 1]$ and CSMA/CA with contention region with radius, $\delta \geq 0$.

- **Slotted ALOHA:** For slotted ALOHA MAC, time axis is divided into slots and each transmitting vehicular node accesses the channel independently at each time-slot with a certain probability, $\rho \in [0, 1]$ on each road [61, 62]. This in turn leads to an independent thinning of the PPPs, so that $\lambda_{MAC} = \rho \lambda_R$. Here, λ_R denotes the intensity of interfering vehicles on each road.

- **CSMA:** For a CSMA MAC, a vehicle is allowed to transmit only if it has the lowest random timer within its contention region (sensing range). This implies that (i) the intensity is a function of transmitter's location as other transmitting vehicles (interferers) in its contention region are forced to keep silent when the desired vehicle is active; (ii) the interference from the H - and V -roads is not independent. When the desired vehicle is active and transmitting at a distance, say $R(= \sqrt{D^2 - h^2})$, the resulting intensity of the PPPs used to approximate the PP of interferers can be expressed as[61]

$$\lambda_{MAC}^H = \begin{cases} p_A(x)\lambda_R & \text{if } x < -R - \delta, x > \delta - R \\ 0; & \text{otherwise,} \end{cases} \quad (3.4)$$

$$\lambda_{MAC}^V = \begin{cases} p_A(y)\lambda_R & \text{if } \|y\| > \sqrt{\delta^2 - R^2}, \\ 0; & \text{if } \|y\| \leq \sqrt{\delta^2 - R^2}, \end{cases} \quad (3.5)$$

In (3.4) and (3.5), $p_A(x)$ and $p_A(y)$ denotes the access probability of interfering vehicle from H -road and V -road respectively. The access probability (which is used to thin the original process) is the probability that the given node has the smallest random timer in the corresponding contention region [61]. For CSMA MAC protocol, access probability is governed by [61, Eq.12]. In next section, we briefly describe various performance metrics such as outage probability, throughput, DOR and IOR for all slotted ALOHA based network configurations. Note that the closed form results using CSMA are hard to obtain, consequently it can be evaluated numerically as in [61].

3.3 Performance Evaluation

3.3.1 Outage Probability

In this subsection, we characterize the performance of the V-VLC in the presence of the aggregate interference and noise variance, σ^2 in terms of outage probability as a performance metric using moment generating functional (MGF) approach. In an interference limited channels, an outage occurs when the SINR falls below a given SINR threshold, β [63]. Mathematically,

$$\begin{aligned} P_{out,VLC}(\beta) &= \mathbb{P}(SINR < \beta), \\ &= \mathbb{P}\left(\frac{S}{I_{VLC} + \sigma^2} < \beta\right). \end{aligned} \quad (3.6)$$

The desired electrical signal power \mathcal{S} and interference \mathcal{I} can be formulated as

$$\begin{aligned} S &= \mathcal{R}^2 Z_o P_{VLC}, \\ I_{VLC} &= \sum_{x_k \in \Phi_{PPP}} \mathcal{R}^2 Z_k P_{VLC}. \end{aligned} \quad (3.7)$$

In above, P_{VLC} and \mathcal{R} denote the transmission power for V-VLC and the responsivity of PD respectively. The electrical SINR can be represented as:

$$SINR = \frac{1}{\frac{\mathcal{I}}{\mathcal{R}^2 Z_o P_{VLC}} + \frac{1}{\alpha_0}}, \quad (3.8)$$

where $\alpha_0 = \frac{\mathcal{R}^2 Z_o P_{VLC}}{\sigma^2}$. From [3.8], the outage probability for V-VLC assuming that desired vehicle is transmitting can be given as:

$$P_{out,VLC}(\beta) = \mathbb{P}\left(\frac{\mathcal{I}}{\mathcal{R}^2 Z_o P_{VLC}} + \frac{1}{\alpha_0} > \frac{1}{\beta}\right). \quad (3.9)$$

We define random variable W as

$$W = \frac{\mathcal{I}}{\mathcal{R}^2 Z_o P_{VLC}} + \frac{1}{\alpha_0}, \quad (3.10)$$

Hence, Eq. (3.9) can be rewritten as

$$P_{out,VLC}(\beta) = \mathbb{P}(W > \beta^{-1}) = 1 - \mathcal{F}_W(\beta^{-1}). \quad (3.11)$$

In general, it is quite difficult to obtain a closed-form solution for $\mathcal{F}_W(\beta^{-1})$. Hence, we make use of numerical inversion of Laplace transform to find CDF, $\mathcal{F}_W(\beta^{-1})$. The CDF of a random variable W is related to the Laplace transform of $\mathcal{F}_W(w)$ as

$$\mathcal{F}_W(w) = \frac{1}{2\pi j} \int_{c-j\infty}^{c+j\infty} L_{\mathcal{F}_W(w)} \exp(sw) ds. \quad (3.12)$$

where j denotes imaginary unit ($\sqrt{-1}$). The above integral can be discretized to get a series using the trapezoid rule and then the infinite series can be truncated to get a finite sum using the Euler summation [64]. Also, $L_{\mathcal{F}_W(w)}(s) = \frac{L_W(s)}{s}$. Moreover, (3.11) can be approximated as

$$P_{out,VLC}(\beta) \approx 1 - \frac{2^{-B} \exp(\frac{A}{2})}{\beta^{-1}} \sum_{b=0}^B \binom{B}{b} \sum_{c=0}^{C+b} \frac{(-1)^c}{D_c} \text{Re} \left\{ \frac{L_W(s)}{s} \right\}. \quad (3.13)$$

where $D_c = 2$ (if $c = 0$) and $D_c = 1$ (if $c = 1, 2, 3, \dots$) and $s = \frac{(A+j2\pi c)}{2\beta^{-1}}$. The estimation error is controlled by three parameters A , B and C . Using the well established result given in [64] and [65], in order to achieve an estimation accuracy of $10^{-\eta}$ (i.e., having the $(\eta - 1)$ th decimal correct), A , B and C have to be at least equal to $\eta \ln 10$, $1.243\eta - 1$, and 1.467η , respectively. Setting $A = 8 \ln 10$, $B = 11$, $C = 14$ achieves stable numerical inversion with an estimation error of 10^{-8} .

Using the definition of the Laplace transform of the probability distribution of a random variable,

$$\begin{aligned} L_W(s) &= \mathbb{E}_{\mathcal{I}} \left[\exp \left(-s \left(\frac{\mathcal{I}}{\mathcal{R}^2 Z_o P_{VLC}} + \frac{1}{\alpha_0} \right) \right) \right], \\ &= \mathbb{E}_{\mathcal{I}} \left[\exp \left(-\frac{s}{\alpha_0} \right) \exp \left(-\frac{s \mathcal{I}}{\mathcal{R}^2 Z_o P_{VLC}} \right) \right], \\ &= \exp \left(-\frac{s}{\alpha_0} \right) \mathbb{E}_{\phi_{PPP}} \left[\prod_{x \in \phi_{PPP}} \exp \left(-\frac{sk'x^{2(m+1)}}{Z_o(h^2 + x^2)^{(m+3)}} \right) \right]. \end{aligned} \quad (3.14)$$

Here $k' := \left(\frac{(m+1)A_R}{2\pi} T_s(\psi) G(\psi) \right)^2$. The expectation in (3.14) can be solved using probability generating functional Laplace (PGFL)¹ defined for a homogeneous Poisson point process [63, Th 4.9].

$$\mathbb{E}_{\phi_{PPP}} \left[\prod_{x \in \phi_{PPP}} \exp \left(-\frac{sk'x^{2(m+1)}}{Z_o(h^2 + x^2)^{(m+3)}} \right) \right] = \exp \left[-\lambda_{MAC} \int_{-\infty}^{-R} \left(1 - \exp \left(-\frac{sk'x^{2(m+1)}}{Z_o(h^2 + x^2)^{(m+3)}} \right) \right) dx \right]. \quad (3.15)$$

$0 \leq \phi_k \leq \Psi_{FOV}$

The Eq. (3.15) can be determined numerically using standard software tools like MATLAB or MATHEMATICA.

Assuming free space path loss propagation model, the interference experienced at RSU for RF based V2V communication can be expressed as sum of RF power received from all the interferers as

$$I_{RF} = \sum_{x \in \Phi_{PPP}} P_{RF} G_t G_r \ell h_x (h^2 + x^2)^{-\frac{\alpha}{2}}, \quad (3.16)$$

¹The PGFL can be envisioned as an equivalent for point process of the characteristic function (CF) or moment generating function (that provide an alternative description of random variables). It enables to compute the Laplace transform (LT) of random variables of the form $F = \sum_{X_i \in \Psi_{PPP}} g(X_i)$. In mathematical form, LT of such function can be given as:

$$L(s) = \mathbb{E}[e^{-sF}] = \mathbb{E} \left[\exp \left(-s \sum_{X_i \in \Psi} g(X_i) \right) \right] = \mathbb{E} \left[\prod_{X_i \in \Psi} e^{-sg(X_i)} \right]$$

where $\ell = \frac{c^2}{(4\pi)^2 f_0^2}$. In above expression, P_{RF} , α , G_t and G_r are the transmission power for V-RF, the path loss exponent, the antenna gains for transmitter and receiver respectively [66]. In order to calculate outage probability $P_{out,RF}(\zeta)$, it is more convenient to express it as a function of probability of successful transmission, $P_s(\zeta)$, where $P_{out,RF}(\zeta)$ can be expressed as

$$P_{out,RF}(\zeta) = 1 - P_s(\zeta) \quad (3.17)$$

The probability of successful transmission, $P_s(\zeta)$ can be calculated as

$$\begin{aligned} P_s(\zeta) &= \mathbb{P}(SINR > \zeta), \\ &= \mathbb{P}\left(\frac{P_{RF}G_tG_r\ell h_x D^{-\alpha}}{I_H + I_V + \mathcal{N}_0} > \zeta\right), \\ &= \mathbb{E}_{I_H+I_V} \left[\mathbb{P}\left(h_x > \frac{\zeta}{P_{RF}G_tG_r\ell D^{-\alpha}}(I_H + I_V + \mathcal{N}_0)\right) \right], \\ &= \exp\left(-\frac{\zeta\mathcal{N}_0}{P_{RF}G_tG_r\ell D^{-\alpha}}\right) \mathbb{E}_{I_H+I_V} \left[\exp\left(-\frac{\zeta(I_H + I_V)}{P_{RF}G_tG_r\ell D^{-\alpha}}\right) \right], \\ &= \underbrace{\mathcal{L}_{I_H}\left(\frac{\zeta}{P_{RF}G_tG_r\ell D^{-\alpha}}\right)}_{1^{st}} \underbrace{\mathcal{L}_{I_V}\left(\frac{\zeta}{P_{RF}G_tG_r\ell D^{-\alpha}}\right)}_{2^{nd}} \underbrace{\exp\left(-\frac{\zeta\sigma^2}{P_{RF}G_tG_r\ell D^{-\alpha}}\right)}_{3^{rd}}. \end{aligned} \quad (3.18)$$

where $\mathcal{L}(\cdot)$, I_H and I_V denote the Laplace transform, the interference from H-road and V-road respectively. Kindly note that there are three factors in (3.18) which can be interpreted as follows: the first and second factor represent the reduction in probability of successful transmission taking into consideration the impact of interference from the interferers from H-road and V-road respectively; the third factor denotes the probability of successful transmission for interference-free scenario. For a one-dimensional PPP, the Laplace transform of the

aggregate interference originating from the interferers can be given as

$$\begin{aligned}
\mathcal{L}_{I_V}(s) &= \mathbb{E}[\exp(-sI_{RF})], \\
&= \mathbb{E} \left[\prod_{x \in \phi} \exp(-sP_{RF}G_tG_r\ell h_x(h^2 + x^2)^{-\frac{\alpha}{2}}) \right], \\
&\stackrel{(a)}{=} \mathbb{E}_x \left[\prod_{x \in \phi} \mathbb{E}_{h_x} \{ \exp(-sP_{RF}G_tG_r\ell h_x(h^2 + x^2)^{-\frac{\alpha}{2}}) \} \right], \\
&= \mathbb{E}_x \left[\prod_{x \in \phi} \frac{1}{1 + sP_{RF}G_tG_r\ell(h^2 + x^2)^{-\frac{\alpha}{2}}} \right], \\
&\stackrel{(b)}{=} \exp \left(-2\lambda_{MAC} \int_0^\infty \frac{1}{1 + (h^2 + x^2)^{\frac{\alpha}{2}}/sP_{RF}G_tG_r\ell} dx \right),
\end{aligned} \tag{3.19}$$

Here (a) holds due to independence of fading coefficients h_x , (b) uses the definition of PGFL for PPP.

Special Case: The step (b) can be further expressed in simplified form by setting the path loss exponent, $\alpha = 2$ as

$$\mathbb{E}[\exp(-sI_{RF})] = \exp \left(-\lambda_{MAC} \frac{\pi(sP_{RF}G_tG_r\ell)}{\sqrt{h^2 + sP_{RF}G_tG_r\ell}} \right), \tag{3.20}$$

Substituting $s = \frac{\zeta}{P_{RF}G_tG_r\ell D^{-\alpha}}$ yields the result as

$$\mathcal{L}_{I_V} \left(\frac{\zeta}{P_{RF}G_tG_r\ell D^{-\alpha}} \right) = \exp \left(-\lambda_{MAC} \frac{\pi\zeta D^\alpha}{\sqrt{h^2 + \zeta D^\alpha}} \right). \tag{3.21}$$

Corollary: When the height of RSU is very low, the step (b) can also be expressed in alternative form as:

$$\mathbb{E}[\exp(-sI_{RF})] = \exp \left(-2\lambda_{MAC}(sP_{RF}G_tG_r\ell)^{\frac{1}{\alpha}} \frac{\pi}{\alpha} \csc \left(\frac{\pi}{\alpha} \right) \right), \tag{3.22}$$

Substituting $s = \frac{\zeta}{P_{RF}G_tG_r\ell D^{-\alpha}}$ yields the result as

$$\mathcal{L}_{I_V} \left(\frac{\zeta}{P_{RF}G_tG_r\ell D^{-\alpha}} \right) = \exp \left(-2\lambda_{MAC}(\zeta)^{\frac{1}{\alpha}} D \frac{\pi}{\alpha} \csc \left(\frac{\pi}{\alpha} \right) \right). \tag{3.23}$$

$$\mathcal{L}_{IH} \left(s = \frac{\zeta}{P_{RF} G_t G_r \ell D^{-\alpha}} \right) = \exp \left(-\lambda_{MAC} \left[\int_{-\infty}^{-R} \frac{1}{1 + (h^2 + x^2)^{\frac{\alpha}{2}} / s \zeta D^\alpha} dx + \int_0^{\infty} \frac{1}{1 + (h^2 + x^2)^{\frac{\alpha}{2}} / s \zeta D^\alpha} dx \right] \right). \quad (3.24)$$

We now derive the expression for outage probability of a hard-switching based hybrid V-VLC/V-RF network. Hard switching based hybrid V-VLC/V-RF network considers only single link to be operational. For simple receiver implementation, it is assumed that only one of the links is active at a certain point. The outage probability of such hybrid network configuration can given as²

$$P_{out,hyb}(\beta, \zeta) \geq P_{out,VLC}(\beta) P_{out,RF}(\zeta). \quad (3.25)$$

3.3.2 Throughput

From a system design perspective, the outage probability can not be considered as sufficient metric to characterize the performance, since a MAC that allows few concurrent transmissions leads to high packet reception probabilities but low throughput as well. Hence, to suitably compare the impact of different MAC protocols, it is necessary to characterize the throughput for the intersection scenario for different network configuration. For the case with desired transmitter located at x_{tx} , the throughput for a specific network configuration with system bandwidth, B_s and SINR threshold, β can be expressed as[61]

$$\mathcal{T} = p_A(x_{tx})(1 - P_{out}) \log_2(1 + \beta) B_s. \quad (3.26)$$

where $p_A(x_{tx})$ denotes the access probability of a transmitter located at x_{tx} [61].

3.3.3 Data Oriented Characterization: DOR and IOR

Many safety/warning related messages are so critical that a large latency is intolerable especially during accident prone scenarios. DOR and IOR can be of strong interest to vehicular communication and can be used to compare the performances of standalone V-VLC and V-RF based on offering high reliability as well as low latency. Any vehicular transmission systems should be able to efficiently support the large amount of data traffics with tolerable latency. As such, we make use of a data-oriented metric, minimum transmission time (MTT) which is defined as the minimum time duration required to transmit a certain amount of data, H over a channel with bandwidth, B . Then, the DOR can be defined as the probability that MTT required

²Note that the equality holds when V-VLC and V-RF links are considered to be independent.

for transmitting a certain amount of data is greater than a predefined delay threshold duration [67]. Mathematically,

$$DOR^{MAC} = \mathbb{P}(MTT > T_{th}), \quad (3.27)$$

where T_{th} denotes the delay threshold duration and can be related to the delay requirement of the data to be transmitted. As a matter of fact, DOR may serve as an statistical measure for the quality of service experienced by individual data transmission for stringent delay requirement by a particular network. Irrespective of multiple access scheme, the DOR for small data transmission within a given coherence time can be defined as

$$DOR^{MAC} = \mathbb{P}(SINR < 2^{\frac{H}{BT_{th}}} - 1). \quad (3.28)$$

Apart from DOR analysis, the characterization of the amount of data that can be successfully transmitted over a specific spectral-temporal resource block also needs to be taken into account for any vehicular transmission system. We make use of another data oriented metric, maximum entropy throughput (MET) which is defined as the maximum amount of information that can be transmitted over a certain time duration, T and system channel bandwidth B . Then, the IOR can be defined as the probability that MET over a certain time duration is less than a threshold entropy value, represented by H_{th} [67]. Mathematically,

$$IOR^{MAC} = \mathbb{P}(SINR < 2^{\frac{H_{th}}{BT}} - 1). \quad (3.29)$$

3.4 Numerical Results and Discussion

In this section, we present numerical results that substantiate our theoretical findings. The system model parameters are adopted in accordance with practical vehicular scenario and listed in Table 3.1. Specifically, we show the potential benefit of standalone V-VLC/V-RF links or hybrid V-VLC/V-RF links. In order to validate the accuracy of our theoretical findings, Monte Carlo simulations are performed by averaging over 10,000 realizations of PPPs and fading channel parameters. We consider a worst case scenario where interference from interferers arise from infinite road segment ($\mathcal{B} = \mathbb{R}^1$).

Fig. 3.4 gives comparison of outage performance for standalone V-VLC links, V-RF links and hybrid V-VLC/V-RF links with slotted ALOHA protocol. We observe that when desired transmitter's location from RSU increases, the outage probability increases. Also, the outage performance of standalone V-VLC links is comparatively better than standalone V-RF for low communication range. For instance, when access probability, $\rho=0.01$, the outage performance of standalone V-VLC links is better compared to V-RF links when desired transmitter's location

Table 3.1: V-VLC and V-RF system parameters

Parameter	Symbol	Value
Lambertian Order	m	1
PD active detection area	A_d	1 cm^2
Half angle of PD's field of view (FOV)	Ψ_{FOV}	60°
LED semi-angle	$\Phi_{\frac{1}{2}}$	70°
Transmission power for V-VLC	P_{VLC}	36.5 dBm [68]
Transmission power for V-RF	P_{RF}	23 dBm[69]
Noise PSD in VLC	σ^2	10^{-22} W/Hz
Noise PSD in RF	\mathcal{N}_0	-174 dBm/Hz
RF path loss exponent	α	4
Absolute temperature	T_k	298° K
System Bandwidth	B_s	20 MHz
Optical filter gain	$T_s(\Psi_k)$	1
Carrier frequency for V-RF	f_c	5.9 GHz
Refractive index	n	1.5
Height of LED traffic light	h	8 m
Access Probability	ρ	0.01-0.9
Traffic Intensity	λ_R	0.01
Carrier frequency for V-VLC	f_c	450 THz

is upto 80 m. However, standalone V-RF is reliable option for long distance communication. It can also be noted that there exists limitation of standalone V-VLC over V-RF when distance between the desired vehicle and RSU is less than 5 m which comes at the cost of restricted receiver's FOV. We consider the lower bound of Eq. 3.25 for plotting simulation results for outage probability associated with hybrid V-VLC/V-RF network configuration. It is worth mentioning here that irrespective of distance between the desired vehicle and RSU, a hybrid V-VLC/V-RF links outperforms standalone V-VLC or V-RF link as expected. Let us recall that hybrid outage is a joint event of V-VLC and V-RF links wherein the outage probability of hybrid V-VLC/V-RF will be less than the outage probability associated with either standalone V-VLC or V-RF links. However, this comes at the expense of extra resources required during practical implementation of a hybrid V-VLC/V-RF links.

We further study the performance gain achieved in proposed scenario by using CSMA over slotted ALOHA. We set CSMA contention radius, $\delta=10$ m. Fig. 3.5 illustrates that for access probability, $\rho=0.01$, the outage performance of standalone V-VLC links is better compared to V-RF links when desired transmitter's location, $R < 120$ m. However, standalone V-RF is reliable option when desired transmitter's location, $R > 120$ m. As before, hybrid V-VLC/V-RF links outperforms standalone V-VLC and V-RF links. Interestingly, a low access

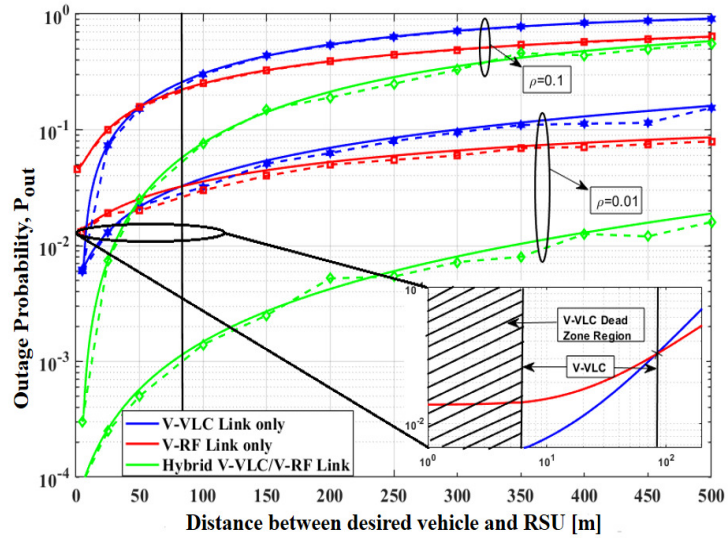


Figure 3.4: Comparison of analytical (solid line) and simulation (dashed line) results for outage probability, P_{out} versus distance for V-VLC links only (blue), V-RF links only (red) and hybrid V-VLC/V-RF Links (green) with slotted ALOHA protocol.

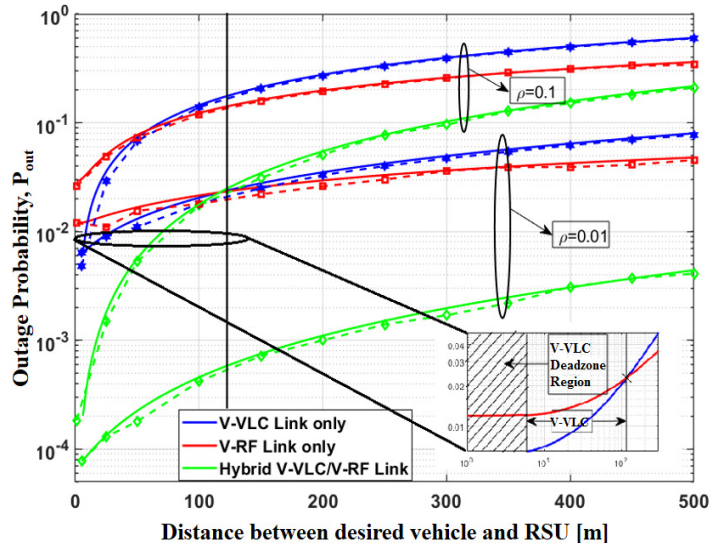


Figure 3.5: Comparison of analytical (solid line) and simulation (dashed line) results for outage probability, P_{out} versus distance for V-VLC link only (blue), V-RF link only (red) and hybrid V-VLC/V-RF link (green) with CSMA CA protocol.

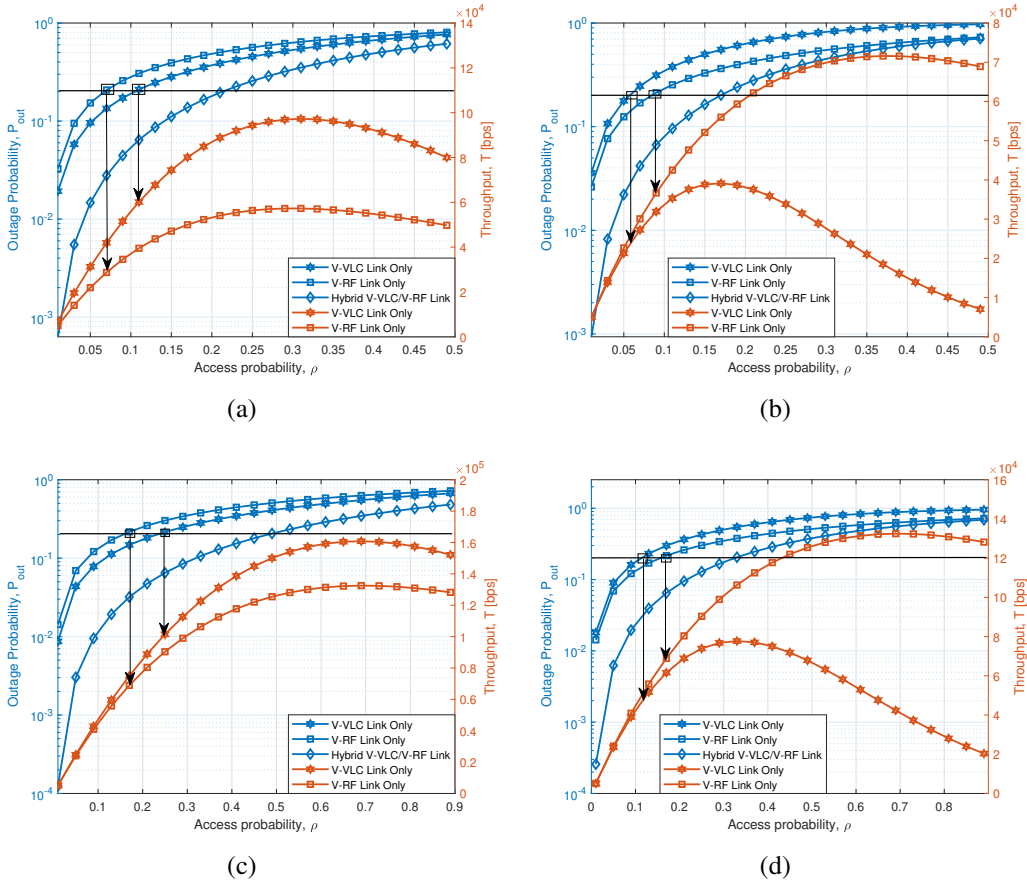


Figure 3.6: Outage probability, P_{out} and throughput, T as a function of access probability, ρ for standalone V-VLC link, V-RF link and hybrid V-VLC/VRF link for two different distance between the desired vehicle and RSU, R . (a) ALOHA case, $R=50$ m; (b) ALOHA case, $R=150$ m; (c) CSMA case, $R=50$ m; and, (d) CSMA case, $R=150$ m.

probability reduces the outage probability. For ease of validation and visualization, we plot outage probability, P_{out} as a function of access probability, ρ as can be seen in Fig. 3.6.

We observe from Fig. 3.6a that for ALOHA case, with an increase in access probability, ρ outage probability increases due to the availability of more interferers. Also, the throughput first increases (due to more active transmitters) with increase in access probability and then decreases (due to extensive amount of interference), leading to an optimal value of access probability, ρ . Nevertheless, in order to ensure a certain quality of service, one must also consider a guarantee on the outage performance as well. With an outage probability below 20% when distance between the desired vehicle and RSU, $R = 50$ m, the optimal value of access probability for standalone V-VLC link, $\rho=0.12$, results in a throughput of about 60 Kbps as can be seen in Fig. 3.6a. In addition, the outage performance of standalone V-VLC is better than standalone V-RF. However, increasing the distance, R , the opposite trend can be observed

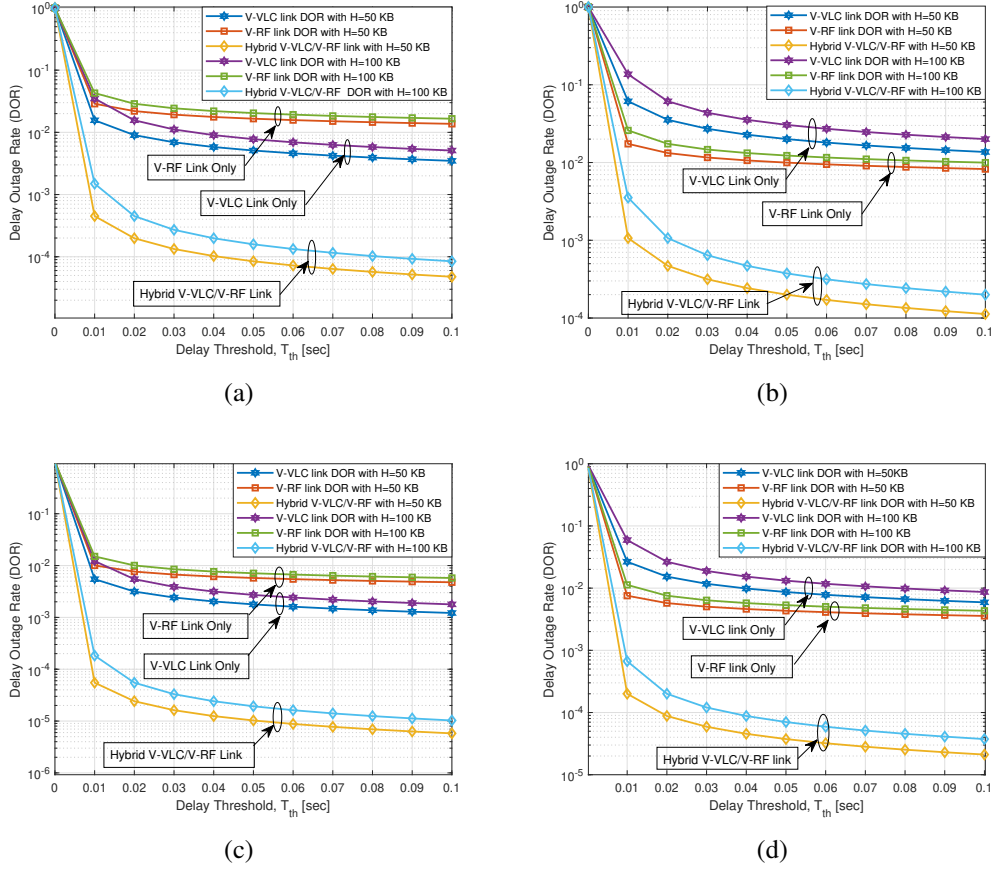


Figure 3.7: Delay outage performance of V-VLC Link only, V-RF Link only and hybrid V-VLC/V-RF Link for CSMA case for two different distance between the desired vehicle and RSU. Here, access probability, ρ is 0.01.: (a) ALOHA case, $R = 50m$; (b) ALOHA case, $R = 150m$; (c) CSMA case, $R = 50m$; and, (d) CSMA case, $R = 150m$

in Fig. 3.6b. As expected, hybrid V-VLC/V-RF outperforms standalone V-VLC or V-RF in terms of outage performance. Kindly note that the throughput of hybrid V-VLC/V-RF system depends on maximum throughput offered by either standalone V-VLC or standalone V-RF system.

For CSMA (Fig. 3.6c), large contention region (i.e., low access probability) reduces the outage probability. Analogous to ALOHA, the throughput first increases with increase in access probability, ρ and then decreases. To ensure an outage probability below 20% when distance between the desired vehicle and RSU, $R = 50$ m, the optimal value of access probability for standalone V-VLC link, $\rho=0.25$, results in a throughput of about 100 Kbps. Hence, in this scenario, the use of CSMA instead of ALOHA leads to more increase in the throughput for the same transmitter location. It can be inferred from above comparison that implementation of hybrid V-VLC/V-RF link leads to considerable improvement in throughput and outage

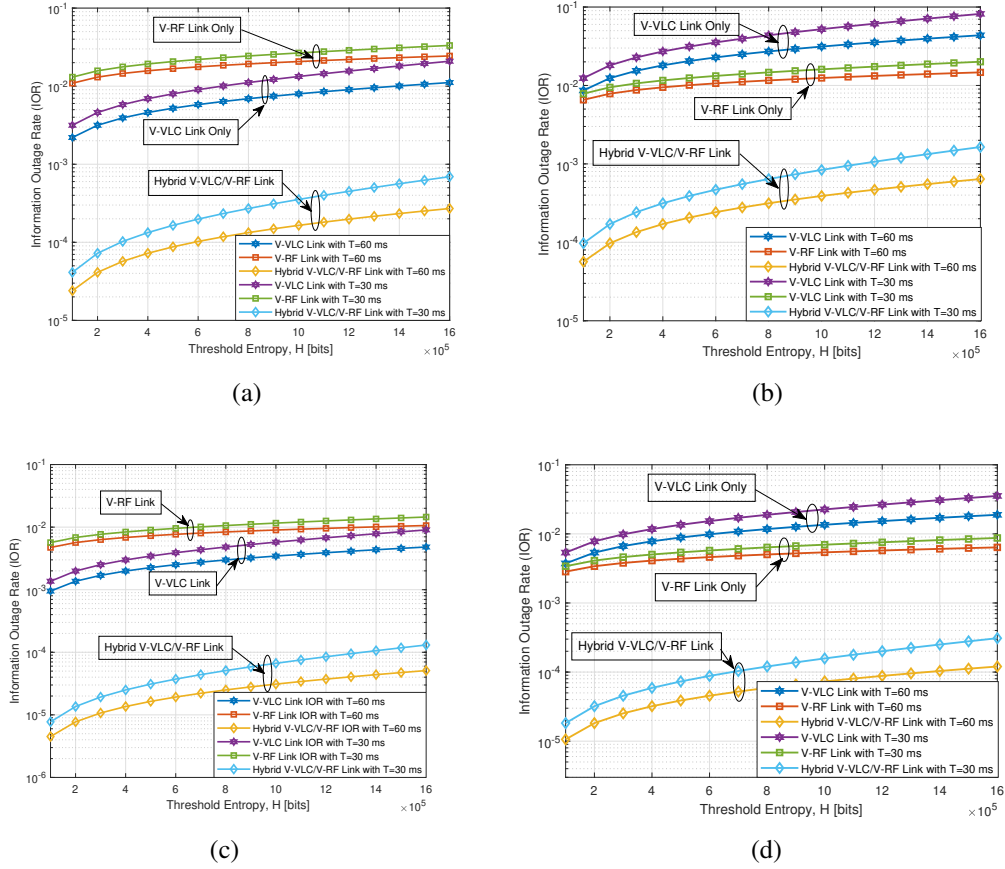


Figure 3.8: Information Outage Rate of V-VLC Link only, V-RF Link only and hybrid V-VLC/V-RF Link for ALOHA case for two different distance between the desired vehicle and RSU. Here, access probability, ρ is 0.01: (a) ALOHA case, $R = 50m$; (b) ALOHA case, $R = 150m$; (c) CSMA case, $R = 50m$; and, (d) CSMA case, $R = 150m$.

probability improvement, compared to scenarios utilizing either V-VLC link or V-RF link separately.

Fig. 3.7a compares DOR performance comparison for standalone V-VLC link, V-RF link and hybrid V-VLC/V-RF link with ALOHA protocol. In particular, we plot DOR of both strategies as function of the delay threshold, T_{th} for different data amount $H \in \{50 \text{ KB}, 100 \text{ KB}\}$. We can observe that for both the choices of H , there exists complementary behaviour in DOR performance of standalone V-VLC and V-RF network depending on distance between the desired vehicle and RSU, R . Specifically, with access probability, $\rho = 0.01$ and transmitter's location, $R=50 \text{ m}$, DOR performance of standalone V-VLC is comparatively better than V-RF as can be seen from Fig. 3.7a. The opposite is true when R is 150 m as shown in Fig. 3.7b. As before, we observe DOR performance improvement by employing CSMA for both standalone V-VLC as well as V-RF network as depicted in Fig. 3.7c and Fig. 3.7d. The reason is as follows:

DOR typically depends on SINR which is better for proposed scenario with CSMA/CA (due to low interference). It is interesting to note that for data traffic with stringent delay requirement, hybrid V-VLC/V-RF ensures minimum delay in transmitting given amount of information between the desired vehicle and RSU as compared to standalone V-VLC or V-RF network.

We now compare the IOR performance of standalone V-VLC, V-RF and hybrid V-VLC/V-RF network configuration for two different values on transmitter's location, $R \in \{50 \text{ m}, 150 \text{ m}\}$. In Fig. 3.8, we plot IOR for all network configuration with ALOHA and CSMA as a function of threshold entropy, H_{th} for two different time duration, $T \in \{60 \text{ ms}, 30 \text{ ms}\}$. In particular, Fig. 3.8a shows that for a given IOR performance with slotted ALOHA, standalone V-VLC Link is reliable option over standalone V-RF link when distance between the desired vehicle and RSU, R is 50 m. However, the complementary insights stands true when D is 150 m as evident from Fig 3.8b.

In Fig. 3.8c, we again observe the improvement in IOR performance of all the network configuration by using CSMA over ALOHA. The reason is as follows: IOR typically depends on SINR which is better for proposed scenario with CSMA/CA (due to low interference). Again, the performance of standalone V-VLC or V-RF link depends on distance between legitimate vehicle and RSU, R as evident from Figs 3.8c and 3.8d. It is worth mentioning that irrespective of distance, R , hybrid V-VLC/V-RF system always guarantees maximum amount of information flow between the desired vehicle and RSU as compared to standalone V-VLC or V-RF network in the given time duration.

3.5 Concluding remarks

In this work, we have shown the potential benefit of employing hybrid V-VLC/V-RF over standalone V-VLC or V-RF network configuration for BSMs dissemination at road intersection ensuring high reliability and low latency. Depending on transmitter's location, it is found that the standalone V-VLC and V-RF exhibit complementary roles in terms of outage probability, throughput, DOR and IOR. The presented framework also show the limitation of standalone V-VLC over V-RF communication when the distance between desired vehicle and RSU is less than the critical distance defined for V-VLC system. We have also found that hybrid V-VLC/V-RF outperforms standalone V-VLC or V-RF network, thus serving as a better alternative option to meet diverse application needs for future intelligent transportation system. It is expected that this comparative analysis may stimulate more innovations for hybrid VLC/RF based vehicular networks.

Part II

3.6 Overview of Part II

Traffic safety at road intersections can be enhanced by improving opportunistic exchange of safety messages between vehicles. In urban intersection scenario, obstacles such as buildings and road side installations/signboards block the line-of-sight communication between vehicles. In order to enhance the reliability of communication link, the existing vehicular solution utilizes relay placement at road intersection. However, as the vehicular density increases, the existing vehicular-radio frequency (V-RF) communication with relaying tends to suffer from higher interference, lower packet reception rate, and longer communication delays due to channel congestion. In contrast to the existing solutions, we propose to use practical deployment strategies namely hybrid vehicular-visible light communication (V-VLC)/V-RF with relaying and reconfigurable intelligent surface (RIS) aided V-RF solutions to improve the communication range for urban vehicle-to-vehicle (V2V) communication. We present stochastic geometry based analytical framework to analyze the performance of proposed solutions in terms of outage probability, throughput and delay outage rate (DOR).

3.6.1 Motivation and Contributions

Traffic safety at road intersections can be enhanced by improving opportunistic exchange of BSMs/CAMs between vehicles. There are two major causes of packet loss in vehicular communication (VC) namely: (a) *Obstruction*: As direct LOS link is blocked by obstruction such as building/obstacles, diffuse and specular scatterings may enable non-line-of-sight (NLOS) reception, however resulting in low SNR at receiver. As a consequence, inducing heavy packet drop due to the poor received signal strength at receiver. (b) *Interference/Packet collision*: The PRP at road side unit (RSU) may be heavily impacted due to interference caused from concurrent transmission from other source vehicles. Further, the hidden node problem arises due to building/obstruction at intersection scenario, where some vehicles are completely unaware about the ongoing transmission and assume the channel in idle state. This induces multiple transmissions to occur at the same time, which result in lower PRP at the receiver.

To overcome lower PRP issues at intersection, we propose to use hybrid V-VLC/V-RF with relaying and V-RF with RIS for vehicular communication system. More specifically, the novelty and major contributions of our research work are summarized below:

- We propose two different solutions namely, relayed transmission (RT) based hybrid V-VLC/V-RF and RIS assisted V-RF for establishing reliable communication between

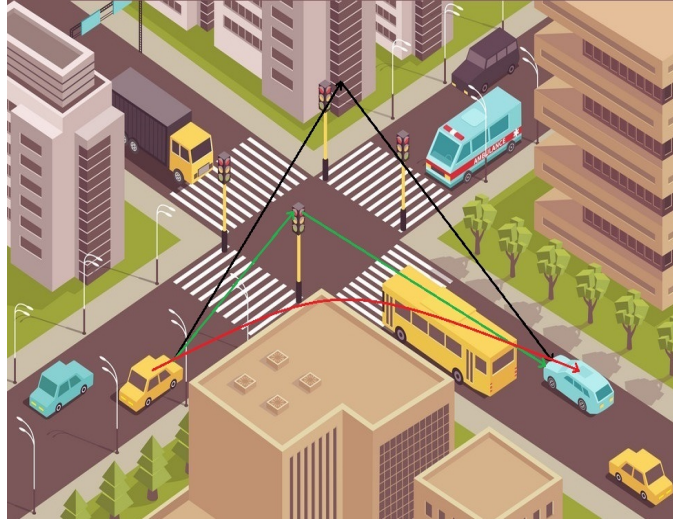


Figure 3.9: Illustration of road intersection scenario where vehicles in blocked line-of-sight (solid red line) can communicate via Hybrid V-VLC/V-RF with relaying (solid green line) and V-RF with RIS (solid black line).

vehicles at road intersection. For an interference limited scenario, we carry out comprehensive qualitative and quantitative performance comparison of our proposed solutions with classic decode and forward relaying based V-RF communication by utilizing stochastic geometry tools.

- We show the impact of various design parameters such as access probability, delay threshold which play critical role in deciding the performance of proposed V2X solutions. Moreover, depending on distance between the vehicular nodes and number of IRS elements used, we illustrate to show trade-offs between these two proposed V2X solutions.
- We also investigate the impact of latency in terms of data oriented performance limit known as delay outage rate (DOR) for the proposed V2X solutions. For delay sensitive application, a large latency is intolerable for many safety/warning related messages. DOR serves as an statistical measure for the effective design of ultra-reliable low latency communication (URLLC) transmission schemes.

Numerical results reveal that the proposed V2X deployment strategies can achieve considerable performance improvement in terms of outage, throughput while achieving low latency as compared to traditional V-RF based V2X network.

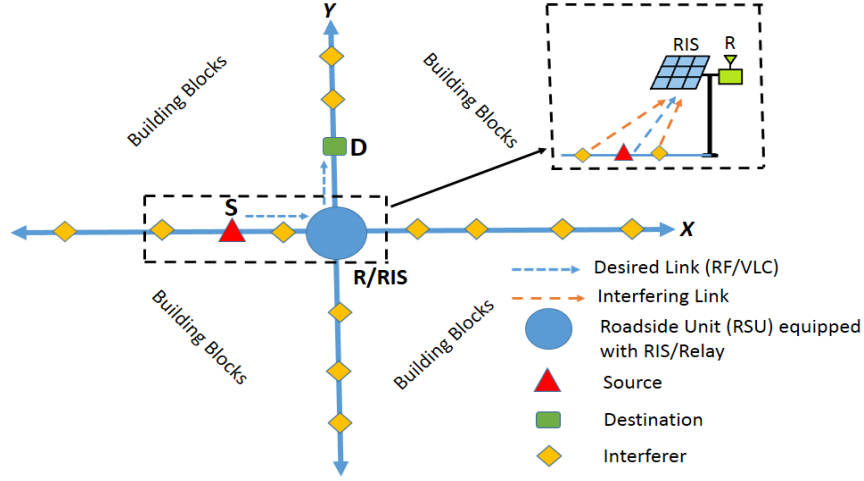


Figure 3.10: Abstraction system model for vehicular communications involving a source S , relay R /RIS and a destination D in presence of one dimensional Poisson field of interference.

3.7 Network model and preliminaries

3.7.1 Scenario Description

A typical road intersection scenario has been depicted in Fig.3.9. We investigate the transfer of safety messages between single source and destination node via relay/RIS in the presence of interference. The primary cause of interference are concurrent transmission caused from same lane or perpendicular lane road side vehicles³. It is assumed that the direct link from a vehicular node to the desired receiver is blocked by obstacles, such as buildings [72], which is indeed a realistic assumption especially when high frequency bands are considered (eg., mmWave based V2X communication). Fig. 3.10 portrays a simplified abstraction of the proposed intersection scenario. For relaying case, we consider a half-duplex transmission wherein transmission occurs during two phases. The duration of each phase is one time-slot. In the first phase, the source transmits the message to the relay ($S \rightarrow R$). While, in second phase, relay broadcast message to destination ($R \rightarrow D$). The transmission is subject to interference originating from a set of interfering vehicles that are located on roads. We assume that the set of interfering vehicles on axis X (Fig. 3.10), denoted by Φ_X with traffic intensity, λ_X (respectively on axis Y , denoted by Φ_Y with traffic intensity, λ_Y) are distributed as per one-dimensional homogeneous Poisson point process (1D-HPPP). The amount of interference experienced by the receiver depends on the selection of medium access control (MAC) protocol. For a carrier sense multiple access with collision avoidance (CSMA/CA) MAC protocol, a vehicle is allowed to

³A similar traffic scenario has been reported in [61, 62, 70, 71], however this work also considers relay/RIS placement at the road intersection centre.

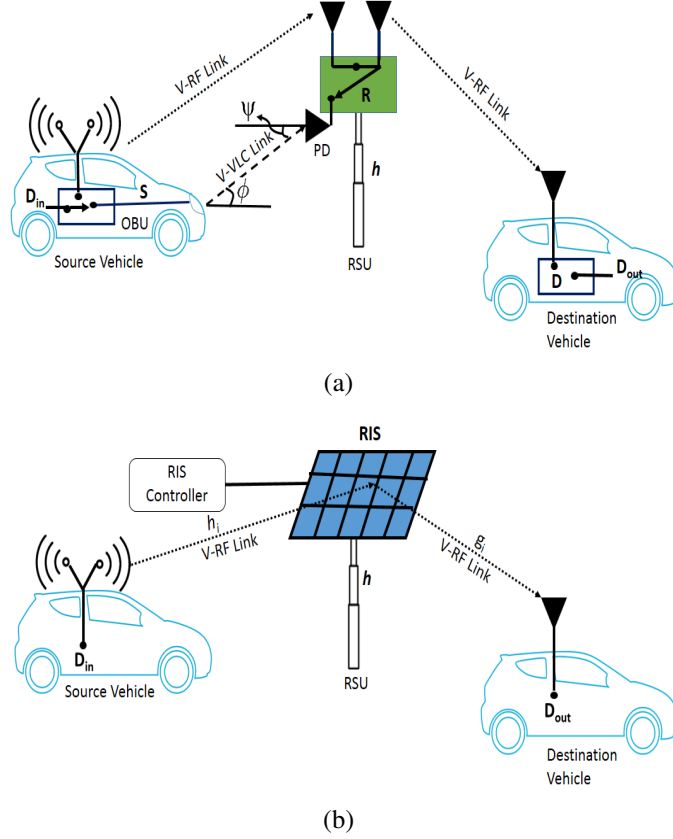


Figure 3.11: Illustration of proposed V2X deployment strategies: (a) Hybrid V-VLC/V-RF scheme and (b) V-RF with RIS scheme.

transmit only if it has the lowest random timer within its contention region (sensing range), δ . This implies that (i) the traffic intensity depends on transmitter's location as other transmitting vehicles (interferers) in its contention region are forced to keep silent when the desired vehicle is active; (ii) the interference from the X- and Y-roads is not independent. When the desired vehicle is active and transmitting at a distance, x_{tx} from RSU, the resulting intensity of the PPPs used to approximate the PP of interferers can be expressed as[61]

$$\lambda_{MAC}^X(x) = \begin{cases} p_A(x)\lambda_X & \text{if } \|x - x_{tx}\| > \delta \\ 0; & \text{otherwise,} \end{cases} \quad (3.30)$$

$$\lambda_{MAC}^Y(y) = \begin{cases} p_A(y)\lambda_Y & \text{if } \|y\| > \sqrt{\delta^2 - x_{tx}^2}, \\ 0; & \text{if } \|y\| \leq \sqrt{\delta^2 - x_{tx}^2}, \end{cases} \quad (3.31)$$

In (3.30) and (3.31), $p_A(x)$ and $p_A(y)$ denotes the access probability of interfering vehicle from X-road and Y-road respectively. The access probability is defined as the probability that the given node has the smallest random timer in the corresponding contention region [61]. For CSMA MAC protocol, access probability is governed by [61, Eq.(12)]. Further, we consider low speed vehicular (LSV) mobility model⁴ where it is assumed that interferer vehicles remain static during consecutive time slots of the transmission [62]. The theoretical framework is unified to capture the performance of desired vehicles for various deployment strategies namely: (i) *Conventional V-RF with relaying*: In order to enhance the reliability of communication links between vehicles which are not in LOS at road intersection, a road side unit (RSU) is employed at the intersection-center to relay the BSMs. In this case, we employ a decode-and-forward (DF) transmission scheme, i.e., the node R decodes and re-encodes the message then forwards it. Here, both source-to-relay and relay-to-destination are assumed to be an RF link. The improved communication performance by such configuration has been briefly discussed in [73, 74]. For sake of analysis, we consider communication from a single-antenna source to a single antenna destination with an aid of classic decode and forward relaying. Although relaying is not a part of conventional standardized V2X, however the relaying solutions are proposed in literature for improving performance of conventional V-RF communication near road intersection[73].

(ii) *Hybrid V-VLC/V-RF with relaying*: We assume that vehicles are equipped with both VLC and IEEE 802.11p transceivers. As shown in Fig.3.11a, SR link can be either V-VLC link or V-RF link, while relay-to-destination is an RF link. It is assumed that information is transmitted with hard-switching either V-VLC or V-RF link depending on the predefined quality of service (QoS) requirements (eg., desired SINR), i.e., only one of the links is allowed to operate at a given time instant. When SINR of V-VLC link remains above a certain threshold, the system keeps working on V-VLC. As soon as the quality of V-VLC link degrades below the predefined threshold (i.e. usually when distance of source from intersection is large), V-RF link is then activated. The SR link goes into outage when both V-VLC and V-RF link are in outage. For simplicity, it is assumed that at least one link (usually V-VLC as primary link) always remains active at a certain time and the system does not interrupt the hybrid V-VLC/V-RF link. This reduces power consumption and makes receiver design less complex with easier decoding as in [75, 76]. Further, the end-to-end system performance improves due to high SINR gain achieved by usage of V-VLC link from source-to-relay which has been later validated through simulation results.

(iii) *V-RF with RIS*: Fig.3.11b shows V-RF with RIS where an RIS composed of N reflecting elements is deployed to assist in the communication from source vehicle. The RIS reflecting

⁴This is a realistic assumption, especially at road intersections and urban scenarios where the vehicles tend to drive slowly across the junctions, intersections etc.

elements are programmable via a RIS controller. The source vehicle, S transmits a signal to RIS over an RF link. Then, the RIS reflects the signal by using appropriate phase shifts to D . For sake of analysis, we consider a $2L$ -path loss model for electrically small RIS [77, 78]. For the system considered, we assume that the CSI of all channels are known at the RIS controller such that the RIS-induced phases can be adjusted by fine tuning of RIS reflecting elements to maximize the received SNR through appropriate phase cancellations and proper alignment of reflected signals from the intelligent surface [45, 79]. Further, it is also assumed that the multipath fading induced inter symbol interference (ISI) can also be eliminated by optimizing the phase shifts at the RIS. In [80], the authors propose to use an RIS as a spatial equalizer to address the well-known multi-path fading phenomenon.

3.8 Performance Evaluation

The outage probability is defined as the probability that the instantaneous SINR falls below than a certain SINR threshold. For a system employing DF protocol, the outage probability is given as[81]

$$\mathcal{P}_{out}^{DF} = 1 - (1 - \mathcal{P}_{out,SR})(1 - \mathcal{P}_{out,RD}), \quad (3.32)$$

where $\mathcal{P}_{out,SR}$ and $\mathcal{P}_{out,RD}$ denote the outage probability associated with SR and RD link respectively.

3.8.1 Outage Probability for V-RF with relaying

We consider a vehicular network with interferers distributed according to a PPP, Φ_{PPP} with a locally finite and diffuse intensity, λ . All interferers transmit with same transmission power, P_{RF} . Let $\Phi_i \subseteq \Phi$ denote the set of interferers that are active in slot i . The interference experienced at R and D for V-RF communication are modeled by[61]

$$\begin{aligned} I_R &= \underbrace{\sum_{x \in \Phi_i} P_{RF} |h_{Rx}|^2 \ell_{Rx}}_{I_{Rx}} + \underbrace{\sum_{y \in \Phi_i} P_{RF} |h_{Ry}|^2 \ell_{Ry}}_{I_{Ry}}, \\ I_D &= \sum_{y \in \Phi_i} P_{RF} |h_{Dy}|^2 \ell_{Dy}, \end{aligned} \quad (3.33)$$

where $\ell_{ab} = A_0 \|a - b\|_2^{-\alpha}$ denotes the euclidean path loss function, $\alpha > 0$ is the the path loss index, $\|\cdot\|_2$ is the ℓ_2 norm and A_0 denotes a constant that depends on several factors such as antenna characteristics, propagation environment and carrier frequency[61]. In order to calculate outage probability $P_{out,RF}(\zeta)$ associated with direct DSRC V2I link, it is more convenient

to express it as a function of probability of successful transmission, $P_s(\zeta)$. Mathematically,

$$\mathcal{P}_{out,RF}(\zeta) = 1 - \mathcal{P}_s(\zeta) \quad (3.34)$$

The probability of successful transmission, $P_{s,SR}(\zeta)$ at relay R can be calculated as

$$\begin{aligned} \mathcal{P}_{s,SR}(\zeta) &= \mathbb{P}(SINR > \zeta), \\ &= \mathbb{P}\left(\frac{P_{RF}|h_{SR}|^2\ell_{SR}}{I_R + \sigma^2} > \zeta\right), \\ &= \mathbb{E}_{I_R}\left[\mathbb{P}\left(|h_{SR}|^2 > \frac{\zeta}{P_{RF}\ell_{SR}}(I_R + \sigma^2)\right)\right], \\ &\stackrel{(a)}{=} \exp\left(-\frac{\zeta\sigma^2}{P_{RF}\ell_{SR}}\right)\mathbb{E}_{I_R}\left[\exp\left(-\frac{\zeta I_R}{P_{RF}\ell_{SR}}\right)\right], \\ &\stackrel{(b)}{=} \exp\left(-\frac{\zeta\sigma^2}{P_{RF}\ell_{SR}}\right)\mathcal{L}_{I_R}\left(\frac{\zeta}{P_{RF}\ell_{SR}}\right) \end{aligned} \quad (3.35)$$

where ζ is SINR threshold, σ^2 is noise variance at R , and \mathcal{L}_{I_R} denotes the Laplace transform of the interference from X -road and Y -road at R . In (3.35), Step (a) follows from fact that the channel fading gain, $|h|^2 \sim \exp(1)$ due to Rayleigh fading, and Step (b) results from definition of Laplace transform. Similarly, the probability of successful transmission, $P_{s,RD}(\zeta)$ at destination D can be given as

$$\mathcal{P}_{s,RD}(\zeta) = \exp\left(-\frac{\zeta\sigma^2}{P_{RF}\ell_{RD}}\right)\mathcal{L}_{I_D}\left(\frac{\zeta}{P_{RF}\ell_{RD}}\right). \quad (3.36)$$

where \mathcal{L}_{I_D} denotes the Laplace transform of the interference from same lane vehicles at D . The expression for Laplace transform of interference at relay R and destination D can be expressed as

$$\mathcal{L}_{I_R}(s) = \exp\left(-\int_{-\infty}^{\infty} \frac{\lambda_{MAC}^X(x)}{1 + (h^2 + x^2)^{\frac{\alpha}{2}}/sP_{RFA_0}} dx\right) \exp\left(-\int_{-\infty}^{\infty} \frac{\lambda_{MAC}^Y(y)}{1 + (h^2 + y^2)^{\frac{\alpha}{2}}/sP_{RFA_0}} dy\right), \quad (3.37)$$

$$\mathcal{L}_{I_D}(s) = \exp\left(-\int_{-\infty}^{\infty} \frac{\lambda_{MAC}^Y(y)}{1 + ||y||^{\alpha}/sP_{RFA_0}} dy\right). \quad (3.38)$$

Proof: Note that for a general transmitter location x_{ix} , we are not able to evaluate the integrals in (3.37) and (3.38) in closed form, consequently it will be evaluated numerically. However, for sake of mathematical tractability, the closed form expressions have also been

provided for high traffic density scenario assuming ALOHA protocol⁵ where each interfering vehicle access the channel in each time slot independently with probability, ρ [61].

The Laplace transform (LT) of interference at relay R can be expressed as

$$\begin{aligned}\mathcal{L}_{I_R}(s) &= \mathbb{E}[\exp(-sI_{Rx}) \exp(-sI_{Ry})], \\ &= \underbrace{\mathbb{E}\left[\prod_x \exp(-sP_{RF}|h_{Rx}|^2 \ell_{Rx})\right]}_{\mathcal{L}_{Rx}(s)} \underbrace{\mathbb{E}\left[\prod_y \exp(-sP_{RF}\ell_{Ry})\right]}_{\mathcal{L}_{Ry}(s)},\end{aligned}\quad (3.39)$$

where $\mathcal{L}_{Rx}(\cdot)$ and $\mathcal{L}_{Ry}(\cdot)$ denote the interference from X and Y road at relay R respectively. The LT of interference from X-road at relay R can be calculated as

$$\begin{aligned}\mathcal{L}_{Rx}(s) &\stackrel{(a)}{=} \mathbb{E}\left[\prod_x \mathbb{E}_{|h_{Rx}|^2} \left\{ \exp(-sP_{RF}|h_{Rx}|^2 A_0 (h^2 + x^2)^{-\frac{\alpha}{2}}) \right\}\right], \\ &= \mathbb{E}\left[\prod_x \frac{1}{1 + sP_{RF}A_0 (h^2 + x^2)^{-\frac{\alpha}{2}}}\right], \\ &\stackrel{(b)}{=} \exp\left(-\int_{-\infty}^{\infty} \frac{\lambda_{MAC}^X(x)}{1 + (h^2 + x^2)^{\frac{\alpha}{2}}/sP_{RF}A_0} dx\right),\end{aligned}\quad (3.40)$$

In above, (a) holds due to independence of fading coefficients $|h_{Rx}|^2$, (b) uses the definition of PGFL for PPP. For slotted ALOHA case, the integral can be expressed in closed form, hence we can obtain closed form expression for LT of the interference. In this case, we can calculate the integral for $\mathcal{B} = \mathbb{R}^1$, $\lambda_X = \lambda_Y = \lambda$ and $\alpha = 2$ in simplified form as

$$\mathcal{L}_{Rx}(s) = \exp\left(-\rho\lambda \frac{\pi s P_{RF} A_0}{\sqrt{h^2 + s A_0 P_{RF}}}\right).\quad (3.41)$$

Following same steps as above, we can obtain the similar expression for \mathcal{L}_{Ry} as well. Following [84, Eq. (13)], we can also express \mathcal{L}_{I_D} in closed form. Now, substituting $s = \frac{\zeta}{P_{RF}\ell_{SR}}$ and $\ell_{SR} = A_0(h^2 + d_{SR}^2)^{-\frac{\alpha}{2}}$ yields the following result

$$\begin{aligned}\mathcal{L}_{I_R}\left(\frac{\zeta}{P_{RF}\ell_{SR}}\right) &= \exp\left(-2\rho\lambda \frac{\pi\zeta(h^2 + d_{SR}^2)}{\sqrt{h^2 + \zeta(h^2 + d_{SR}^2)}}\right), \\ \mathcal{L}_{I_D}\left(\frac{\zeta}{P_{RF}\ell_{RD}}\right) &= \exp\left(-\rho\lambda\pi\sqrt{\zeta}\sqrt{h^2 + d_{RD}^2}\right).\end{aligned}\quad (3.42)$$

⁵Note that the closed form Laplace transform expressions considering CSMA CA protocols are hard to obtain. In addition, [82, 83] showed that the CSMA CA performance tends to the ALOHA performance in dense networks.

where h , d_{SR} and d_{RD} denote the height of RSU, the horizontal distance of source and destination from RSU respectively.

3.8.2 Outage Probability for hybrid VLC-RF with relaying

In this subsection, we characterize the performance of the hybrid V-VLC/V-RF communication system in the presence of the aggregate interference and noise variance, N_0 in terms of outage probability. Firstly, we calculate the outage probability associated with V-VLC link using moment generating functional (MGF) based unified framework.

$$\begin{aligned} P_{out,VLC}(\zeta) &= \mathbb{P}(SINR < \zeta), \\ &= \mathbb{P}\left(\frac{\mathcal{S}}{\mathcal{I}_{VLC} + N_0} < \zeta\right). \end{aligned} \quad (3.43)$$

The desired electrical signal power S from source vehicle and interference \mathcal{I}_{VLC} is given as

$$\begin{aligned} S &= \mathcal{R}^2 Z_o P_{VLC}, \\ \mathcal{I}_{VLC} &= \sum_{x_k \in \Phi_{PPP}} \mathcal{R}^2 Z_k^{VLC} P_{VLC}. \end{aligned} \quad (3.44)$$

In above, Z_o and \mathcal{R} denote the channel power gain associated with source vehicle, and the responsivity of PD respectively. The electrical SINR can be represented as:

$$SINR = \frac{1}{\frac{\mathcal{I}_{VLC}}{\mathcal{R}^2 Z_o P_{VLC}} + \frac{1}{\beta_0}}, \quad (3.45)$$

where $\beta_0 = \frac{\mathcal{R}^2 Z_o P_{VLC}}{N_0}$. From [3.45], the outage probability for V-VLC assuming that desired vehicle is transmitting can be given as:

$$P_{out,VLC}(\zeta) = \mathbb{P}\left(\frac{\mathcal{I}_{VLC}}{\mathcal{R}^2 Z_o P_{VLC}} + \frac{1}{\beta_0} > \frac{1}{\zeta}\right). \quad (3.46)$$

We define random variable W as

$$W = \frac{\mathcal{I}_{VLC}}{\mathcal{R}^2 Z_o P_{VLC}} + \frac{1}{\beta_0}, \quad (3.47)$$

Using above, Eq. (3.47) can be rewritten as

$$P_{out,VLC}(\zeta) = \mathbb{P}(W > \zeta^{-1}) = 1 - \mathcal{F}_W(\zeta^{-1}). \quad (3.48)$$

In above, a tractable solution for CDF, $\mathcal{F}_W(\zeta^{-1})$ is quite challenging to obtain. Thus, we perform numerical inversion of Laplace transform. The relationship between CDF of a rv W and the Laplace transform of $\mathcal{F}_W(w)$ is given as

$$\mathcal{F}_W(w) = \frac{1}{2\pi j} \int_{c-j\infty}^{c+j\infty} L_{\mathcal{F}_W(w)} \exp(sw) ds. \quad (3.49)$$

where $j \triangleq \sqrt{-1}$. The discretization of integral in (3.49) can be realized to get a series using the trapezoid rule and then the infinite series can be truncated to get a finite sum using the Euler summation [64]. Also, $\mathcal{L}_{\mathcal{F}_W(w)}(s) = \frac{\mathcal{L}_W(s)}{s}$. Thus, we apply the MGF based numerical technique developed in [65] and after some algebraic manipulation, (17) can be approximated as [85, 86]

$$P_{out,VLC} \approx 1 - \frac{2^{-Q} e^{\frac{A}{2}}}{\zeta^{-1}} \sum_{q=0}^Q \binom{Q}{q} \sum_{n=0}^{N+q} \frac{(-1)^n}{D_n} \text{Re} \left\{ \frac{L_W(s)}{s} \right\}. \quad (3.50)$$

where $D_0=2$ and $D_n=1$ ($n=1, 2, 3, \dots, N+Q$) and $s = \frac{A+2\pi ni}{2\zeta^{-1}}$. The triplet (A, Q, N) are the positive integers for the accuracy control of the estimation, where $(8\ln 10, 11, 14)$ is a typical parameters choice that achieves stable numerical inversion with an estimation error of 10^{-8} [64].

The Laplace transform of random variable, W can be expressed as

$$\begin{aligned} L_W(s) &= \mathbb{E}_{\mathcal{I}_{VLC}} \left[\exp \left(-s \left(\frac{\mathcal{I}_{VLC}}{\mathcal{R}^2 Z_o P_{VLC}} + \frac{1}{\beta_0} \right) \right) \right], \\ &= \mathbb{E}_{\mathcal{I}_{VLC}} \left[\exp \left(-\frac{s}{\beta_0} \right) \exp \left(-\frac{s \mathcal{I}_{VLC}}{\mathcal{R}^2 Z_o P_{VLC}} \right) \right], \\ &= \exp \left(-\frac{s}{\beta_0} \right) \mathbb{E}_{\Phi_i} \left[\prod_{x \in \Phi_i} \exp \left(-\frac{sk'x^{2(m+1)}}{Z_o(h^2+x^2)^{(m+3)}} \right) \right]. \end{aligned} \quad (3.51)$$

Here $k' := \left(\frac{(m+1)A_R}{2\pi} T_s(\psi) G(\psi) \right)^2$. The last expectation term in (3.51) can be solved using probability generating functional Laplace (PGFL) defined for a homogeneous Poisson point process over region of interest, \mathbb{R} [27, Th 4.9].

$$\mathbb{E}_{\Phi_{PPP}} \left[\prod_{x \in \Phi_i} \exp \left(-\frac{sk'x^{2(m+1)}}{Z_o(h^2+x^2)^{(m+3)}} \right) \right] = \exp \left[- \int_{\mathbb{R}} \lambda_{MAC}^X(x) \left(1 - \exp \left(-\frac{sk'x^{2(m+1)}}{Z_o(h^2+x^2)^{(m+3)}} \right) \right) dx \right]. \quad (3.52)$$

$0 \leq \Psi_k \leq \Psi_{FOV}$

The Eq. (3.52) can be determined using numerical methods⁶

For an *SR*-link assuming both V-VLC and V-RF links to be independent, the outage probability is given as[75]

$$\mathcal{P}_{out,SR} = \mathcal{P}_{out,VLC}(\zeta) \mathcal{P}_{out,RF}(\zeta) \quad (3.53)$$

3.8.3 Outage Probability for V-RF with RIS

For an interference limited system, the received signal at *D* can be expressed as⁷

$$y_D = \sqrt{P_t C_t} \left(\sum_{i=1}^N h_i v_i g_i \right) x + \sqrt{I_D} + \sqrt{I_{RIS}}, \quad (3.54)$$

where x denotes the transmit signal with power, P_t , I_D and I_{RIS} are the interference from same lane's vehicles and the interference from RIS aided links at the destination D respectively, C_t is path loss function that depends on length of RIS[88], $v_i = \rho_i(\Psi_i)e^{j\Psi_i}$, ρ_i denotes the reflectance caused by the i -th reflecting surface of the RIS, and for ideal phase shifts, $\rho_i(\Psi_i) = 1, \forall i$. The channel gains of the RIS-involved links are represented as $h_i = \sqrt{d'_{SR}{}^{-\varepsilon}} \alpha_i e^{-j\theta_i}$ and $g_i = \sqrt{d'_{RD}{}^{-\varepsilon}} \beta_i e^{-j\Phi_i}$, $i \in \{1, 2, \dots, N\}$ respectively, ε is the path-loss exponent, $d'_{SR} (= \sqrt{h^2 + d_{SR}^2})$ and $d'_{RD} (= \sqrt{h^2 + d_{RD}^2})$ denote the distances of the links between S-RIS and RIS-D, α_i and θ_i denote the channel amplitude and phase of h_i , and β_i and Φ_i represent the channel amplitude and phase of g_i , respectively. In addition, the reconfigurable phase Ψ_i is set to $\Psi_i = \theta_i + \Phi_i$ to maximize the SIR at D [89]. The instantaneous SIR, γ_D at D can be formulated as

$$\gamma_D = \frac{P_t A^2 C_t (d'_{SR} d'_{RD})^{-\varepsilon}}{I_D + I_{RIS}}. \quad (3.55)$$

where $A = \sum_{i=1}^N \alpha_i \beta_i$. In particular, A follows distribution of sum of independent and identically distributed (i.i.d) double Rayleigh fading random vectors which aptly capture the channel characteristics of vehicular communication networks [90–92]. The outage probability can be

⁶The numerical methods can easily be implemented in standard mathematical software packages such as *MATLAB* and *MATHEMATICA*.

⁷For purpose of fair comparison, we assume source transmit with transmission power, $P_t = 2P_{RF}$ [87].

expressed as⁸

$$\begin{aligned}\mathcal{P}_{out,RIS} &= 1 - \mathbb{P}(\gamma_D > \zeta), \\ &= 1 - \mathbb{E}_{I_D} \left[\mathbb{P} \left(A^2 > \frac{\zeta (I_{RIS} + I_D)}{P_t C_t (d'_{SR} d'_{RD})^{-\varepsilon}} \right) \right].\end{aligned}\quad (3.56)$$

Now, we make use of the boundary condition for Gamma distribution, $\mathbb{P}(A^2 < x) = (1 - \exp(-\beta_t x))^N$, with $\beta_t = \frac{1}{b} (a!)^{-\frac{1}{a}}$ [94]. Finally, invoking binomial expansion, (3.56) can be approximately expressed as

$$\begin{aligned}\mathcal{P}_{out,RIS} &\approx 1 - \sum_{k=1}^a (-1)^{(k+1)} \binom{a}{k} \mathbb{E} \left[\exp \left(-\frac{k\beta_t \zeta (I_D + I_{RIS})}{P_t C_t (d'_{SR} d'_{RD})^{-\varepsilon}} \right) \right] \\ &\approx 1 - \sum_{k=1}^a (-1)^{(k+1)} \binom{a}{k} \mathcal{L}_{I_D} \left(\frac{k\beta_t \zeta}{P_t C_t (d'_{SR} d'_{RD})^{-\varepsilon}} \right) \mathcal{L}_{I_{RIS}} \left(\frac{k\beta_t \zeta}{P_t C_t (d'_{SR} d'_{RD})^{-\varepsilon}} \right)\end{aligned}\quad (3.57)$$

where $\mathcal{L}_{I_{RIS}}(\cdot)$ denotes the Laplace transform of the interference from RIS aided links which can be expressed as

$$\mathcal{L}_{I_{RIS}}(s) = \exp \left(-\int_0^\infty \lambda_{MAC}^X(x) \left(1 - \left(1 + \frac{s P_t C_t (u d'_{RD})^{-\varepsilon}}{a} \right)^{-a} \right) dx \right).\quad (3.58)$$

where $u = \sqrt{h^2 + x^2}$.

Proof: The Laplace transform for the interference from RIS aided links can be expressed as

$$\begin{aligned}\mathcal{L}_{I_{RIS}}(s) &= \mathbb{E} \left[\exp \left(-\sum_{x \in \Phi_t} s P_t C_t A^2 (d'_{SR} d'_{RD})^{-\varepsilon} \right) \right], \\ &\stackrel{(a)}{=} \mathbb{E} \left[\prod_x \left(1 + \frac{s P_t C_t (d'_{SR} d'_{RD})^{-\varepsilon}}{a} \right)^{-a} \right], \\ &\stackrel{(b)}{=} \exp \left(-\int_0^\infty \lambda_{MAC}^X \left(1 - \left(1 + \frac{s P_t C_t (u d'_{RD})^{-\varepsilon}}{a} \right)^{-a} \right) dx \right).\end{aligned}\quad (3.59)$$

where $u = \sqrt{h^2 + x^2}$, (a) follows from the properties of fading parameter, (b) utilizes the definition of PGFL for HPPP. For slotted ALOHA case, the integral can be expressed in closed form as

$$\mathcal{L}_{I_{RIS}}(s) = \exp \left(-\rho \lambda h \left({}_2F_1 \left(-\frac{1}{2}, a; \frac{1}{2}; -\frac{s P_t C_t}{a (h d'_{RD})^2} \right) - 1 \right) \right).\quad (3.60)$$

⁸Kindly note that the distribution of A^2 also follows gamma distribution which can be verified via method of moment matching[93].

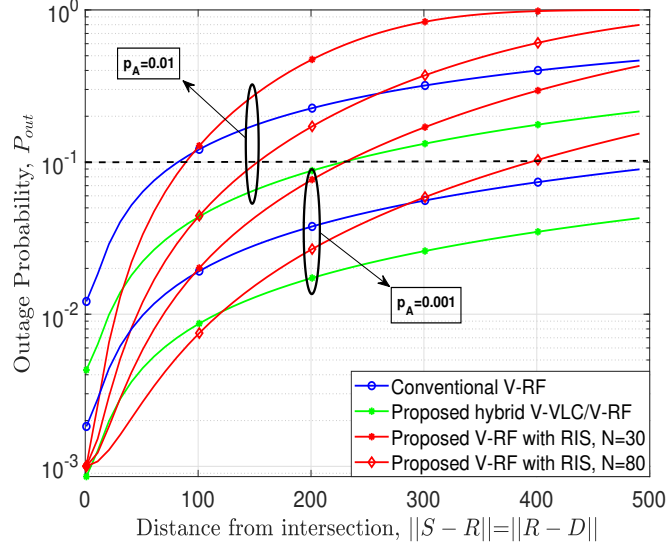


Figure 3.12: Analytical (solid line) and simulation (markers) results for outage probability, \mathcal{P}_{out} versus distance from intersection, i.e $\|S - R\| = \|R - D\|$ for conventional V-RF, proposed hybrid V-VLC/V-RF and RIS aided V-RF communication.

Eq. (3.60) assumes $\varepsilon=2$ and utilizes substitution, $t = \sqrt{x^2 + h^2}$, $t \gg h$ and uses $\int_A^\infty \left(1 - \left(1 + \frac{s}{x^2}\right)^{-N}\right) dx = A \left({}_2F_1\left(-\frac{1}{2}, N; \frac{1}{2}; -\frac{s}{A^2}\right) - 1 \right)$. Note that height, h is greater than close-in distance, D_0 defined for an electrically small RIS.

3.9 Numerical Results and analysis

This section shows the numerical as well as simulation results to show the performance of the proposed solutions. The system model parameters are adopted in accordance with practical vehicular scenario as used in Part I analysis. Unless otherwise specified explicitly, we assume, for simplicity, $d_{SR} = d_{RD} = d_0$, i.e., the RIS/relay is located equidistantly from the source and destination. Unless otherwise stated, we assume $\lambda_X = \lambda_Y = 0.01$. In order to corroborate the accuracy of our analytical findings, we also perform Monte Carlo (MC) simulations by averaging over 10^4 realizations of PPPs and fading channel parameters. We have considered an extreme case when the interference from same lane or perpendicular lane vehicles are originated from an infinite road segment ($\mathcal{B} = \mathbb{R}^1$).

Fig. 3.12 shows the impact of distance, d_0 on the outage performance of conventional V-RF, proposed hybrid V-VLC/V-RF, and RIS assisted V-RF ($N=30, 80$). As intuitive, the outage probability increases with increase in distance, d_0 . We can observe from Fig. 3.12 that irrespective of any d_0 and p_A values, proposed hybrid V-VLC/V-RF scheme always

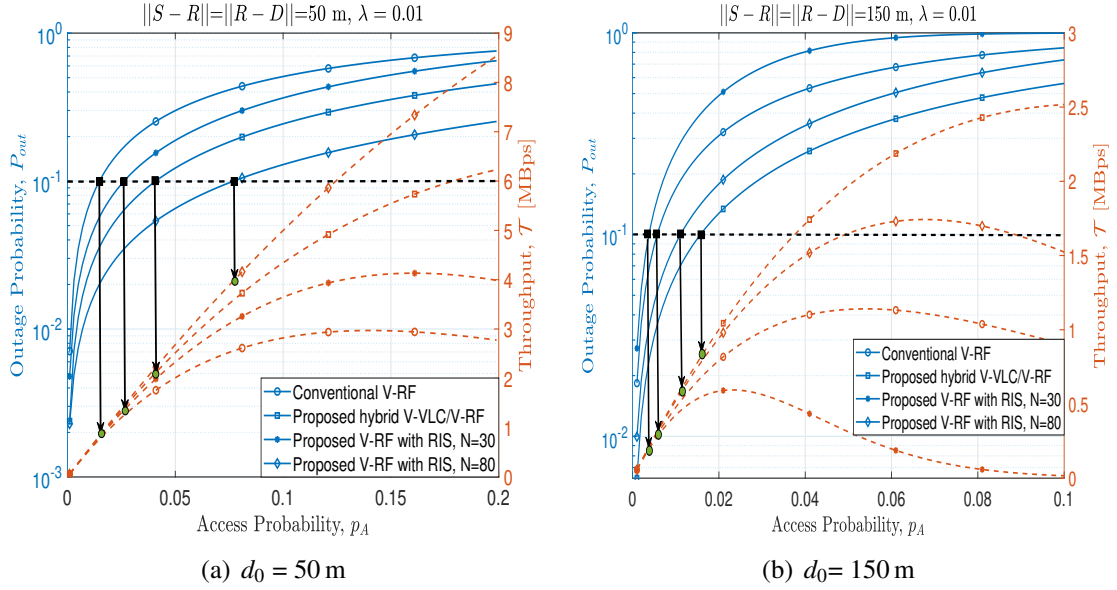


Figure 3.13: Outage probability, \mathcal{P}_{out} and throughput, \mathcal{T} variation with access probability, p_A for two different distances between the source and destination, $d_0 \in (50\text{ m}, 150\text{ m})$.

outperforms conventional V-RF communication in terms of outage probability. Further, the outage performance of proposed hybrid V-VLC/V-RF scheme is better as compared to V-RF with RIS ($N=80$) for $d_0 > 100\text{ m}$ and $p_A=0.01$. Further, with decrease in access probability, p_A , the outage performance of proposed hybrid V-VLC/V-RF as well as V-RF with RIS improves. In order to gain more insights, we next plot outage probability of proposed schemes as a function of access probability. A low access probability ensures low outage probability. This is due to fact that smaller values of p_A implies probability for the vehicles to access the medium is lower, resulting in less interference, and thereby increasing the SIR and reduce the outage. Fig. 3.13 shows outage probability, \mathcal{P}_{out} as a function of access probability, p_A for $d_0 \in (50\text{ m}, 150\text{ m})$. For $d_0 < 100\text{ m}$, proposed V-RF with RIS ($N = 80$) is reliable option over proposed hybrid V-VLC/V-RF scheme as can be seen in Fig. 3.13a. However, the complementary insights can be ruled out when $d_0 > 100\text{ m}$ as shown in Fig. 3.13b. From a system design perspective, the outage probability is not sufficient metric to characterize the performance, since a MAC that allows few concurrent transmissions may lead to high PRP however it will also yield low throughput [61]. Hence, we also plot the throughput as a function of p_A , where the throughput \mathcal{T} is defined as follows[61]

$$\mathcal{T} = p_A(x_{tx})(1 - \mathcal{P}_{out}) \log_2(1 + \zeta) B_s \quad (3.61)$$

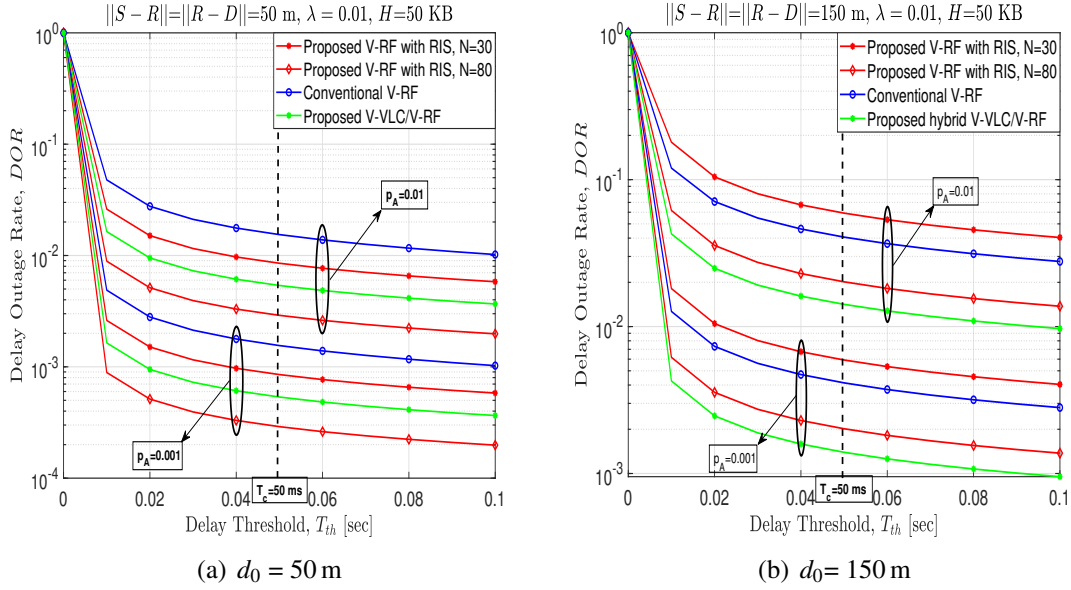


Figure 3.14: Delay outage performance of Conventional V-RF with relaying, hybrid VLC-RF with relaying, and RIS aided V-RF ($N = 30, 80$) for two different distance between the source and destination, $d_0 \in (50m, 150m)$.

The throughput first rises (due to active transmitter) and then declines (due to enormous amounts of interference), leading to an optimum value of p_A . However, in order to ensure a certain QoS, one must also consider a guarantee on the outage probability. For instance, to ensure an outage probability below 10% when $d_0 = 50m$, the optimal value of access probability for proposed V-RF with RIS ($N=80$), $p_A \approx 0.077$, results in a throughput of about 4 MBps. However, when $d_0 = 150m$, the opposite trend can be observed in Fig. 3.13b wherein proposed hybrid V-VLC/V-RF scheme guarantees more throughput as compared to proposed V-RF with RIS ($N=80$) for same outage performance. Notice that for given d_0 and p_A , the performance of the proposed V-RF with RIS scheme can be improved by increasing RIS elements, N without an increase in power consumption of the transceiver. Next, we also plot DOR performance for V2X deployment strategies ensuring different delay threshold requirements. In particular, we plot DOR performance of deployment strategies as a function of the delay threshold, T_{th} for sending data amount, $H=50KB$. It is interesting to note that for data traffic with stringent delay requirements, the proposed V-RF with RIS ($N=80$) ensures minimum delay in transmitting a given amount of information from source to destination as compared to the proposed hybrid V-VLC/V-RF or conventional V-RF when $d_0 = 50m$ and $p_A = 0.01$ as can be seen from Fig 3.14a. We can also observe that when $d_0 = 150m$, there exists complementary behaviour in DOR performance of proposed schemes as evident from Fig. 3.14b. For sake of analysis, for given $T_{th} = 50ms$, we also plot the DOR performance of V-RF with RIS, by varying the number of RIS

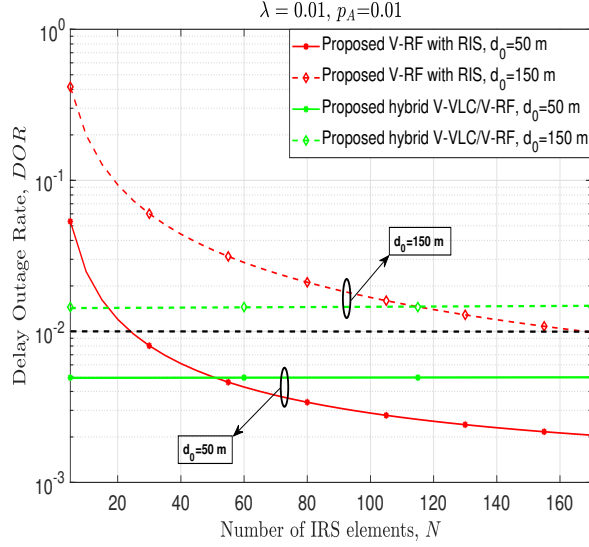


Figure 3.15: Delay outage rate variation with increasing value of RIS elements, N for two different distances between the source and destination, $d_0 \in (50m, 150m)$.

elements as shown in Fig. 3.15. With DOR of 1×10^{-2} as performance constraint, the proposed hybrid V-VLC/V-RF scheme are acceptable for $d_0 < 150m$. However, V-RF with RIS requires $N > 20$ and $N > 170$ for $d_0=50m$ and $d_0=150m$ respectively in order to ensure DOR within acceptable limit.

3.10 Concluding remarks

In this work, we proposed hybrid V-VLC/V-RF and V-RF with RIS schemes to facilitate vehicular communication at road intersections in order to enable uninterrupted connectivity, enhanced coverage, and ultra reliable low latency communications. The obtained results show that the proposed V2X deployment strategies can achieve considerable performance improvement in outage, throughput while ensuring low latency as compared to conventional V-RF with relaying. Undoubtedly, V-RF with RIS with sufficiently large, N always outperforms either hybrid V-VLC/V-RF with relaying or V-RF with relaying. Irrespective of distance between source and destination vehicles, the proposed hybrid V-VLC/V-RF will always outperform conventional V-RF communication in terms of outage and DOR. However, the number of RIS elements, N decides the performance of proposed V-RF with RIS. The proposed solution may serve as better alternative ITS solution as compared to conventional V-RF solution to meet the ultra-high reliable and ultra low latency communication requirements for B5G vehicular networks. Further investigations will be devoted to gain more useful insights when there exists an integration of optical RIS with V-VLC technology.

OPD NOMA for Vehicular Communication

This chapter investigates the performance of optical power domain non orthogonal multiple access (OPD NOMA) for vehicular communication. Specifically, the first part of this chapter investigates the applicability of downlink OPD NOMA enabled V2X network for typical infrastructure-to-vehicle (I2V) communication in presence of interference caused from concurrent vehicle-to-vehicle (V2V) transmissions with an aid of stochastic geometry. In part II, we analyze the performance of a novel cooperative NOMA (C-NOMA) enabled hybrid vehicular visible light communication (V-VLC)/V-RF communication for improving safety message dissemination and enabling massive connectivity among vehicles for road intersection scenarios.

4.1 OPD NOMA for Vehicular Networks

The next generation vehicular network will require reliable massive connectivity, higher spectral efficiency and reduced resource collision, hence a suitable multiple access (MA) scheme should be adopted that can cater for 6G Key Performance Indicators (KPIs) requirements. In this work, we aim to understand the potential benefits and practical challenges associated with employing downlink OPD NOMA based V2X network. The major contributions and findings of our work are summarized below:

- We explore the potential benefits of downlink NOMA using VLC in vehicular scenario for broadcasting road safety related information. We carry out performance analysis of the proposed downlink OPD NOMA based V2X network against the OMA counterpart

with aid of stochastic geometry tools. This is carried out by considering the impact of interference from other vehicular transmission by V2V at the receiving nodes.

- We develop a novel tractable framework in terms of outage probability and achievable rate as performance metrics when a light source (e.g., traffic lamp post) transmits a message to two destination vehicles through visible light by assuming both perfect SIC and imperfect SIC decoding at the receiver.
- In order to verify the efficacy of the proposed OPD-NOMA technique, we compare the performance of downlink OPD NOMA based V2X network with conventional RF NOMA based V2X network. Depending upon the locations of NOMA users from source, we illustrate the trade-offs between these two different technologies.

4.2 System Model and Preliminaries

4.2.1 System Model

We consider an uni-directional traffic stream wherein either NOMA enabled VLC or RF downlink exists between road side unit (RSU) (mounted on LED traffic lamp) and vehicles as depicted in Fig. 4.1. We assume that a light source (e.g., traffic lamp post) sends a message to destination nodes through visible light. However, such VLC transmission is subject to interference originating from neighbouring vehicles that are located on the roads. At transmitter side, as shown in Fig. 4.2, light source transmits the composite signal, which is a superposition of desired optical signals of user pairs with different power allocation. We consider the existence of a central information center (CIC) that collects and keeps track of some key system information (such as location and speed of each vehicle, road condition, BSMs dissemination) about the on-road vehicles. The communication between LED Traffic light and CIC is established via back-haul connectivity and to vehicles through free-space optical wireless transmission. For ease of understanding, Fig. 4.3 provides the schematic layout of proposed system model.

We consider a set of interfering vehicles which are distributed according to a one-dimensional homogeneous Poisson point process (1D-HPPP), represented as $\Psi_{PPP} \sim 1D\text{-HPPP}(\lambda, r)$, where r and λ denote the positions of the interferer vehicles and their intensity, respectively. Further, we assume that interfering vehicles follow Aloha MAC protocol with parameter ρ , i.e., every node can access the medium with an access probability, ρ [95]. We considered low speed vehicles (LSV) mobility model where we assume that interferer vehicles do not move or move slowly, that is, their positions remain the same during the two time slots of the transmission [96].



Figure 4.1: Typical I2V and V2V-VLC scenario.

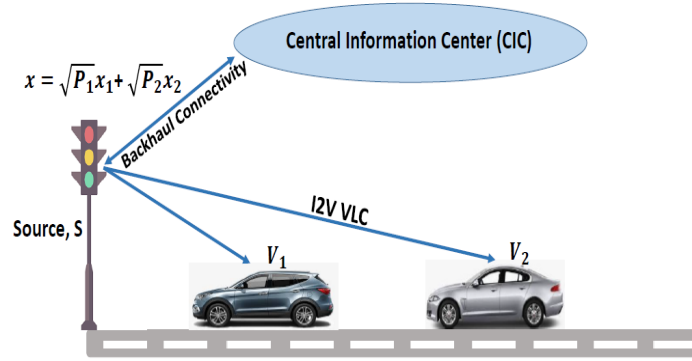


Figure 4.2: OPD NOMA based V2X system model.

The proposed work is also in line with previous work proposed in [97] and [98]. The Doppler shift and time-varying effect of V2V and V2I channel on the performance of OPD-NOMA enabled V2X networks has been left as a subject of future investigation.

4.2.2 Practical Challenges

In order to achieve the same quality of service (QoS) for each received signal, we derive the general formula for the transmit power level required for each vehicular node. Recently, the authors in [99] have experimentally validated an adaptive energy saving technique that can be adopted to compensate the saturation effects in an outdoor VLC by varying transmitting vehicle's power. With no loss of generality, let us consider that a NOMA group consists of k vehicles, which are categorized based on their channel gain conditions in ascending order as $h_1 \leq h_2 \dots \leq h_k$. Based on such ordering, NOMA technique can permit V_i to decode the interfering NOMA signals originating from $V_k, k \leq i$ and then eliminate the interfering NOMA

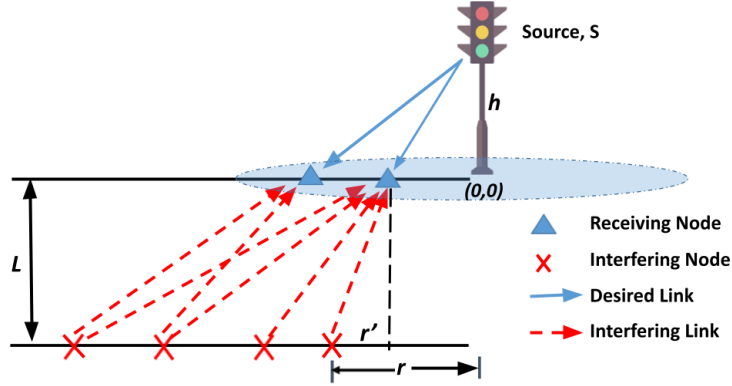


Figure 4.3: Abstraction used for modelling. The desired vehicles are marked in triangle, while interferers are marked in cross marks. Here, L and h denotes the inter lane distance and height of traffic lamp respectively.

signals from the received signal, in a successive manner. According to the NOMA principle and the order of channel gains, power P_i is allocated in descending order, i.e., $P_1 \geq \dots \geq P_k$, which is reverse to the order of h_i .

The received optical signal at V_i can be represented as

$$y_i = \mathcal{R}h_i s + n, \quad (4.1)$$

where s denotes composite optical transmitted from LED, \mathcal{R} denotes the responsivity of PD, n denotes the additive white Gaussian noise with zero mean and variance, σ^2 . We assume that there is a perfect interference cancellation through SIC at the each receiving node. Hence, the SIC enabled receiver first decodes the strongest signal and then subtracts it from the composite received signal. This process continues until all the signals are properly detected. Due to non-uniform power allocation at all the transmitting vehicles, OPD-NOMA with SIC exploits the signal-to-interference plus noise ratio (SINR) difference among vehicles. It is assumed that the required electrical SINR, γ at each receiving node is same (say, constant, c). Mathematically,

$$\gamma = \frac{(\mathcal{R}P_{r_k})^2}{\sigma_k^2} = c \quad \forall k, \quad (4.2)$$

where P_{r_k} denotes optical power received from the k -th vehicle. The transmitter power, P_1 is set such that symbol s_1 can be received accurately, that is

$$\begin{aligned} P_{r1} &= \frac{\sigma_1}{\mathcal{R}} \sqrt{\gamma}, \\ P_1 &= \frac{\sigma_1}{\mathcal{R}h_1} \sqrt{\gamma}. \end{aligned} \quad (4.3)$$

The same can be extended for the vehicle V_2 transmitter power P_2 which is computed as:

$$\begin{aligned}\gamma &= \frac{(\mathcal{R}P_{r_2})^2}{(\mathcal{R}P_{r_1})^2 + \sigma_2^2}, \\ P_{r_2} &= \frac{\sigma_2}{\mathcal{R}} \sqrt{\gamma(\gamma+1)}, \\ P_2 &= \frac{\sigma_2}{\mathcal{R}h_2} \sqrt{\gamma(\gamma+1)}.\end{aligned}\tag{4.4}$$

This approach is iteratively applied to determine vehicle V_3 transmit power, P_3 , which depends on the past values of P_1 and P_2 and can be given in simplified form as

$$P_3 = \frac{\sigma_3}{\mathcal{R}h_3} \sqrt{\gamma(\gamma^2 + 2\gamma + 1)}.\tag{4.5}$$

In general, the same concept can be extended to N transmitting vehicles. Further, the transmit power for the i -th vehicle can be given as a function of the noise variance σ_i , channel gain coefficient h_i , and the required SINR¹ as

$$P_i = \frac{\sigma_i}{\mathcal{R}h_i} \sqrt{\gamma(\gamma+1)}^{\frac{i-1}{2}}, i = 1, 2, 3, \dots, N.\tag{4.6}$$

For transmitting information in power domain, recognising that vehicle V_i has worse channel conditions, PD-NOMA allocates a greater amount of power P_i to that vehicle depending on channel conditions. Thus, there exists non-uniform transmit power allocation among vehicles which is critical for designing a practical V-VLC system. Several open issues such as power imbalance and maintaining fairness among vehicles need to be addressed carefully before practical deployment of OPD-NOMA to vehicular communication systems. Further, in the OPD-NOMA downlink, the unavailability of channel state knowledge impacts the overall system performance, since the channel state information (CSI) for each vehicular node must be known by all users and the light source allocates power to each vehicular node based on its CSI which brings further challenges for NOMA implementation in vehicular scenario.

4.3 Performance Analysis

For the sake of analysis, we specifically consider interference limited scenario wherein two vehicular nodes, V_1 and V_2 are selected to perform NOMA jointly since asking all the vehicles in network to participate is not preferable in practice. However, the proposed analysis can be

¹Note that the transmit power allocation adopted among vehicles is critical for a practical V-VLC system design. For sake of analysis, we assume that each vehicle is allocated power more than certain minimum threshold power which can suffice illumination as well as communication constraint.

easily extended to a generic NOMA scheme with M vehicles, $M \geq 2$. We also consider that the receiving vehicular nodes are sorted according to their preset QoS priorities [100, 101]. In other words, V_1 has to be served immediately with a lower data rate whereas V_2 needs a higher data rate but can be served later. Even in real life, not all users require the same amount of data rate. Let the signals intended to V_1 and V_2 are denoted as x_1 and x_2 , respectively, where $\mathbb{E}[|x_i|^2] = 1$. As per NOMA principle [102], the transmitted optical signal from LED is coded as the composite signal from V_1 and V_2 ,

$$x = \sqrt{P_1}x_1 + \sqrt{P_2}x_2. \quad (4.7)$$

Thus the received signal at V_i can be represented in an interference limited system as

$$y_i = \mathcal{R}h_i x + \sqrt{\mathcal{I}_i}. \quad (4.8)$$

In following subsection, we derive analytical expression for NOMA outage probability and average achievable rate for two-vehicular case.

4.3.1 NOMA Outage Expression for V-VLC

An outage is said to occur when the instantaneous SINR falls below a certain SINR threshold. For V-VLC, noise variance is negligible as compared to aggregate interference [68]. For such interference limited scenario, we first calculate the signal-to-interference ratio (SIR) at each receiving vehicular node, then define outage probability associated to them. As V_1 is assumed to be received with higher power, therefore it will be firstly decoded according to SIC decoding. Subsequently, interference would be V_2 , and SIR at V_1 , denoted as SIR_{V_1} , can be expressed as

$$SIR_{V_1} = \frac{k\xi_1 P_{VLC} r_1^{2(m+1)} (h^2 + r_1^2)^{-(m+\gamma+1)}}{k\xi_2 P_{VLC} r_1^{2(m+1)} (h^2 + r_1^2)^{-(m+3)} + \mathcal{I}_{\mathcal{V}\mathcal{L}\mathcal{C}}}. \quad (4.9)$$

In [4.9], ξ_1 , and P_{VLC} denote the power allocation coefficient associated with vehicle, V_1 and the transmission power for VLC respectively. $\mathcal{I}_{\mathcal{V}\mathcal{L}\mathcal{C}}$ denotes the aggregate interference experienced at the receiving node from vehicles in adjacent lane (VLC-V2V). Referring to Fig. 4.3, we can deduce $\cos(\phi) = \cos(\psi) = \frac{r'}{\sqrt{(L^2 + r'^2)}}$ for given system model based on simple geometrical argument. The interference $\mathcal{I}_{\mathcal{V}\mathcal{L}\mathcal{C}}$ can be given as

$$\mathcal{I}_{\mathcal{V}\mathcal{L}\mathcal{C}} = \sum_{i=1}^N k \frac{r_i'^{2(m+1)}}{(L^2 + r_i'^2)^{(m+3)}} P_{VLC}; \quad (4.10)$$

Here $k = \left(\frac{\mathcal{R}^{(m+1)A_R}}{2\pi} T_s(\psi)G(\psi) \right)^2$. In contrary, as V_2 comes second in decoding order, it has to first retrieve V_1 message, denoted as $SIR_{V_{2-1}}$, is expressed as,

$$SIR_{V_{2-1}} = \frac{k\xi_1 P_{VLC} r_2^{2(m+1)} (h^2 + r_2^2)^{-(m+3)}}{k\xi_2 P_{VLC} r_2^{2(m+1)} (h^2 + r_2^2)^{-(m+3)} + \mathcal{I}'_{\psi, \mathcal{L}^c \mathcal{E}}}. \quad (4.11)$$

The SIR at V_2 to decode its own message, denoted as SIR_{V_2} , is expressed as

$$SIR_{V_2} = \frac{k\xi_2 P_{VLC} r_2^{2(m+1)} (h^2 + r_2^2)^{-(m+3)}}{\mu k\xi_1 P_{VLC} r_2^{2(m+1)} (h^2 + r_2^2)^{-(m+3)} + \mathcal{I}'_{\psi, \mathcal{L}^c \mathcal{E}}}. \quad (4.12)$$

where $\mu \in (0, 1)$ denotes residual factor accounting for interference fraction that remains due to imperfect SIC at the receiver. For the case of perfect SIC, $\mu = 0$. Let us denote outage event related to V_1 as O_{V_1} , which is expressed as

$$O_{V_1} = \{SIR_{V_1} < \beta_1\}, \quad (4.13)$$

where, $\beta_1 = \frac{2\pi}{e} (2^{2R_1} - 1)$ and R_1 is target data rate of V_1 . At any NOMA receiver, the overall decoding mechanism is considered to be in outage if instantaneous user rates associated with either Eq.(4.9) or Eq.(4.12) do not suffice the respective target rates. Let $O_{V_{2-1}}$ denote the outage event when V_2 cannot decode V_1 message, expressed as

$$O_{V_{2-1}} = \{SIR_{V_{2-1}} < \beta_1\}, \quad (4.14)$$

Now, let O_{V_2} denote the outage event when V_2 cannot retrieve its own message, expressed as

$$O_{V_2} = \{SIR_{V_2} < \beta_2\}, \quad (4.15)$$

where $\beta_2 = \frac{2\pi}{e} (2^{2R_2} - 1)$ and R_2 is target data rate of V_2 . Having this background, we are now in position to calculate the outage probability related to V_1 and V_2 . We make use of moment generating functional (MGF) approach to solve for the outage probability.

V_1 outage probability:

$$\mathcal{P}_{O_{V_1}} = \mathbb{P}\left(\frac{\mathcal{I}_{\psi, \mathcal{L}^c \mathcal{E}}}{k(\xi_1 - \beta_1 \xi_2) P_{VLC} r_1^{2(m+1)} (h^2 + r_1^2)^{-(m+3)}} > \frac{1}{\beta_1} \right). \quad (4.16)$$

Let us define random variable Z as

$$Z = \frac{\mathcal{I}_{\psi, \mathcal{L}^c \mathcal{E}}}{k(\xi_1 - \beta_1 \xi_2) P_{VLC} r_1^{2(m+1)} (h^2 + r_1^2)^{-(m+3)}} \quad (4.17)$$

Hence, (4.16) can be rewritten as

$$P_{out} = \mathbb{P}(Z > \beta^{-1}) = 1 - F_Z(\beta^{-1}). \quad (4.18)$$

In general, a closed-form solution for $F_Z(\beta^{-1})$ is quite difficult to obtain. Hence, we utilize numerical inversion of Laplace transform to find CDF, $F_Z(\beta^{-1})$. The CDF of a random variable Z is related to the Laplace transform of $F_Z(z)$ as [64]

$$F_Z(z) = \frac{1}{2\pi j} \int_{c-j\infty}^{c+j\infty} \mathcal{L}_{F_Z(z)} \exp(sw) ds. \quad (4.19)$$

where j is imaginary number ($\sqrt{-1}$). The above integral can be discretized to get a series using the trapezoid rule and then the infinite series can be truncated to get a finite sum using the Euler summation [64]. Also, $\mathcal{L}_{F_Z(z)}(s) = \frac{\mathcal{L}_Z(s)}{s}$. Eq.(4.18) can be approximated as

$$P_{out} \approx 1 - \frac{2^{-B} \exp(\frac{A}{2})}{\beta^{-1}} \sum_{b=0}^B \binom{B}{b} \sum_{c=0}^{C+b} \frac{(-1)^c}{D_c} \text{Re} \left\{ \frac{\mathcal{L}_Z(s)}{s} \right\}. \quad (4.20)$$

where $D_c = 2$ (if $c = 0$) and $D_c = 1$ (if $c = 1, 2, 3, \dots$) and $s = \frac{(A+j2\pi c)}{2\beta^{-1}}$. The estimation error is controlled by three parameters A , B and C . Using the well established result given in [65],[64], in order to achieve an estimation accuracy of $10^{-\eta}$ (i.e., having the $(\eta - 1)$ th decimal correct), A , B and C have to be at least equal $\eta \ln 10$, $1.243\eta - 1$, and 1.467η , respectively. Setting $A=8\ln 10$, $B=11$, $C=14$ achieves stable numerical inversion with an estimation error of 10^{-8} .

The Laplace transform of the probability distribution of a random variable can be computed as

$$\mathcal{L}_Z(s) = \mathbb{E}_{\mathcal{S}} \left\{ \exp \left(- \frac{s \mathcal{I} \mathcal{V} \mathcal{L} \mathcal{C}}{k(\xi_1 - \beta_1 \xi_2) P_{VLC} r_1^{2(m+1)} (h^2 + r_1^2)^{-(m+3)}} \right) \right\} \quad (4.21)$$

$$= \mathbb{E}_r \left\{ \prod_{i=1}^N \exp \left(- \frac{s}{k(\xi_1 - \beta_1 \xi_2) P_{VLC} r_1^{2(m+1)} (h^2 + r_1^2)^{-(m+3)}} \frac{kr_i'^{2(m+1)}}{(L^2 + r_i'^2)^{(m+3)}} \right) \right\}, \quad (4.22)$$

The expectation in Eq.(4.22) can be solved using probability generating functional Laplace (PGFL) defined for a homogeneous Poisson point process [103, Th 4.9].

$$\mathbb{E}_r \left\{ \prod_{i=1}^N \exp \left(- \frac{s}{k(\xi_1 - \beta_1 \xi_2) P_{VLC} r_1^{2(m+1)} (h^2 + r_1^2)^{-(m+3)}} \frac{kr_i'^{2(m+1)}}{(L^2 + r_i'^2)^{(m+3)}} \right) \right\}$$

$$= \exp \left[-\rho\lambda \int_{r_1}^{\infty} \left(1 - \exp \left(-\frac{s}{k(\xi_1 - \beta_1\xi_2)} \frac{kr^{2(m+1)}}{P_{VLC}r_1^{2(m+1)}(h^2 + r_1^2)^{-(m+3)}(L^2 + r^2)^{(m+3)}} \right) \right) dr \right]. \quad (4.23)$$

V_2 outage probability

In order to calculate $\mathcal{P}_{O_{V_2}}$, we express $\mathcal{P}_{O_{V_2}}$ as a function of success probability, $\mathcal{P}_{O_{V_2-1} \cap O_{V_2}}^C$ that is

$$\mathcal{P}_{O_{V_2}} = 1 - \mathcal{P}_{O_{V_2}}^C = 1 - \mathcal{P}_{O_{V_2-1} \cap O_{V_2}}^C, \quad (4.24)$$

$$\mathcal{P}_{O_{V_2-1} \cap O_{V_2}}^C =$$

$$\begin{aligned} & \mathbb{P} \left(\frac{\mathcal{I}'_{\mathcal{V}\mathcal{L}\mathcal{C}}}{k(\xi_1 - \beta_1\xi_2)P_{VLC}r_2^{2(m+1)}(h^2 + r_2^2)^{-(m+3)}} < \frac{1}{\beta_1}, \frac{\mathcal{I}'_{\mathcal{V}\mathcal{L}\mathcal{C}}}{k(\xi_2 - \beta_2\mu\xi_1)P_{VLC}r_2^{2(m+1)}(h^2 + r_2^2)^{-(m+3)}} < \frac{1}{\beta_2} \right), \\ & = \mathbb{P} \left(\frac{\mathcal{I}'_{\mathcal{V}\mathcal{L}\mathcal{C}}}{kP_{VLC}r_2^{2(m+1)}(h^2 + r_2^2)^{-(m+3)}} < \frac{(\xi_1 - \beta_1\xi_2)}{\beta_1}, \frac{\mathcal{I}'_{\mathcal{V}\mathcal{L}\mathcal{C}}}{kP_{VLC}r_2^{2(m+1)}(h^2 + r_2^2)^{-(m+3)}} < \frac{(\xi_2 - \beta_2\mu\xi_1)}{\beta_2} \right), \\ & = \mathbb{P} \left(\frac{\mathcal{I}'_{\mathcal{V}\mathcal{L}\mathcal{C}}}{kP_{VLC}r_2^{2(m+1)}(h^2 + r_2^2)^{-(m+3)}} < \min(J_1, J_2) \right). \end{aligned} \quad (4.25)$$

where $J_1 = \frac{(\xi_1 - \beta_1\xi_2)}{\beta_1}$ and $J_2 = \frac{(\xi_2 - \beta_2\mu\xi_1)}{\beta_2}$. Following same steps as (4.18)-(4.23), (4.25) can be solved using similar approach.

OPD-NOMA Extension to M -nodes

Now, we extend OPD NOMA results to M -destination nodes. The expression for SIR at node V_i to retrieve V_t message can be expressed as

$$SIR_{V_i \rightarrow t} = \frac{k\xi_t P_{VLC}r_i^{2(m+1)}(h^2 + r_i^2)^{-(m+3)}}{kP_{VLC}r_i^{2(m+1)}(h^2 + r_i^2)^{-(m+3)} \left[\mu \sum_{k=1}^{t-1} \xi_k + \sum_{n=t+1}^M \xi_n \right] + \mathcal{I}_{VLC}^i}. \quad (4.26)$$

Observe that, when $k > t - 1$, then $\sum_{k=1}^{t-1} \xi_k = 0$ and when $n > M$, then $\sum_{n=t+1}^M \xi_n = 0$. In order to calculate outage probability $\mathcal{P}_{O_{V_i}}$ at node V_i , we express a successful transmission at node V_i as

$$O_{V_i}^C = \bigcap_{n=M-i+1}^M \{SIR_{V_i \rightarrow i-(M-n)} > R_{i-(M-n)}\}, \quad (4.27)$$

Finally, the outage probability can be expressed as

$$\mathcal{P}_{O_{V_i}} = \begin{cases} 1; & \text{if } \bigcup_{t=1}^M \frac{\xi_t}{\mu \sum_{k=1}^t \xi_k + \sum_{n=t+1}^M \xi_n} < \beta_t, \\ 1 - \mathbb{P} \left(\frac{\mathcal{I}_{VLC}^i}{k P_{VLC} r_i^{2(m+1)} (h^2 + r_i^2)^{-(m+3)}} < J_{(i)min} \right); & \text{otherwise,} \end{cases} \quad (4.28)$$

where $J_{(i)min}$ is given by

$$J_{(i)min} = \min \left(\frac{\xi_{i-(M-1)} - \beta_{i-(M-1)} \left[\mu \sum_{k=1}^{i-(M-1)-1} \xi_k + \sum_{n=i-(M-1)+1}^M \xi_n \right]}{\beta_{i-(M-1)}}, \right. \\ \left. \frac{\xi_{i-(M-2)} - \beta_{i-(M-2)} \left[\mu \sum_{k=1}^{i-(M-2)-1} \xi_k + \sum_{n=i-(M-2)+1}^M \xi_n \right]}{\beta_{i-(M-2)}}, \dots, \right. \\ \left. \frac{\xi_{i-(M-\ell)} - \beta_{i-(M-\ell)} \left[\mu \sum_{k=1}^{i-(M-\ell)-1} \xi_k + \sum_{n=i-(M-\ell)+1}^M \xi_n \right]}{\beta_{i-(M-\ell)}} \right). \quad (4.29)$$

where $\ell \in (1, 2, \dots, M)$. We set the condition that $\ell > M - i$. Intuitively, as the number of destination nodes, M increases, NOMA performance become better over OMA.

4.3.2 NOMA Outage Expression for V-RF

For V-RF, assuming free space path loss propagation model, the interference at the receiver can be given as aggregate of all the RF power received from N interferers as:

$$\mathcal{I}_{\mathcal{R}\mathcal{F}} = \sum_{i=1}^N P_{RF} G_t G_r \ell h_k (L^2 + r_i^2)^{-\frac{\alpha}{2}}, \quad (4.30)$$

Here, $\ell = \frac{c^2}{(4\pi)^2 f_0^2}$; c is speed of light and f_0 is carrier frequency. In above expression, P_{RF} , α , G_t and G_r are the the RF transmission power, the path loss exponent, the antenna gains for transmitter and receiver respectively [66].

V_1 outage probability

The outage probability ($\mathcal{P}_{O_{V_1}}^{RF}$) related to V_1 in case of RF based vehicular communication can

be given as

$$\begin{aligned}
\mathcal{P}_{O_{V_1}}^{RF} &= 1 - \mathbb{P} \left(\frac{\xi_1 P_{RF} G_t G_r \ell h_1 (h^2 + r_1^2)^{-\frac{\alpha}{2}}}{\xi_2 P_{RF} G_t G_r \ell h_1 (h^2 + r_1^2)^{-\frac{\alpha}{2}} + \mathcal{I}_{RF}} > \zeta_1 \right), \\
&= 1 - \mathbb{P} \left(h_1 > \frac{\zeta_1 \mathcal{I}_{RF}}{(\xi_1 - \zeta_1 \xi_2) P_{RF} G_t G_r \ell (h^2 + r_1^2)^{-\frac{\alpha}{2}}} \right), \\
&= 1 - \left[\mathcal{L}_{I_{RF}} \left(\frac{\zeta_1}{(\xi_1 - \zeta_1 \xi_2) P_{RF} G_t G_r \ell (h^2 + r_1^2)^{-\frac{\alpha}{2}}} \right) \right],
\end{aligned} \tag{4.31}$$

where $\zeta_1 = 2^{R_1} - 1$ and $\mathcal{L}(\cdot)$ denotes for Laplace transform which is given as²

$$\mathcal{L}_{I_{RF}} \left(\frac{\zeta_1}{(\xi_1 - \zeta_1 \xi_2) P_{RF} G_t G_r \ell (h^2 + r_1^2)^{-\frac{\alpha}{2}}} \right) = \exp \left(-\rho \lambda \left(\frac{\zeta_1}{(\xi_1 - \zeta_1 \xi_2)} \right)^{\frac{1}{\alpha}} (h^2 + r_1^2)^{\frac{1}{2}} \frac{\pi}{\alpha} \csc \left(\frac{\pi}{\alpha} \right) \right). \tag{4.32}$$

Proof: The Laplace transform, $L_{I_{RF}}(s)$ can be computed as:

$$\begin{aligned}
L_{I_{RF}}(s) &= \mathbb{E}[\exp(-sI_{RF})] \\
&= \mathbb{E} \left[\prod_r \exp(-sP_{RF} G_t G_r \ell h ||r'||^{-\alpha}) \right] \\
&\stackrel{(a)}{=} \mathbb{E}_r \left[\prod_r \mathbb{E}_h \{ \exp(-sP_{RF} G_t G_r \ell h ||r'||^{-\alpha}) \} \right] \\
&= \mathbb{E}_r \left[\prod_r \frac{1}{1 + sP_{RF} G_t G_r \ell ||r'||^{-\alpha}} \right] \\
&\stackrel{(b)}{=} \exp \left(-\rho \lambda \int_{r_1}^{\infty} \frac{1}{1 + ||r'||^{\alpha} / sP_{RF} G_t G_r \ell} dr \right) \\
&\stackrel{(c)}{=} \exp \left(-\rho \lambda (sP_{RF} G_t G_r \ell)^{\frac{1}{\alpha}} \int_{r_1}^{\infty} \frac{1}{1 + v^{\alpha}} dv \right) \\
&\stackrel{(d)}{=} \exp \left(-\rho \lambda (sP_{RF} G_t G_r \ell)^{\frac{1}{\alpha}} \frac{\pi}{\alpha} \csc \left(\frac{\pi}{\alpha} \right) \right)
\end{aligned} \tag{4.33}$$

here, (a) holds due to independence of channel fading coefficients h_x and assumes $L \ll r'$, (b) uses the PGFL for Homogeneous PPP, (c) involves variable transformation $||r|| / (sP_{RF} G_t G_r \ell)^{\frac{1}{\alpha}} \rightarrow v$, and (d) when $r_1 \rightarrow 0$. Substituting $s = \frac{\zeta_1}{(\xi_1 - \zeta_1 \xi_2) P_{RF} G_t G_r \ell (h^2 + r_1^2)^{-\frac{\alpha}{2}}}$ yields the desired result.

²The closed form expression was obtained based on assumption that the inter lane distance, L can be ignored as compared to longitudinal stretch of the road i.e. $L \ll r$

V_2 outage probability

As before, we express $\mathcal{P}_{O_{V_2}}^{RF}$ as a function of success probability, $\mathcal{P}_{O_{V_2-1} \cap O_{V_2}}^C$ that is

$$\mathcal{P}_{O_{V_2}}^{RF} = 1 - \mathcal{P}_{O_{V_2}}^C = 1 - \mathcal{P}_{O_{V_2-1} \cap O_{V_2}}^C, \quad (4.34)$$

$$\begin{aligned} & \mathcal{P}_{O_{V_2-1} \cap O_{V_2}}^C \\ &= \mathbb{P} \left(\frac{\xi_1 P_{RF} G_t G_r \ell h_2 (h^2 + r_2^2)^{-\frac{\alpha}{2}}}{\xi_2 P_{RF} G_t G_r \ell h_2 (h^2 + r_2^2)^{-\frac{\alpha}{2}} + \mathcal{I}'_{RF}} > \zeta_1, \frac{\xi_2 P_{RF} G_t G_r \ell h_2 (h^2 + r_2^2)^{-\frac{\alpha}{2}}}{\mu \xi_1 P_{RF} G_t G_r \ell h_2 (h^2 + r_2^2)^{-\frac{\alpha}{2}} + \mathcal{I}'_{RF}} > \zeta_2 \right), \\ &= \mathbb{P} \left(h_2 > \frac{\zeta_1 \mathcal{I}'_{RF}}{(\xi_1 - \zeta_1 \xi_2) P_{RF} G_t G_r \ell h_2 (h^2 + r_2^2)^{-\frac{\alpha}{2}}}, h_2 > \frac{\zeta_2 \mathcal{I}'_{RF}}{(\xi_2 - \mu \zeta_2 \xi_1) P_{RF} G_t G_r \ell h_2 (h^2 + r_2^2)^{-\frac{\alpha}{2}}} \right), \\ &= \mathcal{L}'_{RF} \left(\frac{J}{P_{RF} G_t G_r \ell h_2 (h^2 + r_2^2)^{-\frac{\alpha}{2}}} \right). \end{aligned} \quad (4.35)$$

where $\zeta_2 = 2^{R_2} - 1$ and $J = \max(J_1, J_2)$. Here, $J_1 = \frac{\zeta_1}{(\xi_1 - \zeta_1 \xi_2)}$ and $J_2 = \frac{\zeta_2}{(\xi_2 - \mu \zeta_2 \xi_1)}$.

V-RF NOMA Extension to M -nodes

Here, we extend the V-RF NOMA results to M -destination nodes. We define the expression of the SIR at V_i to decode V_i message as follows

$$SIR_{V_i \rightarrow t} = \frac{\xi_t P_{RF} G_t G_r \ell h_t (h^2 + r_i^2)^{-\frac{\alpha}{2}}}{P_{RF} G_t G_r \ell h_t (h^2 + r_i^2)^{-\frac{\alpha}{2}} \left[\mu \sum_{k=1}^{t-1} \xi_k + \sum_{n=t+1}^M \xi_n \right] + \mathcal{I}'_{RF}}. \quad (4.36)$$

Same as above, when $k > t - 1$, then $\sum_{k=1}^{t-1} \xi_k = 0$ and when $n > M$, then $\sum_{n=t+1}^M \xi_n = 0$. In this case, the outage probability, $\mathcal{P}_{O_{V_i}}$ can be expressed as $\mathcal{P}_{O_{V_i}}$

$$= \begin{cases} 1; & \text{if } \bigcup_{t=1}^M \frac{\xi_t}{\mu \sum_{k=1}^{t-1} \xi_k + \sum_{n=t+1}^M \xi_n} < \zeta_t, \\ 1 - L_{RF}^i \left(\frac{J^{(i)max}}{P_{RF} G_t G_r \ell h_t (h^2 + r_i^2)^{-\frac{\alpha}{2}}} \right); & \text{if otherwise,} \end{cases} \quad (4.37)$$

where $J_{(i)_{max}}$ is given by

$$J_{(i)_{max}} =$$

$$\max \left(\frac{\zeta_{i-(M-1)}}{\xi_{i-(M-1)} - \zeta_{i-(M-1)} \left[\mu \sum_{k=1}^{i-(M-1)-1} \xi_k + \sum_{n=i-(M-1)+1}^M \xi_n \right]}, \right. \\ \left. \frac{\zeta_{i-(M-2)}}{\xi_{i-(M-2)} - \zeta_{i-(M-2)} \left[\mu \sum_{k=1}^{i-(M-2)-1} \xi_k + \sum_{n=i-(M-2)+1}^M \xi_n \right]}, \dots, \right. \\ \left. \frac{\zeta_{i-(M-\ell)}}{\xi_{i-(M-\ell)} - \zeta_{i-(M-\ell)} \left[\mu \sum_{k=1}^{i-(M-\ell)-1} \xi_k + \sum_{n=i-(M-\ell)+1}^M \xi_n \right]} \right). \quad (4.38)$$

where $\ell \in (1, 2, \dots, M)$.

4.3.3 Average Achievable Rate for V-VLC

In this subsection, we derive the expression for average achievable rate for V_1 and V_2 . Using the fact that $\mathbb{E}[X] = \int_0^\infty \mathbb{P}[X > t] dt$ for real-valued random variables with non-negative support, the expression for \mathcal{R}_{V_1} for OPD NOMA case may be modified as

$$\begin{aligned} \mathcal{R}_{V_1} &= \int_0^\infty \mathbb{P} \left[\frac{1}{2} \log_2 \left(1 + \frac{e}{2\pi} SIR_{V_1} \right) > t \right] dt, \\ &= \int_{t=0}^{\frac{1}{2} \log_2 \left(1 + \frac{e}{2\pi} \xi_1 \right)} \mathbb{P} \left[SIR_{V_1} > \frac{2\pi}{e} (2^{2t} - 1) \right] dt, \end{aligned} \quad (4.39)$$

$$= \int_t \mathbb{P} \left[\mathcal{I}_{VLC} < \frac{k(\xi_1 - \xi_2 \beta) P_{VLC} r_1^{2(m+1)} (h^2 + r_1^2)^{-(m+3)}}{\beta} \right] dt, \quad (4.40)$$

$$= \int_t \mathcal{F}_{\mathcal{I}_{VLC}} \left(\frac{k(\xi_1 - \xi_2 \beta) P_{VLC} r_1^{2(m+1)} (h^2 + r_1^2)^{-(m+3)}}{\beta} \right) dt. \quad (4.41)$$

where $\beta = \frac{2\pi}{e} (2^{2t} - 1)$ and $\mathcal{F}_{\mathcal{I}_{VLC}}(\cdot)$ denotes the CDF of interference caused from V2V communication. This CDF expression can be expressed as [36],

$$\mathcal{F}_{\mathcal{I}_{VLC}}(x) = \xi_c \left(\sqrt{\frac{\pi(\rho\lambda)^2 z}{4x}} \right), \quad (4.42)$$

where ξ_c is the complementary error function.

The average achievable rate associated with vehicle V_2 , denoted by \mathcal{R}_{V_2} is represented as

$$\mathcal{R}_{V_2} = \mathbb{E} \left[\frac{1}{2} \log_2 \left(1 + \frac{e}{2\pi} SIR_{V_2} \right) \right], \quad (4.43)$$

Thus, the expression of \mathcal{R}_{V_2} is given by

$$\mathcal{R}_{V_2} = \int_{t=0}^{\frac{1}{2} \log_2 \left(1 + \frac{e}{2\pi} \frac{\xi_2}{\mu \xi_1} \right)} \mathbb{P} \left[\frac{1}{2} \log_2 \left(1 + \frac{e}{2\pi} SIR_{V_2} \right) > t \right] dt, \quad (4.44)$$

$$= \int_t \mathcal{F}_{\mathcal{I}_{VLC}} \left(\frac{k(\xi_2 - \xi_1 \mu \beta) P_{VLC} r_2^{2(m+1)} (h^2 + r_2^2)^{-(m+3)}}{\beta} \right) dt. \quad (4.45)$$

The expression of the average achievable rate at the user V_i when OPD NOMA is considered is given by

$$\mathcal{R}_{V_i} = \int_{t=0}^{v_{sup}} \mathcal{F}_{\mathcal{I}_{VLC}} \left(\frac{k(\xi_i - \beta [\mu \sum_{h=1}^{i-1} \xi_h + \sum_{n=i+1}^M \xi_n])}{\beta} P_{VLC} r_i^{2(m+1)} (h^2 + r_i^2)^{-(m+3)} \right) dt, \quad (4.46)$$

where $v_{sup} = \frac{1}{2} \log_2 \left(1 + \frac{e}{2\pi} \frac{\xi_i}{\mu \sum_{h=1}^{i-1} \xi_h + \sum_{n=i+1}^M \xi_n} \right)$.

For OMA case, the average achievable rate at the receiving node, V_i , denoted by $\mathcal{R}_{V_i}^{(OMA)}$, can be expressed as³

$$\mathcal{R}_{V_i}^{(OMA)} = \int_{t=0}^{\infty} \mathbb{P} \left[\frac{1}{4} \log_2 \left(1 + \frac{e}{2\pi} SIR_{V_i} \right) > t \right] dt = \int_t \mathcal{F}_{\mathcal{I}_{VLC}} \left(\frac{k P_{VLC} r_i^{2(m+1)} (h^2 + r_i^2)^{-(m+3)}}{\beta'} \right) dt. \quad (4.47)$$

where $\beta' = \frac{2\pi}{e} (2^{4t} - 1)$.

4.3.4 Average Achievable Rate for V-RF

In this case, the maximum achievable capacity for vehicle V_i is given as $\log_2(1 + SIR_{V_i})$. Following the similar steps as in OPD-NOMA, the average achievable rate associated with V_1

³Notice that the achievable rate is multiplied by $\frac{1}{2}$ since we assume bandwidth splitting in OMA.

can be given as

$$\mathcal{R}_{V_1} = \int_{v=0}^{\log_2(1+\frac{\xi_1}{\xi_2})} \mathbb{P}[SIR_{V_1} > 2^v - 1] dv = \int_v \mathcal{L}_{\mathcal{I}_{RF}} \left(\frac{2^v - 1}{(\xi_1 - (2^v - 1)\xi_2) P_{RF} G_t G_r \ell (h^2 + r_1^2)^{-\frac{\alpha}{2}}} \right) dv. \quad (4.48)$$

Then, the average achievable rate related to V_2 can be expressed as

$$\mathcal{R}_{V_2} = \int_{v=0}^{\log_2(1+\frac{\xi_2}{\mu\xi_1})} \mathbb{P}[SIR_{V_2} > 2^v - 1] dv, \quad (4.49)$$

$$= \int_v \mathcal{L}_{\mathcal{I}_{RF}} \left(\frac{2^v - 1}{(\xi_2 - (2^v - 1)\mu\xi_1) P_{RF} G_t G_r \ell (h^2 + r_2^2)^{-\frac{\alpha}{2}}} \right) dv. \quad (4.50)$$

The average achievable rate associated with vehicle V_i , denoted by \mathcal{R}_{V_i} can be expressed as

$$\mathcal{R}_{V_i} = \int_0^{v_{sup}} \mathcal{L}_{\mathcal{I}_{RF}} \left(\frac{2^v - 1}{(\xi_i - \beta \left[\mu \sum_{h=1}^{i-1} \xi_h + \sum_{n=i+1}^M \xi_n \right]) P_{RF} G_t G_r \ell (h^2 + r_2^2)^{-\frac{\alpha}{2}}} \right) dv. \quad (4.51)$$

where $\beta = 2^v - 1$ and $v_{sup} = \log_2(1 + \frac{\xi_i}{\mu \sum_{h=1}^{i-1} \xi_h + \sum_{n=i+1}^M \xi_n})$.

Again for OMA case, the average achievable rate at the receiving node, V_i , denoted by $\mathcal{R}_{V_i}^{(OMA)}$, can be expressed as

$$\mathcal{R}_{V_i}^{(OMA)} = \int_{v=0}^{\infty} \mathcal{L}_{\mathcal{I}_{RF}} \left(\frac{2^{2v} - 1}{P_{RF} G_t G_r \ell (h^2 + r_i^2)^{-\frac{\alpha}{2}}} \right) dv. \quad (4.52)$$

4.4 Numerical Results

In this section, we present results that corroborate our theoretical findings. The system model parameters used for the analysis are summarized in Table 4.1. We present the down link performance of OPD-NOMA with perfect SIC as well as error propagation due to imperfect SIC in presence of several system model parameters. The distance between transmitter and receiver is set to $\|S - V_1\|=40$ m and $\|S - V_2\|=47$ m. In order to validate the accuracy of our theoretical findings, Monte Carlo simulations are performed by averaging over 10,000

realizations of PPPs and fading channel parameters⁴. We consider a worst case scenario where interference from V2V arise from infinite road segment ($\mathcal{B} = \mathbb{R}^1$).

Table 4.1: System Model Parameters

Parameter	Symbol	Value
Lambertian Order	m	1 [104]
PD active detection area	A_d	1 cm^2 [104]
LED semi-angle	$\Phi_{\frac{1}{2}}$	70°
Transmission power for VLC	P_{VLC}	33 dBm[68]
VLC System Bandwidth	B_s	20 MHz
Responsivity of the PD	\mathcal{R}	0.54 A/W [104]
Absolute temperature	T_k	298° K
Transmission power for VLC	P_{VLC}	23 dBm[68]
RF System Bandwidth	B_s	10 MHz
Transmitter antenna gain	G_t	3dBi
Receiver antenna gain	G_r	3dBi
Optical filter gain	$T_s(\Psi_k)$	1
Noise power spectral density	N_o	$10^{-21} A^2 / Hz$
Refractive index	n	1.5
Path loss exponent	α	2
Power allocation coefficient	ζ	0.5-1
Inter-lane spacing	L	10 m[68]
Height of RSU	h	10 m

Fig. 4.4(a) shows the relationship between outage probability of OPD NOMA and vehicular density, λ . In traffic flow theory, the vehicular density denotes the number of vehicles per kilometer (km) in a traffic lane. We set power allocation coefficient, ξ_1 and access probability ρ to be 0.85 and 0.02 respectively. Keeping in view different data requirement by each user, the target data rate of V_2 is assumed to be greater than V_1 . It can be observed from Fig. 4.4(a) that as expected, the outage probability increases as vehicular density increases. We also compare

⁴The Monte carlo simulation procedure are described as follows. It may be noted that the vehicles are deployed over a length of 10,000 m, and the interference is summed at the origin as per (4.12) and preserved. The scenario is repeated for at least 10,000 times in order to obtain the statistics of the interference. Given our simulation settings, we further calculate the SIR as per (4.11) and (4.14) and count the number of times for which SIR not larger than the threshold β , accordingly the simulated outage probability is computed as:

$$\hat{\mathcal{P}}_O = \frac{\sum_{m=1}^N 1_{SIR \leq \beta}}{N} \quad (4.53)$$

where N denotes the total number of simulation runs respectively. The simulation has been performed using the MATLAB software.

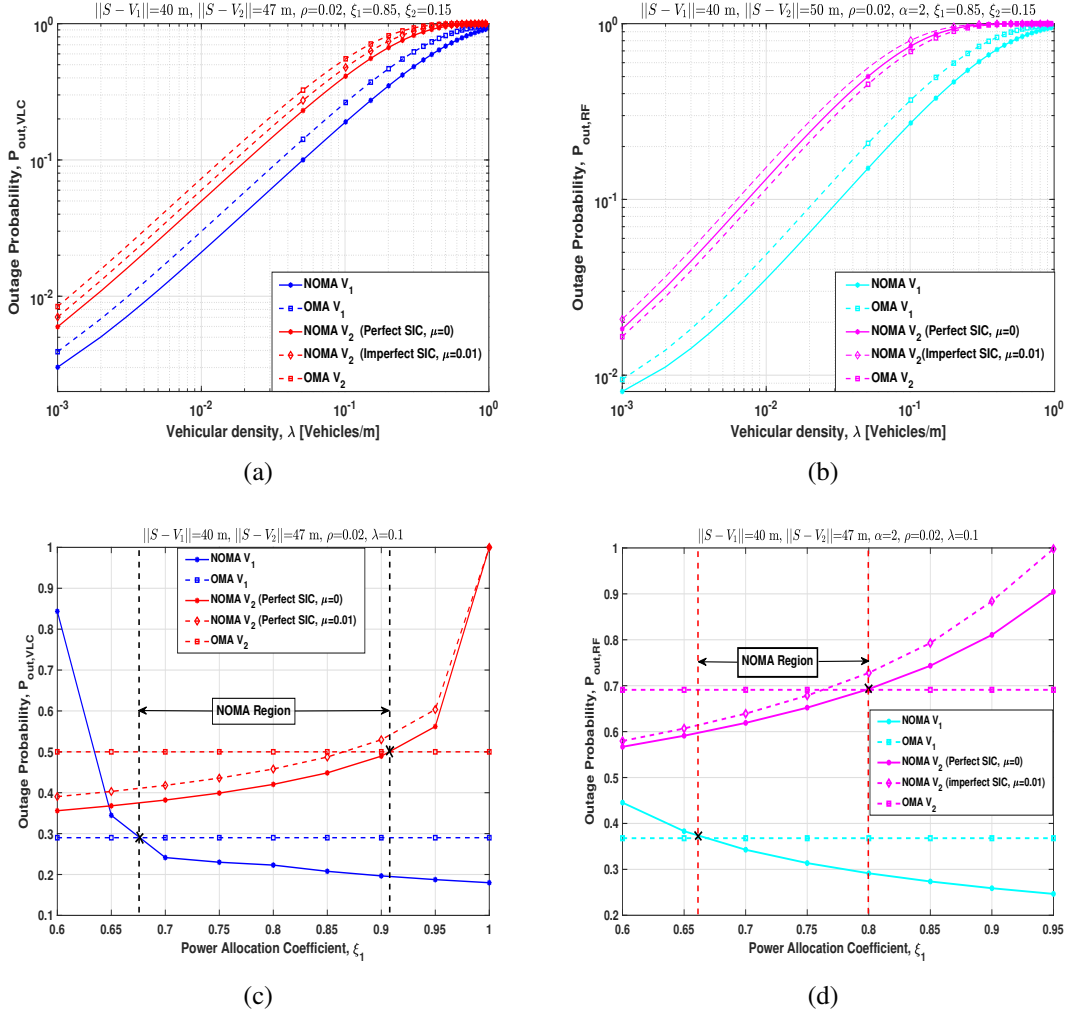


Figure 4.4: Outage Probability, $\mathcal{P}_{out,VLC}$ as a function of vehicular density, λ : (a) V-VLC, and (b) V-RF. Impact of power allocation coefficient, ξ_1 : (c) V-VLC, and (d) V-RF.

the OMA and NOMA systems for the case of two users. We can observe that the outage performance of each vehicle of OPD NOMA system is superior to OMA system for vehicle V_1 as well as V_2 . This is due to fact that the diversity order of the NOMA system is typically higher than OMA system[105]. In order to evaluate the potential trade off between OPD-NOMA based V-VLC systems and V-RF systems, we compare our result with conventional V-RF OMA and NOMA system. It is noteworthy that the outage performance of NOMA is sensitive to the values of power allocation coefficient, source-destination distance and target data rate threshold.

Fig. 4.4(b) depicts outage probability as a function of vehicular density for V-RF communication. Again similar insights can be obtained. Surprisingly, OMA system is superior than that of NOMA system for UE-2. As mentioned before, the power allocation coefficient, ξ_1 indeed

affects the outage performance. Interestingly, a suitable choice of power allocation coefficient decides the NOMA outage probability. For ease of validation and visualization, we also plot outage probability, $\mathcal{P}_{out,VLC}$ as a function of power allocation coefficient, ξ_1 as can be seen in Fig. 4.4(c).

From Fig. 4.4(c), we notice that in OPD NOMA, when power allocation coefficient, ξ_1 increases, $\mathcal{P}_{O_{V_1}}$ decreases, while $\mathcal{P}_{O_{V_2}}$ increases. Next, if we compare NOMA and OMA outage performance, we observe that, for V_1 , OMA performs better as compared to NOMA when $\xi_1 \in [0.6, 0.67]$. This is mainly because lower values of ξ_1 means low power is being allocated to V_1 , while high power is allocated to V_2 which increases the interference at V_1 . Conversely, we can observe that when $\xi_1 \in [0.67, 1]$, OPD NOMA performs superior as compared to OMA. This is due to the fact that V_1 is allocated more power, while less power is allocated to V_2 . For V_2 , we see that OMA outperforms NOMA only when $\xi_1 \in [0.91, 1]$. This is true because, for large values of ξ_1 , V_2 is allocated a small amount of power, thus decreasing the SIR at V_2 and results in increased outage probability. In nutshell, both users exhibit superior NOMA performance over OMA system when $\xi_1 \in [0.67, 0.91]$. In fact, OPD NOMA offers quite wider choice of power allocation coefficient as compared to V-RF NOMA as evident from Fig. 4.4(c). We can observe from Fig. 4.4(d) that for V_1 , when $\xi_1 \in [0.66, 1]$, V-RF NOMA outperforms V-RF OMA system. On other hand, for V_2 , when $\xi_1 < 0.8$, V-RF NOMA outperforms V-RF OMA system. It can be noted that the benefit of NOMA over OMA system can be exploited when $\xi_1 \in [0.66, 0.8]$. However, with error propagation due to imperfect SIC ($\mu = 0.01$), the range of ξ_1 shrinks to $[0.68, 0.76]$. Next, we compare NOMA performance for

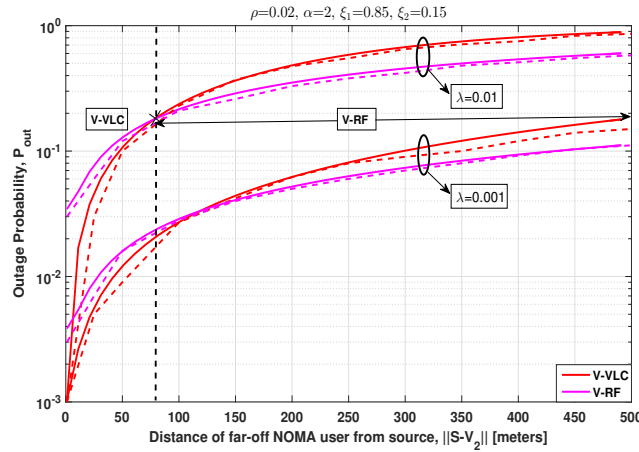


Figure 4.5: Comparison of analytical (solid line) and simulation (dashed line) results for outage probability, \mathcal{P}_{out} versus distance of far-off NOMA user for OPD NOMA based V-VLC link (red) and NOMA based V-RF link (magenta)

V-VLC and V-RF link depending on location of far-off users. We can observe from Fig. 4.5

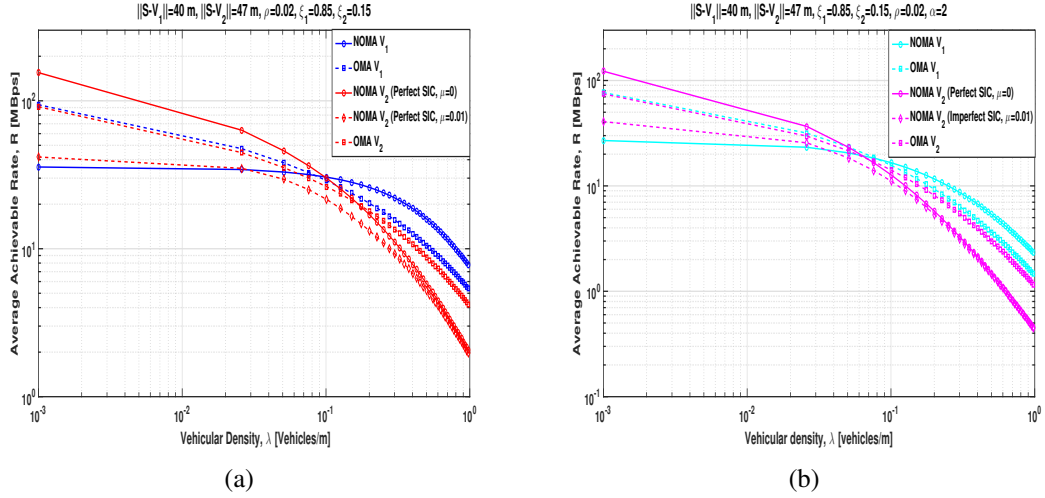


Figure 4.6: Average achievable rate, \mathcal{R} variation with vehicular density, λ : (a) V-VLC, and (b) V-RF.

that when location of far-off NOMA user from source, $\|S - V_2\|$ increases, outage probability also increases. Also, the outage performance of standalone V-VLC link is comparatively better than standalone V-RF for low communication range. For instance, when interfering vehicular density, $\lambda=0.01$, the outage performance of V-VLC link is better compared to V-RF Link when distance of far-off NOMA user from source, $\|S - V_2\|$ is upto 80 m. However, V-RF is reliable option for long distance communication. In nutshell, there exists tradeoff between NOMA based V-VLC and V-RF link depending upon the location of NOMA user from source.

Fig. 4.6 illustrates the relationship between average achievable rate and vehicular density, λ . We observe that the vehicle V_2 has a larger average achievable rate than V_1 . This is due to the fact that V_2 does not experience extra interference. In contrast, this trend holds true only for low values of vehicular density. For high vehicular density, the performance of V_2 decreases drastically. We can also observe that V_1 are more robust to the interference for higher values of λ . For such highly dense environment ($\lambda > 0.1$), V_1 has better achievable rate than V_2 . Fig. 4.6b shows average achievable rate as a function of vehicular density, λ for V-RF communication. Again, the average achievable rate for V_2 is larger than V_1 for low vehicular density. In comparison with OPD NOMA, irrespective of traffic intensity, V-RF NOMA has always lower average achievable rate for both the users especially for lower values of vehicular density ($\lambda < 0.1$). It should be noted again that the average achievable rate also depends on power allocation coefficient, source- destination distance and target rate thresholds.

Next, we plot the behaviour of average achievable rate variation with power allocation coefficient, ξ_1 in Fig. 4.7. We observe from Fig. 4.7a that in OPD NOMA, when power allocation coefficient, ξ_1 increases, \mathcal{R}_{V_2} decreases, while \mathcal{R}_{V_1} increases. In particular when

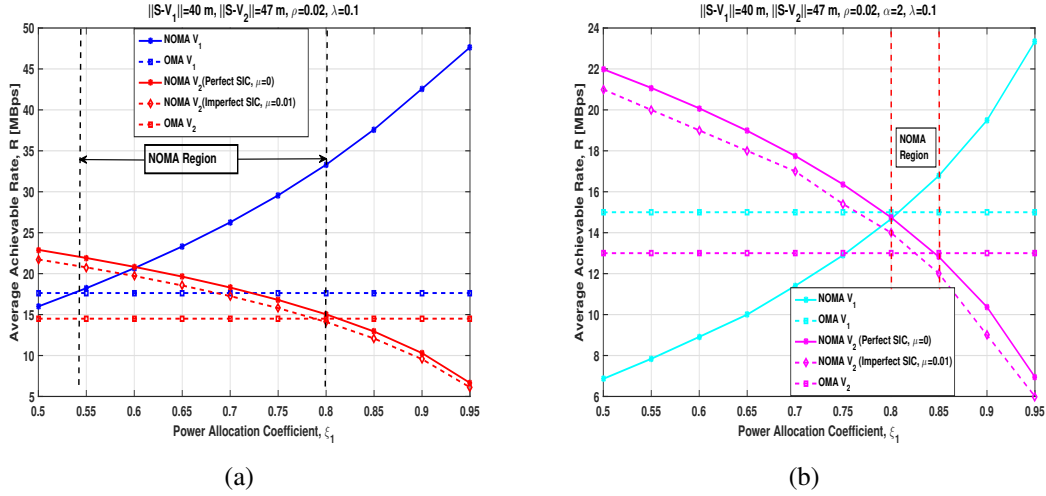


Figure 4.7: Average achievable rate, \mathcal{R} of V-RF as a function of power allocation coefficient, ξ_1 : (a) V-VLC, and (b) V-RF.

$\xi_1 < 0.8$, average achievable rate of V_2 with OPD NOMA is greater than OMA. When $\xi_1 > 0.54$, OPD NOMA exhibits better performance as compared to OMA in terms of average achievable rate for V_1 . This implies that as ξ_1 increases, V_1 is allocated more power, while less power is allocated to V_2 , therefore the average achievable rate of V_1 increases, on other hand, the average achievable rate of V_2 decreases. At same time, we can also observe that when $\xi_1 \in [0.54, 0.8]$, OPD NOMA could able to achieve better average rate for both V_1 and V_2 as compared to OMA system. For comparison purpose, we also plot the average achievable rate as a function of power allocation coefficient for V-RF communication. We can observe from Fig. 4.7b that when $\xi_1 \in [0.8, 0.85]$, NOMA achieves better average rate for both V_1 and V_2 compared to OMA system.

4.5 Concluding Remarks

In this work, we explore the potential benefit and research challenges involved with practical implementation of downlink OPD NOMA based V2X network for broadcasting road safety related information. We compare the performance of proposed downlink OPD NOMA based V2X network with OMA system using stochastic geometry tools. We show that the proposed OPD NOMA based V2X network offers improved performance in terms of outage performance, and average achievable rate as compared to conventional RF NOMA based V2X network. However, there also exists tradeoff between NOMA based V-VLC and V-RF link depending upon the location of NOMA user from source.

It may be noted that several open research challenges such as power imbalance among vehicles, impact of channel symmetry, power allocation techniques under feedback delay, synchronization in a high-mobility scenario, non linear distortion in OPD-NOMA, co-existence of V-VLC and V-RF, etc are yet to be explored. However, we believe that the presented contribution may serve as a valuable resource for future invention, optimal planning and development of next generation VLC based intelligent transportation system. Undoubtedly, uplink OPD NOMA can be a potential future direction of research for beyond 5G enabled V2X network.

Part II

4.6 Overview of Part II

Vehicle-to-everything (V2X) communication aims to achieve significantly improved safety and traffic efficiency, more particularly at road intersection where high percentage of accidents usually occur. The existing vehicular radio frequency (V-RF) based V2X utilizes relaying for improving safety message dissemination at road intersections. For a high traffic density scenario, the V-RF communication with relaying solution may suffer from large latency and low packet delivery rates due to channel congestion. In this work, we propose to use NOMA enabled hybrid V-VLC/V-RF communication systems to address this problem. In particular, the main motivation is to mitigate the effects of shadowing caused by blockages⁵ such as building and other obstructions at road intersection. Moreover, such a scheme can also facilitate more reliable communication in the case of non-line-of-sight (NLoS) transmission. Our novel contributions against previously published works are shown in Table I. More specifically, the main contributions of this research paper are summarized as follows:

1. We explore a cooperative NOMA enabled hybrid V-VLC/V-RF solution for improving safety message dissemination and enabling massive connectivity among vehicles particularly at road intersection scenario. The superiority of the proposed V2X solution is validated by comparing it with conventional V-RF communication system.
2. We develop tractable analytical expression for such NOMA enabled hybrid vehicular communication system in terms of outage probability and average achievable rate using

⁵Empirical measurements showed that due to such blockages, the strength of received V2V signal drops rapidly over distance away from the intersection [106]. As a consequence, vehicles located in perpendicular streets may not be able to communicate well with each other, resulting in a significant decrease in V2V communication performance.

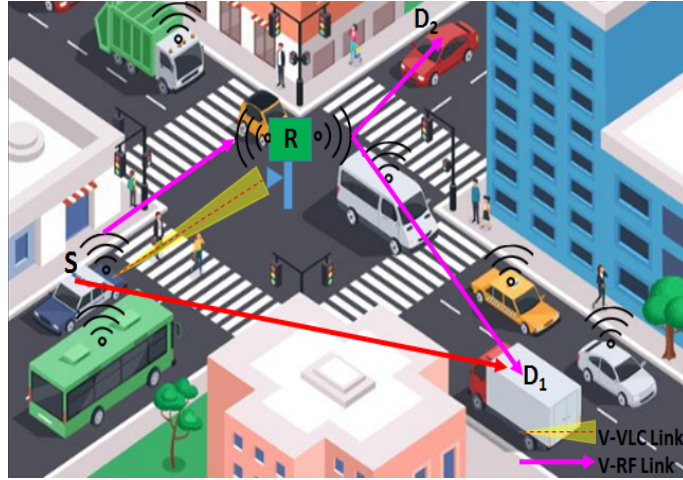


Figure 4.8: Real life application scenario: At road intersection, vehicles in blocked LOS (dashed red line) can communicate via C-NOMA supported hybrid V-VLC/V-RF systems. The SR link can either be V-VLC (red color line) or V-RF (solid magenta line) link, while $RD_{1,2}$ link is a V-RF link.

various analytical tools of stochastic geometry. The proposed analysis is then extended to generic NOMA scheme with K destination vehicles, where $K > 2$.

3. We also examine the impact of vehicles headlights radiation pattern viz. Lambertian and empirical path loss model on statistical characterization of the proposed hybrid solution. Moreover, we compare the performance of NOMA with conventional OMA scheme and show that NOMA leads to improved performance for the proposed system.

4.7 System Model and Assumptions

4.7.1 Network Scenario

A typical road intersection scenario involving cooperative NOMA transmission between a source vehicle, S and two destination vehicles, D_1 and D_2 with the help of a relay node, R has been shown in Fig. 4.8. The proposed analysis can be extended to generalized form for K destination vehicles where $K > 2$. The relay node is assumed to be kept at the road intersection, where the two perpendicular roads, horizontal road X and vertical road Y , cross each other. We assume the communication from a single source vehicle to multiple destination vehicles applying decode and forward (DF) strategy via relay node [107]. For sake of analysis, we consider a realistic scenario, where all the destination vehicles do not require the same amount of data rate, that is, D_1 can be a vehicle which needs to be served immediately with a lower

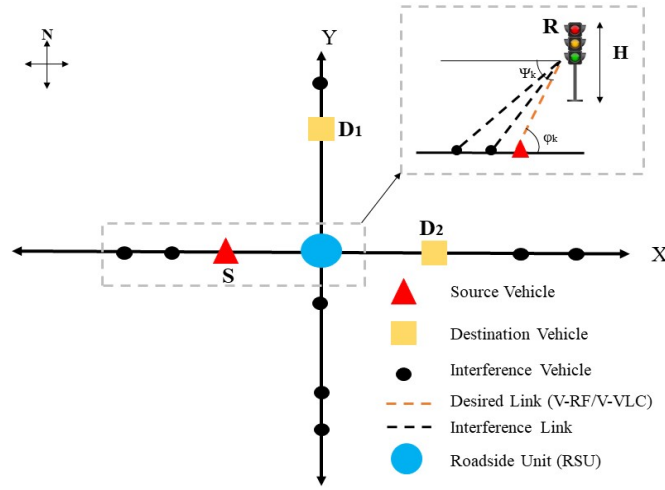


Figure 4.9: Abstraction model of the considered scenario. The source vehicle is marked with red triangle, destination vehicles are marked with yellow squares, and interfering vehicles with black circles. The desired link is represented by red dotted line and the interference link is represented by black dotted line. H denotes the height of the traffic light.

data rate whereas D_2 has a lower priority with a higher data rate⁶. As per insights shared in [99], we also consider that vehicles can control the transmit power of optical signals. Half duplex transmission is employed where the transmission occurs in two phases. In the first phase, reception occurs where R , D_1 and D_2 receives the message from S ($S \rightarrow R$, $S \rightarrow D_1$, $S \rightarrow D_2$) and in the second phase, the message received at R is broadcasted to the destination vehicles D_1 and D_2 ($R \rightarrow D_1$, $R \rightarrow D_2$). Each of these phases lasts one time slot and the message received at D_1 and D_2 in the two phases are decoded after MRC. Fig. 4.9 provides an abstract model of the proposed network scenario.

A hybrid VLC-RF based V2X scenario is considered, where SR link can be either VLC link or an RF link, while SD and RD are RF links as shown in Fig. 4.10. A hybrid transmission without MRC implies that the communication takes place between $S \rightarrow R$ and $R \rightarrow D$, whereas the hybrid transmission with MRC implies that the communication occurs between $S \rightarrow R$, $R \rightarrow D$ and $S \rightarrow D$. During $S \rightarrow R$ transmission, only one of the links is operational at a given time instant based on QoS requirement. For instance, when SIR of V-VLC link is above a threshold value, the system keeps on operating with V-VLC link. However, as distance of the source vehicle S from R becomes large, the quality of V-VLC link degrades, as a consequence V-RF link is then activated. The SR link goes to outage only when both V-VLC and V-RF link falls in outage [112].

⁶Unlike [39, 108], we consider a more realistic assumption that the destination vehicular nodes are prioritize according to their quality of service (QoS) requirements as reported in [109–111].

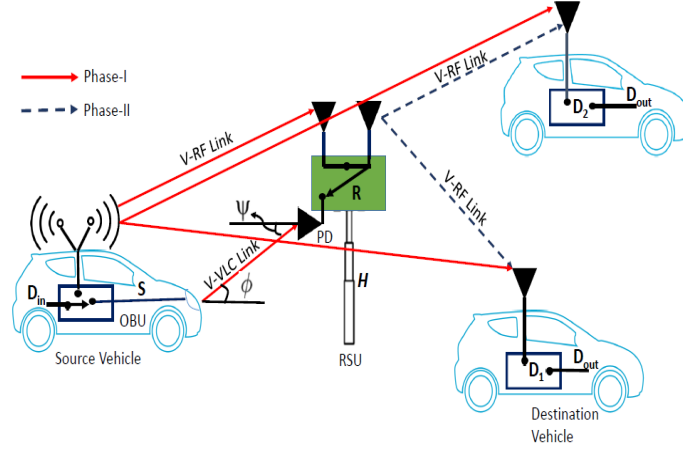


Figure 4.10: Illustration of cooperative NOMA aided hybrid VLC-RF based V2X with relaying.

The triplet set $\{S, R, D\}$ are subject to interference that are originated from vehicles on roads. The set of interfering vehicles can be denoted by φ_X and φ_Y on X and Y road respectively. These are distributed according to 1D-HPPP, expressed as, $\varphi_X \sim 1D\text{-HPPP}(\lambda_X, x)$ and $\varphi_Y \sim 1D\text{-HPPP}(\lambda_Y, y)$, where x and λ_X and y and λ_Y are the position of interfering vehicles and their intensity on the X and Y road respectively. We assume that the vehicular nodes employ slotted Aloha protocol with parameter ρ , where each node can access the medium with an access probability ρ . In this study, we consider Empirical modelling based realistic asymmetrical angular distribution of the radiation intensity pattern of light source. Assuming no attenuation loss, the channel DC gain for V-VLC system can be given as [113],

$$H(0) = \left(\frac{D_R \cos(\psi_i)^{\frac{1}{\varepsilon}}}{\zeta L_i} \right)^2 \quad (4.54)$$

where D_R and ψ denote the aperture diameter and angle of irradiance. Here, $\cos \psi_i = \frac{d_i}{\sqrt{d_i^2 + H^2}}$ and d_i is the distance between i^{th} transmitter and the intersection. The two correction coefficients (ε and ζ) take into account the asymmetrical pattern of the headlamp and weather conditions [113]. $L_i = \sqrt{d_i^2 + H^2}$ which is expressed as the propagation distance between the i^{th} transmitter to the relay.

For V-RF communication, the fading coefficient for the links source-to-relay, source-to-destination and relay-to-destination denoted by, h_{SR} , h_{SD} and h_{RD} respectively are modeled as $\sim \mathcal{N}(0, 1)$. Given a RF link, the power fading coefficient ($|h_{SR}|^2$, $|h_{SD}|^2$, $|h_{RD}|^2$) is an exponential random variable with unit mean. Further, we consider a path loss model l_{pq} between the nodes p and q . For direct LOS between p and q , $l_{pq} = \|p - q\|_2^{-\alpha}$ where $\|p - q\|_2$ is the euclidean distance between node p and q , where $\|\cdot\|_2$ is l_2 norm, and α is the path loss

exponent. For non-line-of-sight propagation (NLOS), Manhattan model is used where $l_{xy} = \|p - q\|_1^{-\alpha}$ where $\|\cdot\|_1$ is l_1 norm [114]. For our case, the distance of vehicles from relay node is represented as, $(\sqrt{H^2 + d^2})^{-\alpha}$, where d is the distance of the vehicle from the intersection point and H is the height of relay.

The signal transmitted by source S , denoted by X_S , is a combination of the data intended to vehicular nodes D_1 and D_2 ,

$$X_S = \sqrt{a_1}X_{D_1} + \sqrt{a_2}X_{D_2}, \quad (4.55)$$

where a_1 and a_2 are the power allocation coefficient to vehicular nodes D_1 and D_2 such that $a_1 + a_2 = 1$. Here X_{D_1} and X_{D_2} are the signals intended to the destination nodes D_1 and D_2 . For V-VLC system, the received optical signal at R due to VLC link, denoted as Y_R^{VLC} , can be given as,

$$Y_R^{VLC} = \mathcal{R}hX_S + \sqrt{I_{VLC}}, \quad (4.56)$$

where \mathcal{R} denotes the responsivity of PD, and I_{VLC} is the combined interference experienced at the relay node R from vehicles in adjacent lanes. It can be given as,

$$I_{VLC} = \sum_{r_i \in \Phi} z \frac{P_{VLC} r_i^{\frac{4}{\epsilon}}}{(H^2 + r_i^2)^{\frac{2\epsilon+2}{\epsilon}}}, \quad (4.57)$$

where $z = \mathcal{R}^2 \left(\frac{D_R}{\zeta}\right)^4$, r_i is the distance of interfering vehicles from intersection and P_{VLC} denotes the transmission power for VLC.

For V-RF link, the signal received at relay node R during $S \rightarrow R$ transmission, denoted as Y_R^{RF} , can be expressed as,

$$Y_R^{RF} = h_{SR}\sqrt{l_{SR}}X_S + \sum_{x \in \Phi_{X_R}} h_{Rx}\sqrt{l_{Rx}}X_x + \sum_{y \in \Phi_{Y_R}} h_{Ry}\sqrt{l_{Ry}}X_y, \quad (4.58)$$

where X_x and X_y represent the message transmitted by the interfering nodes x and y respectively and l_{Rx} and l_{Ry} denote the path loss model between vehicular node R and interfering node x or y . The signal received at the vehicular node D_i during $S \rightarrow D_i$ transmission, denoted as Y_{D_i} , can be given as,

$$Y_{D_i} = h_{SD_i}\sqrt{l_{SD_i}}X_S + \sum_{x \in \Phi_{X_{D_i}}} h_{D_ix}\sqrt{l_{D_ix}}X_x + \sum_{y \in \Phi_{Y_{D_i}}} h_{D_iy}\sqrt{l_{D_iy}}X_y, \quad (4.59)$$

where l_{D_ix} denotes the path loss model between vehicular node D_i and interfering node x . The signal received at vehicular node D_i during $R \rightarrow D_i$ transmission, denoted as Y_{RD_i} , can be

represented as,

$$Y_{RD_i} = h_{RD_i} \sqrt{l_{RD_i}} X_R + \sum_{x \in \Phi_{X_{D_i}}} h_{D_i x} \sqrt{l_{D_i x}} X_x + \sum_{y \in \Phi_{Y_{D_i}}} h_{D_i y} \sqrt{l_{D_i y}} X_y. \quad (4.60)$$

4.8 Performance Analysis

In the following, we evaluate the performance of the system model using outage probability and average achievable rate as the performance metrics.

4.8.1 Outage Probability for V-VLC

An outage is said to occur when the instantaneous SINR drops below a certain threshold value. For an interference limited scenario, we first evaluate the SIR at each of the receiving nodes, and then define outage probability associated with them. The vehicular node D_1 is assumed to receive information with higher power than node D_2 , therefore it will decode first according to SIC decoding and interference would be due to D_2 . The SIR at R due to VLC link, denoted as $\gamma_{SR_1}^{VLC}$, can be expressed as,

$$\gamma_{SR_1}^{VLC} = \frac{z a_1 P_{VLC} d_0^{\frac{4}{\epsilon}} (H^2 + d_0^2)^{-\left(\frac{2\epsilon+2}{\epsilon}\right)}}{z a_2 P_{VLC} d_0^{\frac{4}{\epsilon}} (H^2 + d_0^2)^{-\left(\frac{2\epsilon+2}{\epsilon}\right)} + I_{VLC}}, \quad (4.61)$$

where d_0 is the distance between source node S and relay node R .

The relay R will first retrieve the information from D_1 vehicle, denoted as $\gamma_{SR_{2-1}}^{VLC}$, is expressed as⁷,

$$\gamma_{SR_{2-1}}^{VLC} = \frac{z a_1 P_{VLC} d_0^{\frac{4}{\epsilon}} (H^2 + d_0^2)^{-\left(\frac{2\epsilon+2}{\epsilon}\right)}}{z a_2 P_{VLC} d_0^{\frac{4}{\epsilon}} (H^2 + d_0^2)^{-\left(\frac{2\epsilon+2}{\epsilon}\right)} + I_{VLC}}. \quad (4.62)$$

The SIR at relay node to decode the data associated with vehicular node D_2 , denoted as $\gamma_{SR_2}^{VLC}$, is represented as,

$$\gamma_{SR_2}^{VLC} = \frac{z a_2 P_{VLC} d_0^{\frac{4}{\epsilon}} (H^2 + d_0^2)^{-\left(\frac{2\epsilon+2}{\epsilon}\right)}}{I_{VLC}}. \quad (4.63)$$

Let us denote the outage event associated with vehicular node D_1 at R as $O_{SR_1}^{VLC}$. The outage event at R when vehicular node D_2 is unable to retrieve the data associated with D_1 is denoted as $O_{SR_{2-1}}^{VLC}$. The outage at R when D_2 node is unable to retrieve its own data is denoted by $O_{SR_2}^{VLC}$.

⁷Perfect SIC has been considered which implies that there is no fraction of power left after SIC decoding process [115].

These outage events can be expressed as,

$$\begin{aligned} O_{SR_1}^{VLC} &= \{\gamma_{SR_1}^{VLC} < \theta_1\}, \\ O_{SR_{2-1}}^{VLC} &= \{\gamma_{SR_{2-1}}^{VLC} < \theta_1\}, \\ O_{SR_2}^{VLC} &= \{\gamma_{SR_2}^{VLC} < \theta_2\}, \end{aligned} \quad (4.64)$$

where $\theta_1 = \frac{2\pi}{e}(2^{C_1} - 1)$ and $\theta_2 = \frac{2\pi}{e}(2^{C_2} - 1)$ and C_1 and C_2 are the target data rates of vehicular nodes D_1 and D_2 respectively.

We now calculate the outage probability associated with the relay node R by using the moment generating functional (MGF) approach. The outage probability at R due to vehicular node D_1 , denoted as $P_{O_{R_1}}^{VLC}$, can be calculated by using [116, Eq. (19)],

$$P_{O_{R_1}}^{VLC} \approx 1 - \frac{2^{-F} \exp\left(\frac{E}{2}\right)}{\theta_1^{-1}} \sum_{f=0}^F \binom{F}{f} \sum_{g=0}^{G+f} \frac{(-1)^g}{H_g} \text{Re} \left(\frac{\mathcal{L}_Z(s)}{s} \right). \quad (4.65)$$

In (4.65), $\mathcal{L}_Z(s)$ denotes Laplace transform of the probability distribution of a random variable, Z which can be expressed as [36, Eq. 23],

$$\mathcal{L}_Z(s) = \mathbb{E}_I \left\{ \exp \left(- \frac{sI_{VLC}}{z(a_1 - \theta_1 a_2) P_{VLC} d_0^{\frac{4}{\epsilon}} (H^2 + d_0^2)^{-(\frac{2\epsilon+2}{\epsilon})}} \right) \right\} \quad (4.66)$$

$$= \mathbb{E}_r \left\{ \prod_{i=1}^N \exp \left(- \frac{s}{z(a_1 - \theta_1 a_2) d_0^{\frac{4}{\epsilon}} (H^2 + d_0^2)^{-(\frac{2\epsilon+2}{\epsilon})}} \frac{zr_i^{\frac{4}{\epsilon}}}{(H^2 + r_i^2)^{\frac{2\epsilon+2}{\epsilon}}} \right) \right\}. \quad (4.67)$$

The expectation in (4.67) can be solved using probability generating functional laplace (PGFL) defined for a homogeneous Poisson point process [117].

$$\begin{aligned} & \mathbb{E}_r \left\{ \prod_{i=1}^N \exp \left(- \frac{s}{z(a_1 - \theta_1 a_2) d_0^{\frac{4}{\epsilon}} (H^2 + d_0^2)^{-(\frac{2\epsilon+2}{\epsilon})}} \frac{zr_i^{\frac{4}{\epsilon}}}{(H^2 + r_i^2)^{\frac{2\epsilon+2}{\epsilon}}} \right) \right\} \\ &= \exp \left[- \rho \lambda_D \int_{d_0}^{\infty} \left(1 - \exp \left(- \frac{s}{z(a_1 - \theta_1 a_2) d_0^{\frac{4}{\epsilon}} (H^2 + d_0^2)^{-(\frac{2\epsilon+2}{\epsilon})}} \frac{zr^{\frac{4}{\epsilon}}}{(H^2 + r^2)^{\frac{2\epsilon+2}{\epsilon}}} \right) \right) dr \right], \end{aligned} \quad (4.68)$$

where λ_D denotes the intensity of the interfering vehicles located on the roads. Eq.(4.68) can be solved using numerical methods that can be implemented using MATLAB. The outage probability at R associated with vehicular node D_2 can be calculated by using [36, Eq.(27)],

$$P_{O_{R_2}}^{VLC} = 1 - \mathbb{P}\left(\frac{I_{VLC}}{zP_{VLC}d_0^{\frac{4}{\varepsilon}}(H^2 + d_0^2)^{-\left(\frac{2\varepsilon+2}{\varepsilon}\right)}} < \min(B_1, B_2)\right), \quad (4.69)$$

where $B_1 = \frac{(a_1 - \theta_1 a_2)}{\theta_1}$ and $B_2 = \frac{a_2}{\theta_2}$.

Now, we extend the NOMA results to K vehicular nodes. The SIR at relay R associated with D_i to decode D_w due to the VLC link can be expressed as,

$$\gamma_{SR_i}^{VLC} = \frac{za_i P_{VLC} d_0^{\frac{4}{\varepsilon}} (H^2 + d_0^2)^{-\left(\frac{2\varepsilon+2}{\varepsilon}\right)}}{zP_{VLC} d_0^{\frac{4}{\varepsilon}} (H^2 + d_0^2)^{-\left(\frac{2\varepsilon+2}{\varepsilon}\right)} \left[\sum_{u=w+1}^K a_u \right] + I_{VLC}}, \quad (4.70)$$

here, when $u > K$, then $\sum_{u=w+1}^K a_u = 0$. Then, the outage probability at node R_i is expressed as [36],

$$P_{O_{R_i}}^{VLC} = \begin{cases} 1 - \mathbb{P}\left(\frac{I_{VLC}}{zP_{VLC}d_0^{\frac{4}{\varepsilon}}(H^2+d_0^2)^{-\left(\frac{2\varepsilon+2}{\varepsilon}\right)}} < B_{(i)\min}\right); & \text{else,} \\ 1; & \bigcup_{w=1}^K \frac{a_w}{\sum_{u=w+1}^K a_u} < \theta_w, \end{cases} \quad (4.71)$$

where $B_{(i)\min}$ is given as

$$B_{(i)\min} = \min\left(\frac{a_{i-(K-1)} - \theta_{i-(K-1)} \left[\sum_{u=i-(K-1)+1}^K a_u \right]}{\theta_{i-(K-1)}}, \frac{a_{i-(K-2)} - \theta_{i-(K-2)} \left[\sum_{u=i-(K-2)+1}^K a_u \right]}{\theta_{i-(K-2)}}, \dots, \frac{a_{i-(K-L)} - \theta_{i-(K-L)} \left[\sum_{u=i-(K-L)+1}^K a_u \right]}{\theta_{i-(K-L)}}\right), \quad (4.72)$$

4.8.2 Outage Probability for V-RF

We define the SIR at R due to D_1 as $\gamma_{SR_1}^{RF}$, expressed as,

$$\gamma_{SR_1}^{RF} = \frac{P_{RF}|h_{SR}|^2 l_{SR} a_1}{P_{RF}|h_{SR}|^2 l_{SR} a_2 + I_{X_R} + I_{Y_R}}, \quad (4.73)$$

where P_{RF} is the RF transmission power and I_{X_M} and I_{Y_M} denote the combined interference from perpendicular roads X and Y at M respectively. Here M signifies the receiving nodes, $M \in \{R, D_1, D_2\}$. I_{X_M} and I_{Y_M} can be expressed as,

$$\begin{aligned} I_{X_M} &= \sum_{x \in \Phi_{X_M}} P_{RF} |h_{M_x}|^2 l_{M_x}, \\ I_{Y_M} &= \sum_{y \in \Phi_{Y_M}} P_{RF} |h_{M_y}|^2 l_{M_y}. \end{aligned} \quad (4.74)$$

The SIR at relay node R to first retrieve the information from D_1 , denoted as $\gamma_{SR_{2-1}}^{RF}$, can be expressed as,

$$\gamma_{SR_{2-1}}^{RF} = \frac{P_{RF}|h_{SR}|^2 l_{SR} a_1}{P_{RF}|h_{SR}|^2 l_{SR} a_2 + I_{X_R} + I_{Y_R}}. \quad (4.75)$$

The SIR at node R associated with D_2 to retrieve its own data, denoted as $\gamma_{SR_2}^{RF}$, can be represented as,

$$\gamma_{SR_2}^{RF} = \frac{P_{RF}|h_{SR}|^2 l_{SR} a_2}{I_{X_R} + I_{Y_R}}. \quad (4.76)$$

Let us denote the outage event at R associated with vehicular node D_1 as $O_{SR_1}^{RF}$. Let $O_{SR_{2-1}}^{RF}$ be the outage event at R when vehicular node D_2 cannot retrieve the message associated with D_1 . The outage at R when D_2 vehicle is unable to decode its own data is denoted by $O_{SR_2}^{RF}$. These outage events can be expressed as,

$$\begin{aligned} O_{SR_1}^{RF} &= \{\gamma_{SR_1}^{RF} < \beta_1\}, \\ O_{SR_{2-1}}^{RF} &= \{\gamma_{SR_{2-1}}^{RF} < \beta_1\}, \\ O_{SR_2}^{RF} &= \{\gamma_{SR_2}^{RF} < \beta_2\}, \end{aligned} \quad (4.77)$$

where $\beta_1 = 2^{2C_1} - 1$ and $\beta_2 = 2^{2C_2} - 1$.

Having analysed these expressions, we now calculate the outage probability at relay node R associated with vehicular nodes D_1 and D_2 . The outage probability at R associated with D_1

node, denoted as $P_{O_{R_1}}^{RF}$, can be represented as [118],

$$\begin{aligned} P_{O_{R_1}}^{RF} &= \mathbb{P}(\gamma_{SR_1}^{RF} < \beta_1) \\ &= 1 - \mathcal{L}_{I_{X_R}} \left(\frac{A_1}{P_{RF} l_{SR}} \right) \mathcal{L}_{I_{Y_R}} \left(\frac{A_1}{P_{RF} l_{SR}} \right), \end{aligned} \quad (4.78)$$

where $A_1 = \frac{\beta_1}{a_1 - \beta_1 a_2}$ and $\mathcal{L}_{I_{X_R}}$ and $\mathcal{L}_{I_{Y_R}}$ denotes the Laplace transforms of the interfering vehicles at relay node R from road X and Y whose expressions can be calculated by using [116, Eq. (33)] as,

$$\begin{aligned} \mathcal{L}_{I_{X_R}}(s) &= \exp \left(\frac{-\rho \lambda_X \pi s P_{RF}}{\sqrt{H^2 + s P_{RF}}} \right), \\ \mathcal{L}_{I_{Y_R}}(s) &= \exp \left(\frac{-\rho \lambda_Y \pi s P_{RF}}{\sqrt{H^2 + s P_{RF}}} \right). \end{aligned} \quad (4.79)$$

Eq. (26) can be expressed in simplified form as,

$$P_{O_{R_1}}^{RF} = \begin{cases} 1 - \mathcal{G}_R \left(\frac{A_1}{P_{RF} l_{SR}} \right); & \text{otherwise,} \\ 1; & \beta_1 \geq \frac{a_1}{a_2}, \end{cases} \quad (4.80)$$

where $\mathcal{G}_M \left(\frac{C}{D} \right) = \mathcal{L}_{I_{X_M}} \left(\frac{C}{D} \right) \mathcal{L}_{I_{Y_M}} \left(\frac{C}{D} \right)$.

Similarly, the outage probability at R associated with vehicular node D_2 , denoted as $P_{O_{R_2}}^{RF}$, can be represented as,

$$P_{O_{R_2}}^{RF} = \begin{cases} 1 - \mathcal{G}_R \left(\frac{A_{\max}}{P_{RF} l_{SR}} \right); & \text{otherwise,} \\ 1; & \beta_2 \geq \frac{a_1}{a_2}, \end{cases} \quad (4.81)$$

where $A_2 = \frac{\beta_2}{a_2}$ and $A_{\max} = \max(A_1, A_2)$.

Assuming that V-VLC and V-RF links to be independent, the overall outage performance at relay node R associated with vehicular nodes D_1 and D_2 , denoted as $P_{O_{R_i}}$ where $i \in \{1, 2\}$, can be expressed as,

$$P_{O_{R_i}} = P_{O_{R_i}}^{RF} \times P_{O_{R_i}}^{VLC}. \quad (4.82)$$

The SIR at destination node D_1 to retrieve its own data when transmission occurs from $R \rightarrow D_1$ is expressed as,

$$\gamma_{RD_1} = \frac{P_{RF} |h_{RD_1}|^2 l_{RD_1} a_1}{P_{RF} |h_{RD_1}|^2 l_{RD_1} a_2 + I_{X_{D_1}} + I_{Y_{D_1}}}. \quad (4.83)$$

Now, as D_2 comes second in decoding order, it first retrieves the data associated with D_1 vehicle. The SIR, denoted as $\gamma_{RD_{2-1}}$, can be expressed as,

$$\gamma_{RD_{2-1}} = \frac{P_{RF}|h_{RD_2}|^2 l_{RD_2} a_1}{P_{RF}|h_{RD_2}|^2 l_{RD_2} a_2 + I_{X_{D_2}} + I_{Y_{D_2}}}. \quad (4.84)$$

The SIR at node D_2 to retrieve its own data can be represented as,

$$\gamma_{RD_2} = \frac{P_{RF}|h_{RD_2}|^2 l_{RD_2} a_2}{I_{X_{D_2}} + I_{Y_{D_2}}}. \quad (4.85)$$

Let O_{RD_1} be the outage event associated with D_1 . The outage event when D_2 node is unable to retrieve the data associated with vehicular node D_1 , denoted as $O_{RD_{2-1}}$. The outage when destination node D_2 is unable to decode its own data is denoted by O_{RD_2} . These outage events can be represented as,

$$\begin{aligned} O_{RD_1} &= \{\gamma_{RD_1} < \beta_1\}, \\ O_{RD_{2-1}} &= \{\gamma_{RD_{2-1}} < \beta_1\}, \\ O_{RD_2} &= \{\gamma_{RD_2} < \beta_2\}. \end{aligned} \quad (4.86)$$

The outage probability associated with vehicular node D_1 , denoted as $P_{O_{RD_1}}$, can be expressed as [118],

$$P_{O_{RD_1}} = \mathbb{P}(\gamma_{RD_1} < \beta_1) = 1 - \mathcal{L}_{I_{X_{D_1}}} \left(\frac{A_1}{P_{RF} l_{RD_1}} \right) \mathcal{L}_{I_{Y_{D_1}}} \left(\frac{A_1}{P_{RF} l_{RD_1}} \right),$$

where $\mathcal{L}_{I_{X_M}}$ and $\mathcal{L}_{I_{Y_M}}$ denotes the Laplace transforms of the interfering vehicles at destination nodes, D_1 and D_2 , from road X and Y whose expressions are governed by [115, Eq.(21), Eq.(22)].

Similarly, the outage probability associated with vehicular node D_2 , denoted as $P_{O_{RD_2}}$, can be expressed as,

$$P_{O_{RD_2}} = 1 - \mathbb{P}(\gamma_{RD_{2-1}} < \beta_1) \times \mathbb{P}(\gamma_{RD_2} < \beta_2) = 1 - \mathcal{L}_{I_{X_{D_2}}} \left(\frac{A_{\max}}{P_{RF} l_{RD_2}} \right) \mathcal{L}_{I_{Y_{D_2}}} \left(\frac{A_{\max}}{P_{RF} l_{RD_2}} \right),$$

The overall outage probability associated with nodes D_1 and D_2 for a hybrid transmission without MRC, denoted as P_{Outage, D_i} where $i \in \{1, 2\}$, can be expressed as,

$$P_{Outage, D_i} = 1 - (1 - P_{O_{R_i}}) \times (1 - P_{O_{RD_i}}). \quad (4.87)$$

During the second phase, after applying MRC at destination node D_1 , the SIR associated with D_1 can be expressed as,

$$\gamma_{D_1} = \frac{P_{RF}(|h_{SD_1}|^2 l_{SD_1} + |h_{RD_1}|^2 l_{RD_1})a_1}{P_{RF}(|h_{SD_1}|^2 l_{SD_1} + |h_{RD_1}|^2 l_{RD_1})a_2 + I_{X_{D_1}} + I_{Y_{D_1}}}. \quad (4.88)$$

Similarly, in the second phase, after applying MRC, D_2 first retrieves the message associated with D_1 vehicle. Hence, the SIR at node D_2 to interpret D_1 can be represented as,

$$\gamma_{D_{2-1}} = \frac{P_{RF}(|h_{SD_2}|^2 l_{SD_2} + |h_{RD_2}|^2 l_{RD_2})a_1}{P_{RF}(|h_{SD_2}|^2 l_{SD_2} + |h_{RD_2}|^2 l_{RD_2})a_2 + I_{X_{D_2}} + I_{Y_{D_2}}}. \quad (4.89)$$

Now, the SIR at node D_2 to retrieve its own data after MRC reception, can be expressed as,

$$\gamma_{D_2} = \frac{P_{RF}(|h_{SD_2}|^2 l_{SD_2} + |h_{RD_2}|^2 l_{RD_2})a_2}{I_{X_{D_2}} + I_{Y_{D_2}}}. \quad (4.90)$$

We assume O_{D_1} is the outage event associated with D_1 . The outage event when D_2 is unable to retrieve the message associated with D_1 , denoted as $O_{D_{2-1}}$. The outage when D_2 is unable to retrieve its own message is denoted by $O_{D_{2-2}}$. These outage events can be given as,

$$\begin{aligned} O_{D_1} &= \{\gamma_{D_1} < \beta_1\}, \\ O_{D_{2-1}} &= \{\gamma_{D_{2-1}} < \beta_1\}, \\ O_{D_2} &= \{\gamma_{D_2} < \beta_2\}. \end{aligned} \quad (4.91)$$

We now calculate the outage probability related to vehicular nodes D_1 and D_2 . The outage probability associated with D_1 destination node, denoted by $P_{O_{D_1}}$, can be represented as [115],

$$P_{O_{D_1}} = \mathbb{P}(\gamma_{D_1} < \beta_1) = 1 - \left\{ \frac{l_{RD_1} \mathcal{G}_{D_1}\left(\frac{A_1}{P_{RF} l_{RD_1}}\right) - l_{SD_1} \mathcal{G}_{D_1}\left(\frac{A_1}{P_{RF} l_{SD_1}}\right)}{l_{RD_1} - l_{SD_1}} \right\}. \quad (4.92)$$

The outage probability associated with D_2 destination node, denoted by $P_{O_{D_2}}$, can be expressed as,

$$P_{O_{D_2}} = 1 - \mathbb{P}(\gamma_{D_{2-1}} < \beta_1) \times \mathbb{P}(\gamma_{D_2} < \beta_2) = 1 - \left\{ \frac{l_{RD_2} \mathcal{G}_{D_2}\left(\frac{A_{\max}}{P_{RF} l_{RD_2}}\right) - l_{SD_2} \mathcal{G}_{D_2}\left(\frac{A_{\max}}{P_{RF} l_{SD_2}}\right)}{l_{RD_2} - l_{SD_2}} \right\}.$$

The overall outage probability associated with vehicular nodes D_1 and D_2 after applying MRC, denoted as P_{Outage,D_i}^{MRC} where $i \in \{1, 2\}$, can be expressed as,

$$P_{Outage,D_i}^{MRC} = 1 - (1 - P_{O_{R_i}}) \times (1 - P_{O_{D_i}}). \quad (4.93)$$

Now, we extend the NOMA results to K vehicular nodes. The SIR at relay R associated with D_i to decode the message related to D_w can be represented as,

$$\gamma_{SR_{i \rightarrow w}}^{RF} = \frac{P_{RF} |h_{SR}|^2 l_{SR} a_i}{P_{RF} |h_{SR}|^2 l_{SR} \left[\sum_{u=w+1}^K a_u \right] + I_{X_R} + I_{Y_R}}. \quad (4.94)$$

The outage probability related to R due to RF link can be expressed as [36],

$$P_{O_{R_i}}^{RF} = \begin{cases} 1 - \mathcal{G}_R \left(\frac{A_{(i)\max}}{P_{RF} l_{SR}} \right); & \text{otherwise,} \\ 1; & \bigcup_{w=1}^K \frac{a_w}{\sum_{u=w+1}^K a_u} < \beta_w, \end{cases} \quad (4.95)$$

where $A_{(i)\max}$ is given as

$$A_{(i)\max} = \max \left(\frac{\beta_{i-(K-1)}}{a_{i-(K-1)} - \beta_{i-(K-1)} \left[\sum_{u=i-(K-1)+1}^K a_u \right]}, \frac{\beta_{i-(K-2)}}{a_{i-(K-2)} - \beta_{i-(K-2)} \left[\sum_{u=i-(K-2)+1}^K a_u \right]}, \dots, \frac{\beta_{i-(K-L)}}{a_{i-(K-L)} - \beta_{i-(K-L)} \left[\sum_{u=i-(K-L)+1}^K a_u \right]} \right), \quad (4.96)$$

where $L \in (1, 2, \dots, K)$ and we set the condition that $L > K - 1$

The expression for SIR at destination node D_i to decode D_w data during $R \rightarrow D_i$ transmission, denoted as $\gamma_{RD_{i \rightarrow w}}$, can be given as,

$$\gamma_{RD_{i \rightarrow w}} = \frac{P_{RF} |h_{RD_i}|^2 l_{RD_i} a_i}{P_{RF} |h_{RD_i}|^2 l_{RD_i} \left[\sum_{u=w+1}^K a_u \right] + I_{X_{D_i}} + I_{Y_{D_i}}}. \quad (4.97)$$

The outage probability related to vehicular node D_i , denoted as $P_{OR_{D_i}}$, can be represented as,

$$P_{OR_{D_i}} = \begin{cases} 1 - \mathcal{G}_{D_i}\left(\frac{A^{(i)\max}}{P_{RF}l_{RD_i}}\right); & \text{otherwise,} \\ 1; & \bigcup_{w=1}^K \frac{a_w}{\sum_{u=w+1}^K a_u} < \beta_w. \end{cases} \quad (4.98)$$

During the second phase, after applying MRC, the SIR related to node D_i to retrieve message associated with node D_w , denoted as $\gamma_{D_i \rightarrow w}$, can be expressed as,

$$\gamma_{D_i \rightarrow w} = \frac{P_{RF}(|h_{SD_i}|^2 l_{SD_i} + |h_{RD_i}|^2 l_{RD_i}) a_i}{P_{RF}(|h_{SD_i}|^2 l_{SD_i} + |h_{RD_i}|^2 l_{RD_i}) \left[\sum_{u=w+1}^K a_u \right] + I_{X_{D_i}} + I_{Y_{D_i}}}. \quad (4.99)$$

The outage probability related to vehicular node D_i can be expressed as [115],

$$P_{O_{D_i}} = 1 - \left\{ \frac{l_{RD_i} \mathcal{G}_{D_i}\left(\frac{A^{(i)\max}}{P_{RF}l_{RD_i}}\right) - l_{SD_i} \mathcal{G}_{D_i}\left(\frac{A^{(i)\max}}{P_{RF}l_{SD_i}}\right)}{l_{RD_i} - l_{SD_i}} \right\}. \quad (4.100)$$

4.9 Average Achievable Rate

The average achievable rate at R due to the combined effect of V-VLC and V-RF link associated with D_i message, where where $i \in \{1, 2\}$, can be expressed as⁸,

$$\mathcal{T}_{SR_i} = \max(\mathcal{T}_{SR_i}^{VLC}, \mathcal{T}_{SR_i}^{RF}). \quad (4.101)$$

The average achievable rate at destination node D_1 when R broadcasts the message to D_1 , denoted by \mathcal{T}_{RD_1} , can be given as,

$$\mathcal{T}_{RD_1} = \frac{1}{2} \mathbb{E}[\log_2(1 + \gamma_{RD_1})] = \int_{v=0}^{\frac{1}{2} \log_2(1 + \frac{a_1}{a_2})} \mathcal{G}_{D_1} \left(\frac{2^{2v} - 1}{(a_1 + a_2 - a_2 2^{2v}) P_{RF} l_{RD_1}} \right) dv.$$

The average achievable rate at node D_2 when R broadcasts the message to D_2 , denoted by \mathcal{T}_{RD_2} , can be expressed as,

$$\mathcal{T}_{RD_2} = \frac{1}{2} \mathbb{E}[\log_2(1 + \gamma_{RD_2})] = \int_{v=0}^{\infty} \mathcal{G}_{D_2} \left(\frac{2^{2v} - 1}{a_2 P_{RF} l_{RD_2}} \right) dv.$$

⁸V-RF and V-VLC are two different vehicular technologies. For ease of analysis, we assume that average achievable rate evaluated at relay is maximum of average achievable rate associated with either V-VLC or V-RF link.

The overall average achievable rate at vehicular node D_i due to hybrid transmission without MRC, can be expressed as,

$$\mathcal{T}_{D_i} = \min(\mathcal{T}_{RD_i}, \mathcal{T}_{SR_i}) \quad (4.102)$$

where $i \in \{1, 2\}$. After applying MRC, the average achievable rate associated with vehicular node D_1 is represented as [115],

$$\mathcal{T}_{D_1} = \frac{1}{2} \mathbb{E}[\log_2(1 + \gamma_{D_1})]. \quad (4.103)$$

On further solving the above equation, we obtain (4.104).

$$\mathcal{T}_{D_1} = \int_{v=0}^{\frac{1}{2} \log_2 \left(1 + \frac{a_1}{a_2}\right)} \frac{l_{RD_1} \mathcal{G}_{D_1} \left(\frac{2^{2v}-1}{(a_1 - (2^{2v}-1)a_2) P_{RF} l_{RD_1}} \right) - l_{SD_1} \mathcal{G}_{D_1} \left(\frac{2^{2v}-1}{(a_1 - (2^{2v}-1)a_2) P_{RF} l_{SD_1}} \right)}{l_{RD_1} - l_{SD_1}} dv. \quad (4.104)$$

Similarly, after applying MRC on D_2 node, the average achievable rate, is represented as,

$$\mathcal{T}_{D_2} = \frac{1}{2} \mathbb{E}[\log_2(1 + \gamma_{D_2})] = \int_{v=0}^{\infty} \frac{l_{RD_2} \mathcal{G}_{D_2} \left(\frac{2^{2v}-1}{a_2 P_{RF} l_{RD_2}} \right) - l_{SD_2} \mathcal{G}_{D_2} \left(\frac{2^{2v}-1}{a_2 P_{RF} l_{SD_2}} \right)}{l_{RD_2} - l_{SD_2}} dv.$$

The overall average achievable rate at vehicular node D_i after applying MRC can be represented as,

$$\mathcal{T}_{D_i}^{MRC} = \min(\mathcal{T}_{R_i}, \mathcal{T}_{D_i}). \quad (4.105)$$

where $i \in \{1, 2\}$. The average achievable rate at relay node R_i for K destination nodes can be expressed as [118],

$$\mathcal{T}_{SR_i}^{RF} = \int_{v=0}^{v'} \mathcal{G}_R \left(\frac{2^{2v}-1}{\left(a_i - (2^{2v}-1) \left[\sum_{u=i+1}^K a_u \right] \right) P_{RF} l_{SR}} \right) dv. \quad (4.106)$$

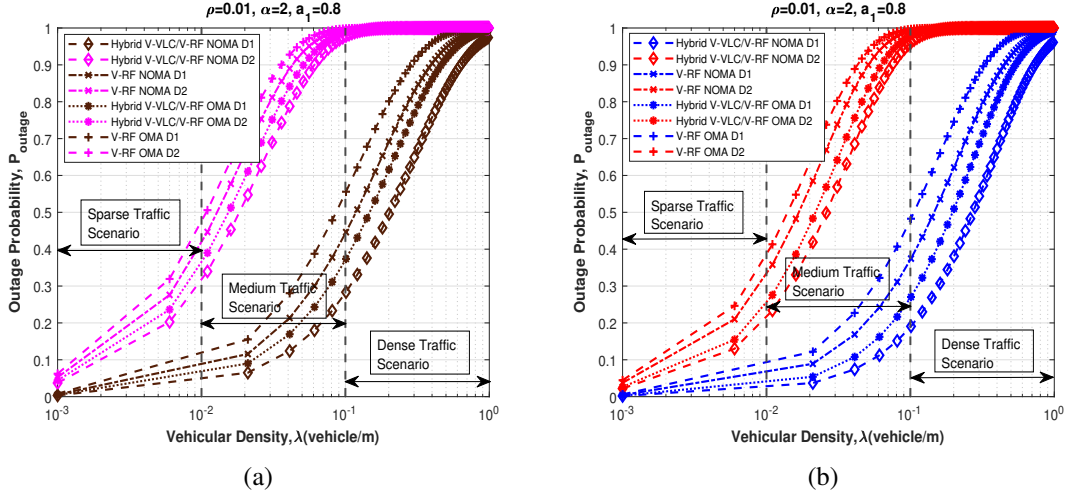


Figure 4.11: Outage probability as a function of vehicular density λ : (a) Hybrid transmission without MRC, and (b) Hybrid transmission with MRC.

where $v' = \frac{1}{2} \log_2 \left(1 + \frac{a_i}{\sum_{u=i+1}^K a_u} \right)$. The average achievable rate at node D_i due to $R \rightarrow D_i$ transmission, denoted as \mathcal{I}_{RD_i} , can be expressed as,

$$\mathcal{I}_{RD_i} = \int_{v=0}^{v'} \mathcal{G}_{D_i} \left(\frac{2^{2v} - 1}{\left(a_i - (2^{2v} - 1) \left[\sum_{u=i+1}^K a_u \right] \right) P_{RF} l_{RD_i}} \right) dv. \quad (4.107)$$

After applying MRC at D_i [115], the average achievable rate, denoted by \mathcal{I}_{D_i} , is given by equation (4.108).

$$\mathcal{I}_{D_i} = \int_{v=0}^{v'} \frac{l_{RD_i} \mathcal{G}_{D_i} \left(\frac{2^{2v} - 1}{\left(a_i - (2^{2v} - 1) \left[\sum_{u=i+1}^K a_u \right] \right) P_{RF} l_{RD_i}} \right) - l_{SD_i} \mathcal{G}_{D_i} \left(\frac{2^{2v} - 1}{\left(a_i - (2^{2v} - 1) \left[\sum_{u=i+1}^K a_u \right] \right) P_{RF} l_{RD_i}} \right)}{l_{RD_i} - l_{SD_i}} dv. \quad (4.108)$$

4.10 Numerical Results

In this section, we present the results of our proposed framework for hybrid transmission with and without MRC. We also compare the results of a hybrid V-VLC/V-RF system with a

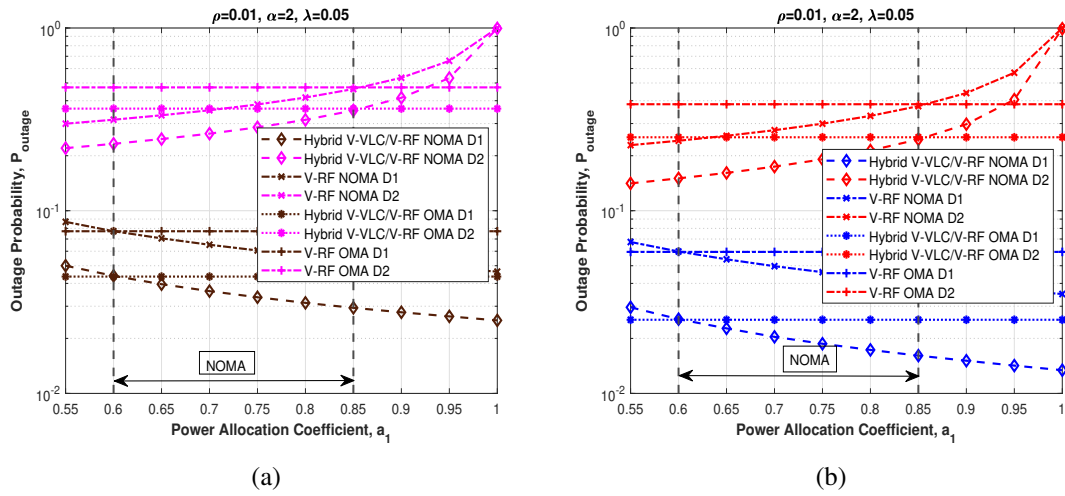


Figure 4.12: Outage probability as a function of power allocation coefficient a_1 : (a) Hybrid transmission without MRC, (b) Hybrid transmission with MRC.

conventional V-RF system. The system model parameters for V-VLC and V-RF system are chosen similar as in [112]. We assume the vehicular intensities at road X and Y to be the same, that is, $\lambda_X = \lambda_Y = \lambda$. As mentioned before, we consider different data requirements of each destination vehicular nodes, the target data rate of vehicular node D_2 is assumed to be more than D_1 node. Monte Carlo simulations are performed to corroborate our theoretical equations. We have considered a worst case scenario when the interference from same lane or perpendicular lane vehicles are originating from an infinite road segment ($\mathcal{B} = \mathbb{R}^1$).

Fig. 4.11 illustrates the performance of outage probability for varying vehicular densities, λ . We observe that as the vehicular density increases, the outage probability associated with destination nodes D_1 and D_2 also increases. To observe the benefits of using a hybrid based system, we evaluate and compare the performance of hybrid V-VLC/V-RF based system with the conventional V-RF. From Fig. 4.11(a) we notice that, for a vehicular density of 0.01, outage probability associated with D_1 for a hybrid V-VLC/V-RF case is 0.05, while for V-RF case, it is approximately 0.12. Similarly, outage probability associated with D_2 for a hybrid V-VLC/V-RF is 0.32, while for V-RF case it is around 0.42. Fig. 4.11(b) represents hybrid transmission without MRC. For vehicular density, $\lambda=0.01$, outage probability associated with D_1 for a hybrid V-VLC/V-RF system is 0.03, whereas for a V-RF system it is approximately 1. Similarly, outage probability associated with D_2 for a hybrid V-VLC/V-RF system is 0.21 whereas for a V-RF system it is 0.34. The outage performance for hybrid transmission with and without MRC is better than a conventional V-RF system. Further, we also analyze the NOMA and OMA results for two user scenarios and observe that for both D_1 and D_2 destination vehicles, the outage performance of the NOMA overpowers that of OMA.

Fig. 4.12 depicts the the impact of varying power allocation coefficient on the outage probability. It is worth mentioning here that as intuitive, with increase in a_1 , the outage probability associated with D_1 decreases, whereas the outage probability of D_2 increases. We observe that the hybrid V-VLC/V-RF link performs better than the conventional V-RF link. From Fig. 4.12(a), for D_1 vehicle, OMA outperforms NOMA when $a_1 \in [0.55, 0.6]$ for a hybrid V-VLC/V-RF system. This is because for lower values of a_1 , lower power is assigned to vehicular node D_1 and more power is assigned to D_2 node, consequently increasing the interference and outage at D_1 . For $a_1 \in [0.6, 0.85]$, NOMA performs better than OMA, this is because, more power is now assigned to vehicular node D_1 . On the other hand, for D_2 vehicle, NOMA performs better than OMA for $a_1 \in [0.85, 1]$. Similarly, we observe from Fig. 4.12(b) that, for a hybrid V-VLC V-RF, OMA outperforms NOMA for $a_1 \in [0.55, 0.6]$. For D_2 vehicle, NOMA provides an enhanced performance over OMA for $a_1 \in [0.85, 1]$. In a hybrid V-VLC/V-VRF scenario, when $a_1 \in [0.6, 0.85]$, NOMA performs better than OMA for both D_1 and D_2 destination nodes. On comparing Fig. 4.12(a) and 4.12(b), we note that the performance of a system using MRC reception is better than the system without MRC. For instance, with $a_1 = 0.8$, MRC reception has reduced the outage probability by 45% compared to the hybrid transmission without MRC.

Fig. 4.13 represents the performance of average achievable rate for varying vehicular densities, λ . For a sparse traffic and medium traffic scenario, vehicle D_1 has a lower achievable rate than vehicle D_2 because the D_2 vehicular node acts as an additional interference term for D_1 vehicle. As the vehicular density increases, D_1 vehicle provides a higher achievable rate than the vehicular node D_2 . This is because, $a_1 > a_2$ and the effect of D_2 interference on D_1 becomes insignificant when compared to the other interfering vehicles on road X and Y . We also note that the performance of achievable rate in case of OMA for D_2 destination vehicle is more than the D_1 destination vehicle. Analysing Fig. 4.13(a) for a hybrid V-VLC/V-RF scenario, vehicular node D_1 has a better performance of NOMA over OMA for $\lambda > 0.2$ vehicles/m. Similarly from Fig. 4.13(b), we observed that when $\lambda > 0.1$ vehicles/m, NOMA performs better than OMA in a hybrid V-VLC/V-RF scenario. Due to the directional property of VLC, the effect of interference on a hybrid V-VLC/V-RF system for a dense traffic scenario is significantly less than the conventional V-RF system. In Fig. 4.13, we also analyse the curves for average achievable rate for different power allocation coefficient a_1 . For higher a_1 , larger amount of power is assigned to node D_1 , therefore we observe that, as the power allocation coefficient increases, the achievable rate associated with vehicular node D_1 increases while that of the D_2 vehicle decreases. From Fig. 4.13(c), when $a_1 > 0.96$, NOMA has an enhanced performance compared to OMA for vehicular node D_1 . Similarly for D_2 vehicle, NOMA performs better than OMA when $a_1 \in [0.55, 0.95]$. We also observe that for the D_2 vehicle,

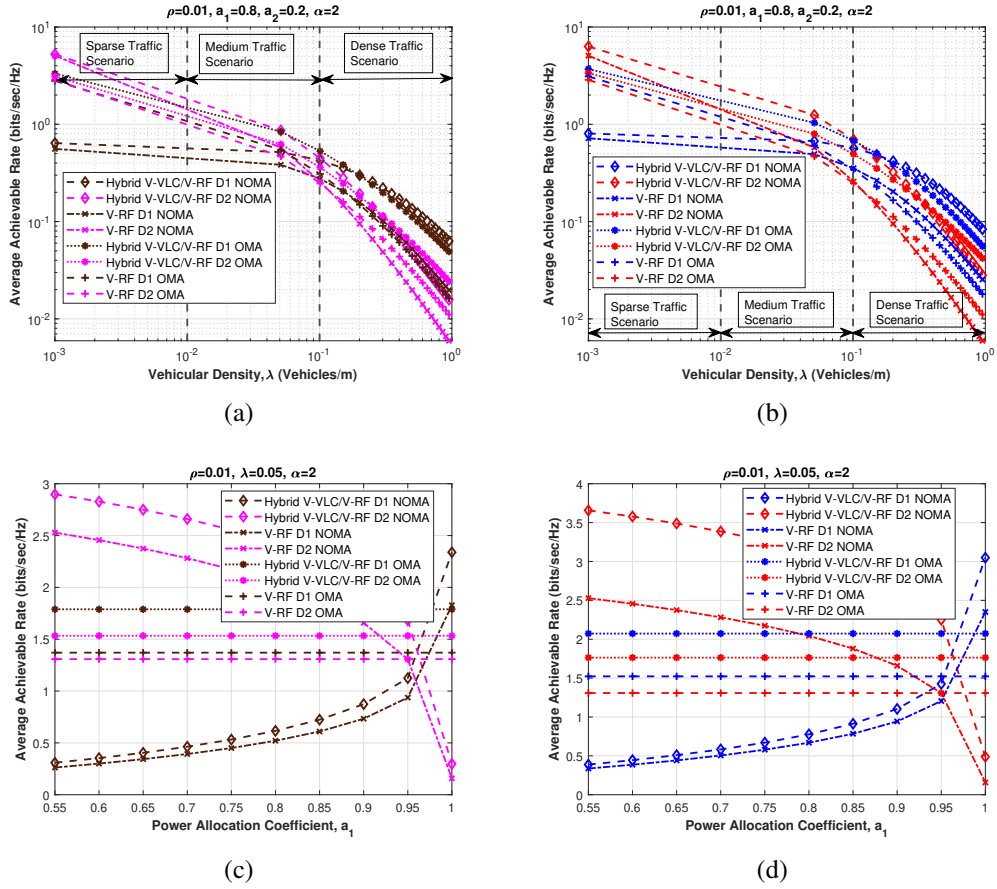


Figure 4.13: Average achievable rate as a function of vehicular density λ : (a) Hybrid transmission without MRC; (b) Hybrid transmission with MRC. Impact of power allocation coefficient a_1 : (c) Hybrid transmission without MRC; and, (d) Hybrid transmission with MRC.

there is a noteworthy improvement in the average achievable rate for a hybrid V-VLC/V-RF based system compared to the conventional V-RF system. Similar analysis has been performed for Fig. 4.13(d). For D_2 destination vehicle, NOMA performs better than OMA when $a_1 \in [0.55, 0.97]$. Analyzing Fig. 4.13(c) and 4.13(d), we notice that on varying the power allocation coefficient, the hybrid transmission with MRC provides slightly better performance compared to the hybrid transmission without MRC. For MRC reception, when $a_1 > 0.98$, D_1 has a higher achievable rate than D_2 whereas for without MRC reception, D_1 has a better achievable rate performance when $a_1 > 0.96$.

Fig. 4.14(a) and 4.14(b) investigate the performance of an empirical model with respect to the Lambertian model in terms of outage performance and average achievable rate. It can be observed that Lambertian model has lower outage probability and high achievable rate as compared to the empirical model while employing the hybrid transmission with MRC. For

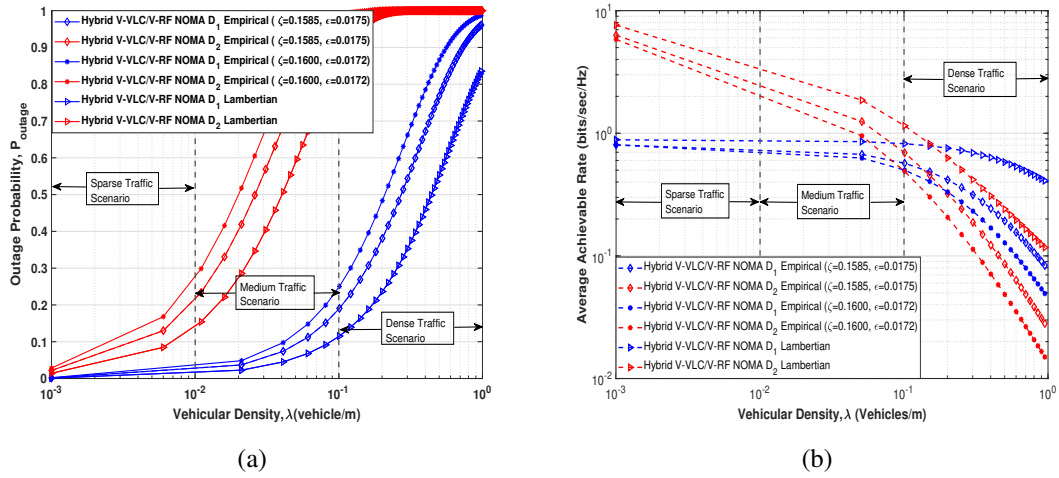


Figure 4.14: (a) Outage probability as a function of vehicular density λ for Lambertian and empirical model (b) Average achievable rate as a function of vehicular density λ for Lambertian and empirical model. Here, $\rho=0.01$, $\alpha=2$ and $a_1=0.8$.

$\lambda = 0.1$, the outage performance of the Lambertian model has decreased by 0.1 as compared to the empirical model. Similarly for D_2 destination vehicle, the outage performance of empirical model is 0.12 more than the Lambertian model. For dense traffic scenarios, Lambertian model offers higher achievable rate for both D_1 and D_2 destination vehicles as compared to the empirical VLC channel model. It has been observed that for $\lambda = 0.1$, the Lambertian model offers an achievable rate of 0.8 bits/s/Hz for D_1 node whereas the empirical model offers an average achievable rate of around 0.6 bits/s/Hz. It can be inferred from the above insights that given our simulation setting, empirical model is lower bound to the Lambertian model in terms of outage and average achievable rate performance.

Next, we employ traffic flow theory (TFT⁹) to investigate the impact of vehicular speed, v_s ¹⁰. Given the traffic flow $q = v_s \times \lambda$, we utilize speed-density flow model [119] to investigate the impact of v_s on the outage probability and average achievable rate. Fig. 4.15 illustrates the impact of vehicular speed on outage performance and average achievable rate for proposed C-NOMA supported V-VLC/V-RF scheme. Under stationary traffic condition, it can be observed that the outage and average rate improves with increase in vehicular speed. This is due to fact that light traffic (low λ) supports high vehicular speed and vice versa obeying speed-density flow model. In more simpler words, in low traffic conditions, increasing the vehicle speed

⁹TFT entails the knowledge of the fundamental characteristics of traffic flows (for instance, the road capacities, the relation between flow and density, and headway distributions) and the associated analytical methods[119].

¹⁰Shown under stationary traffic conditions, please note that under non-stationary traffic conditions, the time varying effects of V2X channels and Doppler shift are beyond the scope of this study and has been left as a subject of future investigation.

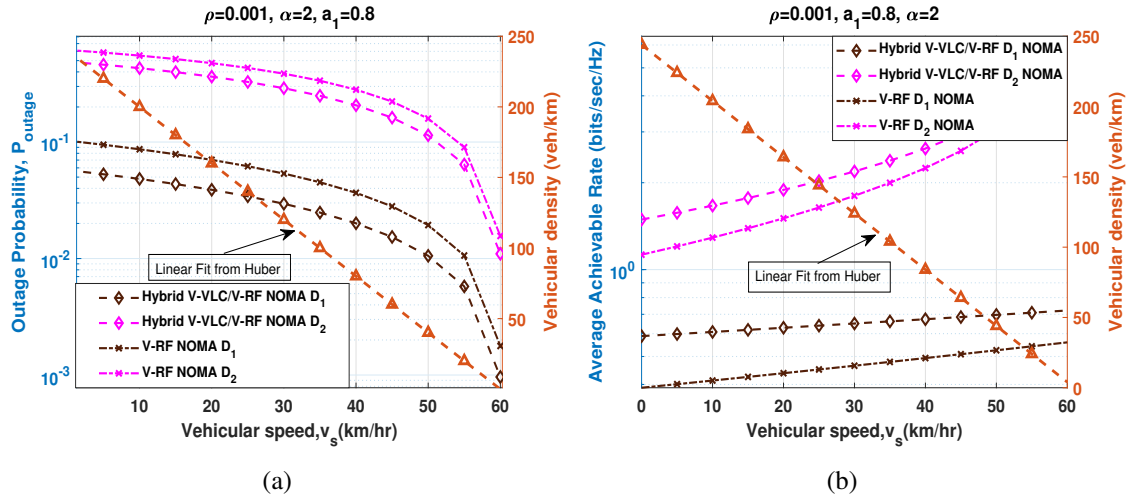


Figure 4.15: Impact of vehicular speed: (a) Outage probability, and (b) average achievable rate.

improves the outage and average achievable rate performance, whereas in high traffic conditions, decreasing the vehicle speed increases the performance.

4.11 Concluding Remarks

In this work, we explored the potential benefit of cooperative NOMA assisted hybrid V-VLC and V-RF solution to the V2X communication at road intersections. It has been shown through simulation results that the performance of the hybrid V-VLC/V-RF network is better than a conventional V-RF system in terms of outage probability and average achievable rate. We compared the performance of a hybrid transmission system with MRC over a hybrid transmission system without MRC and show that the MRC offers considerable improvement in terms of outage probability and average achievable rate. We also compared the performance of the Lambertian model with the empirical model and observed that the empirical model offers a higher outage and lower average achievable rate compared to the Lambertian model. We believe that this performance analysis of NOMA enabled hybrid V-VLC/V-RF network provides significant analytical contributions, while simulating new research direction as a future cooperative intelligent transportation system (C-ITS) alternative to meet diverse application needs for B5G V2X networks.

Optical RIS for Vehicular Network

5.1 Introduction

Recently, Reconfigurable Intelligent Surfaces (RISs) is also emerging as a disruptive communication technology for enhancing signal quality and transmission coverage in wireless vehicular networks [120]. Recent studies have demonstrated that RIS assisted vehicular communication systems are capable of achieving more enhanced wireless vehicular connectivity [47, 48, 121]. Despite the widespread interest in applying RISs in various wireless vehicular environment, there is paucity of intensive research efforts on exploring optical-RIS (O-RIS) for vehicular communication. In optical domain, O-RIS are categorized as: intelligent metasurface reflector (IMR) and intelligent mirror array (IMA) [44]. It is anticipated that 6G-ITS applications viz. autonomous driving, platooning and cooperative driving shall witness proliferation of such O-RIS and hybrid RF-VLC technologies, while fulfilling stringent 6G key performance indicators (KPIs) requirements.

Motivated by the above insights, this work aims to highlight the advantageous amalgamation of O-RIS and hybrid RF-VLC technologies for enhanced vehicular message dissemination particularly at road intersection. We utilize stochastic geometry approach to characterize the performance of proposed framework subject to interference originating from vehicles in the adjacent lane. By intelligently incorporating O-RIS with hybrid RF-VLC V2X systems, our principal objective is to portray improved system reliability, wide coverage range, reduced transmission latency, higher system goodput, reduced power utilization, and enhanced road safety.

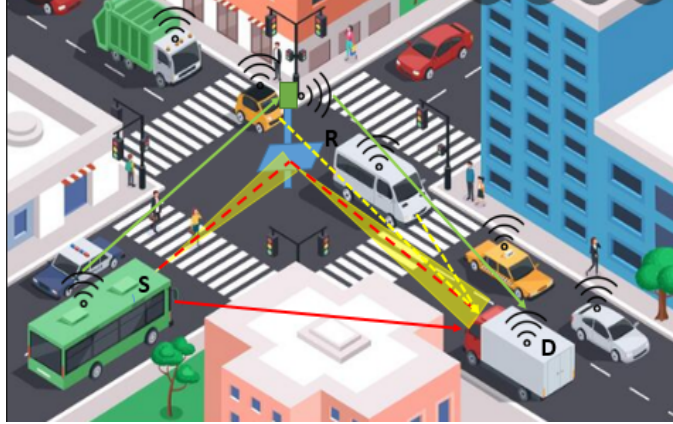


Figure 5.1: Real life application scenario: At road intersection, the vehicles in blocked LOS can communicate via O-RIS (dashed red line) or V-RF links (solid green line) in presence of interference from adjacent lane vehicles (dashed yellow line).

5.2 System Overview

Consider a road intersection scenario as illustrated in Fig. 5.1. We examine traffic safety message dissemination between single source vehicle S and destination vehicle D via O-RIS/Relay R subject to interference caused from adjacent lane vehicles. We assume location of interfering vehicles to be 1D homogeneous Poisson point process, ψ_{PPP} . By enabling an RIS controller to actively relay the RF information from S to D , the O-RIS can not only potentially help improve the transmission rate for standalone V-VLC systems, but also provide wide coverage range using RIS controller. As soon as the quality of primary V-VLC link degrades (eg. long range communication case), the communication between S and D nodes can still be accomplished using conventional V-RF systems employing relaying.

5.3 Performance Analysis

In this section, we mathematically evaluate the performance of proposed framework in terms of outage probability, system goodput and delay outage rate (DOR).

5.3.1 Outage Probability

Fig. 5.2 depicts O-RIS enabled hybrid RF-VLC V2X communication where the O-RIS is placed on a road side unit (RSU). As per insights shared in [44], the IMA outperforms the IMR for VLC system. Hence, we consider intelligent controllable mirror array based O-RIS for the proposed work. O-RIS consists of $n_m \times n_m$ identical mirror elements, where size of each element is $l_m \times w_m$. Each mirror element can be oriented independently in two directions $\gamma_{j,k}$

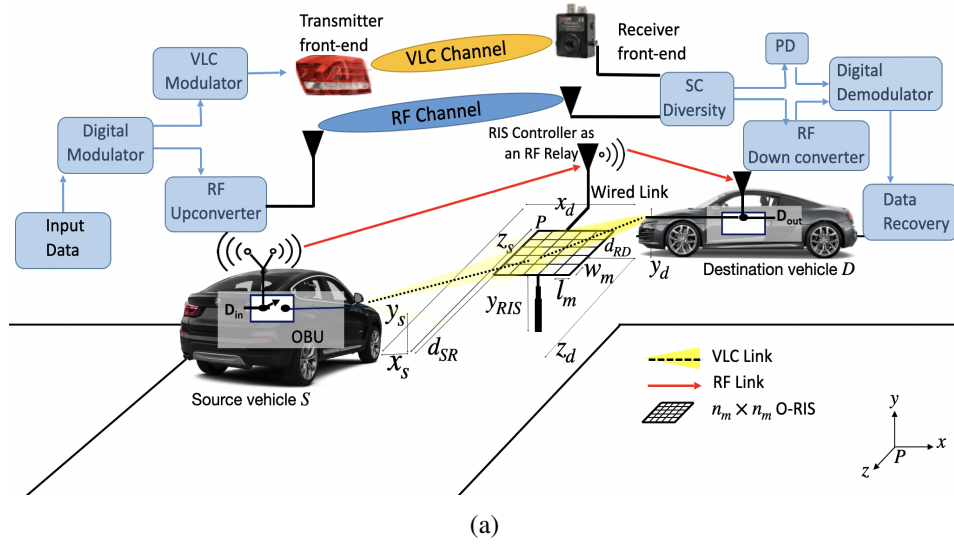


Figure 5.2: 3D coordinate system model: O-RIS can be deployed at road intersection to relax the line-of-sight (LOS) requirement between source and destination vehicles in a V-VLC systems.

(rotation around x -axis) and $\beta_{j,k}$ (rotation around z -axis). The channel gain H_{RIS} is given as follows [51]:

$$H_{RIS} = \sum_{j=1, k=1}^{all\ mirrors} \xi A_R T_s \mathcal{A}_{j,k}(\gamma, \beta) G(\theta_{\mathbf{R}_{j,k}}^{\mathbf{D}}) \cos(\theta_{\mathbf{R}_{j,k}}^{\mathbf{D}}), \quad (5.1)$$

where ξ is the current-to-optical conversion efficiency of the LED, A_R is the area of the receiver, T_s is the optical filter gain, and the irradiance at the receiver contributed by the $(j, k)^{th}$ mirror element, denoted by $\mathcal{A}_{j,k}$ is given by (5.1) [44]. In (5.1), ρ_M is the reflection efficiency of mirror, L_A represents the Lambertian order which is given by $L_A = \frac{-\ln(2)}{\ln(\cos(\frac{\phi_1}{2}))}$ where ϕ_1 is LED semi-angle, and $\mathbb{I}(\cdot)$ denotes the binary indicator function,. Further, $\mathbf{R}_{j,k} = [(x_s + \frac{w_m}{2} + (k-1)w_m); 0; (z_s + \frac{l_m}{2} + (j-1)l_m)]$ represents the centroid coordinates of the mirror in j^{th} row and k^{th} column. The source coordinates are given by the $\mathbf{S} = [(x_s + \frac{w_m}{2} + (k-1)w_m); -(y_{RIS} - y_s); (z_s + \frac{l_m}{2} + (j-1)l_m)]$; x_s and z_s denote x and z component of \mathbf{S} respectively as illustrated in Fig. 5.2. In addition, y_s and y_{RIS} represent the height of the transmitter and the RSU, respectively. Note that the distance of the source vehicle, $d_{SR} = z_s - n_m w_m$.

Similarly, the destination vehicle's coordinates can be interpreted as $\mathbf{D} = [x_d - (x_s + \frac{w_m}{2} + (k-1)w_m); -(y_d - y_{RIS}); z_d - (z_s + \frac{l_m}{2} + (j-1)l_m)]$. In above, x_d and z_d are the x and z component of \mathbf{D} respectively as shown in Fig. 5.2 and y_d is the height of the receiver. Observe that the distance of the destination vehicle, $d_{RD} = x_d - (x_s + n_m l_m)$.

$$\begin{aligned} \mathcal{A}_{j,k}(\gamma, \beta) &= \frac{(L_A + 1)\rho_M}{2\pi} \int_{-\frac{l_m}{2}}^{\frac{l_m}{2}} \int_{-\frac{w_m}{2}}^{\frac{w_m}{2}} \cos^{L_A}(\theta_{\mathbf{R}_{j,k}}^{\mathbf{I}}) \frac{\mathbf{e}_3^T (\mathbf{D} - \mathbf{R}_{j,k}) \widehat{\mathbf{N}}_{j,k}^T (\mathbf{D} - \mathbf{R}_{j,k})}{\|\mathbf{D} - \mathbf{R}_{j,k}\|_2^4} \\ &\quad \times \mathbb{I}\left(\mathbf{e}_1^T \mathbf{S} - \frac{w_m}{2} \leq \mathbf{e}_1^T \mathbf{I} \leq \mathbf{e}_1^T \mathbf{S} + \frac{w_m}{2}, \mathbf{e}_2^T \mathbf{S} - \frac{l_m}{2} \leq \mathbf{e}_2^T \mathbf{I} \leq \mathbf{e}_2^T \mathbf{S} + \frac{l_m}{2}\right) dx'' dz'' \end{aligned} \quad (5.2)$$

\mathbf{I} is the pre-reflection image of \mathbf{D} in the source plane (X-Y plane), and is given as $[\mathbf{e}_1^T (\mathbf{R}_{j,k} + \frac{\mathbf{e}_3^T (\mathbf{S} - \mathbf{R}_{j,k})}{\mathbf{e}_3^T \mathbf{R}_{j,k} \mathbf{I}} \widehat{\mathbf{R}}_{j,k} \mathbf{I}); \mathbf{e}_2^T (\mathbf{R}_{j,k} + \frac{\mathbf{e}_3^T (\mathbf{S} - \mathbf{R}_{j,k})}{\mathbf{e}_3^T \mathbf{R}_{j,k} \mathbf{I}} \widehat{\mathbf{R}}_{j,k} \mathbf{I}); \mathbf{e}_3^T \mathbf{S}]$.

The mirror orientation is configured in such a way that $\widehat{\mathbf{S}}\mathbf{R}_{j,k}$ represents the corresponding incidence direction for the reflection direction $\widehat{\mathbf{R}}_{j,k}\mathbf{D}$. Finally, the mirror orientation is determined by finding a unit vector normal to its surface, $\widehat{\mathbf{N}}_{j,k}$ which can be expressed as: $\widehat{\mathbf{N}}_{j,k} = \frac{\widehat{\mathbf{R}}_{j,k}\mathbf{S} + \widehat{\mathbf{R}}_{j,k}\mathbf{D}}{\sqrt{2 + 2\widehat{\mathbf{R}}_{j,k}\mathbf{S}^T \widehat{\mathbf{R}}_{j,k}\mathbf{D}}}$ [44]. In addition, we obtain $\beta_{j,k}$ and $\gamma_{j,k}$ in terms of $\widehat{\mathbf{N}}_{j,k}$ as:

$\beta_{j,k} = \sin^{-1}(\widehat{\mathbf{N}}_{j,k}^T \mathbf{e}_3)$, and $\gamma_{j,k} = \frac{\sin^{-1}(\widehat{\mathbf{N}}_{j,k}^T \mathbf{e}_1)}{\cos(\beta_{j,k})}$. In (5.1), $G(\theta_{\mathbf{R}_{j,k}}^{\mathbf{D}})$ denotes the gain of an optical concentrator and is expressed as $G(\theta_{\mathbf{R}_{j,k}}^{\mathbf{D}}) = \frac{n^2}{\sin^2(\Psi_c)}$, $0 \leq \theta_{\mathbf{R}_{j,k}}^{\mathbf{D}} \leq \Psi_c$. If $\theta_{\mathbf{R}_{j,k}}^{\mathbf{D}} > \Psi_c$, then $G(\theta_{\mathbf{R}_{j,k}}^{\mathbf{D}}) = 0$. n is the refractive index of optical concentrator and Ψ_c is half the receiver's field of view (FOV). Finally, $\theta_{\mathbf{R}_{j,k}}^{\mathbf{D}}$ denotes the angle between $\mathbf{R}_{j,k}\mathbf{D}$ and the positive z -axis and can be obtained as $\mathbf{e}_3^T (\mathbf{R}_{j,k} - \mathbf{I}) / \|\mathbf{R}_{j,k} - \mathbf{D}\|_2$ [44].

For an interference limited scenario, given the transmitted signal x , the received signal y can be expressed as: $y = \sqrt{P_{VLC}} \mathcal{R} H_{RIS} x + \sqrt{\mathcal{I}_{V2V}} + w$, where \mathcal{R} is the responsivity of the PD, w is additive white Gaussian noise (AWGN) such that $w \sim \mathcal{CN}(0, \sigma^2)$, and the interference experienced at the D from vehicles in adjacent lanes, denoted by \mathcal{I}_{V2V} is given by [122, Eq.12] as: $\mathcal{I}_{V2V} = \sum_{r_i \in \Psi} \mu \frac{P_{VLC} r_i^{2(L_A+1)}}{(L^2 + r_i^2)^{(L_A+3)}}$, where $\mu = \left(\frac{(L_A+1)A_R}{2\pi} T_s(\psi) G(\psi)\right)^2$, L is the inter-lane distance, r_i is the distance of interfering vehicles from destination vehicle and P_{VLC} denotes the transmission power for V-VLC. For given d_{SR} and d_{RD} setting, the outage probability associated with V-VLC can be expressed as:

$$\begin{aligned} \mathcal{P}_{out,VLC}(\zeta) &= 1 - \mathbb{P}(SINR > \zeta), \\ &= 1 - \mathbb{P}\left(\frac{(\mathcal{R} H_{RIS})^2 P_{VLC}}{\mathcal{I}_{V2V} + \sigma^2} > \zeta\right), \\ &= 1 - \mathcal{F}_{I_{V2V}}\left(\frac{(\mathcal{R} H_{RIS})^2 P_{VLC}}{\zeta} - \sigma^2\right). \end{aligned} \quad (5.3)$$

$$\begin{aligned}
& \mathcal{P}_{out,RF}(\zeta) = \\
& \underbrace{1 - \exp\left(-\frac{\zeta\sigma^2}{P_{RF}\ell_{SR}}\right) \exp\left(-2\rho\lambda \frac{\pi\zeta(h^2 + d_{SR}^2)}{\sqrt{h^2 + \zeta(h^2 + d_{SR}^2)}}\right)}_{1 - P_{out,SR}(\zeta)} \underbrace{\exp\left(-\frac{\zeta\sigma^2}{P_{RF}\ell_{RD}}\right) \exp\left(-\rho\lambda\pi\sqrt{\zeta}\sqrt{L^2 + d_{RD}^2}\right)}_{1 - P_{out,RD}(\zeta)}
\end{aligned} \tag{5.5}$$

where, ζ is SINR threshold and we utilize LT to evaluate the CDF of the interference. We begin with the definition of LT of a random variable X as: $\mathbb{E}[e^{-sX}]$. Accordingly, we can write

$$\begin{aligned}
& \mathcal{L}_s\{\mathcal{I}_{V2V}\} = \mathbb{E}[e^{-sI_{V2V}}], \\
& = \mathbb{E}_{r \in \Psi_{PPP}} \left[\exp\left(-s \sum_{r \in \Psi_{PPP}} \mu \frac{P_{VLC}r^{2(L_A+1)}}{(L^2 + r^2)^{(L_A+3)}}\right) \right], \\
& = \mathbb{E}_{r \in \Psi_{PPP}} \left[\prod_{r \in \Psi_{PPP}} \exp\left(-s\mu \frac{P_{VLC}r^{2(L_A+1)}}{(L^2 + r^2)^{(L_A+3)}}\right) \right], \\
& \stackrel{(a)}{=} \exp\left(-\int_{\mathbb{R}} \left[1 - \exp\left(-s\mu \frac{P_{VLC}r^{2(L_A+1)}}{(L^2 + r^2)^{(L_A+3)}}\right)\right] \rho\lambda dr\right),
\end{aligned} \tag{5.4}$$

where final step (a) follows from definition of probability generating functional (PGFL) for homogeneous PPP over region of interest, \mathbb{R} [63, Th 4.9]. Utilizing (5.4), CDF of the interference can be obtained by inverting the LT by using Talbot inversion method with the unified numerical inversion frame work[123] as: $\mathcal{F}_{I_{V2V}}(x) = L^{-1}\left[\frac{1}{s}\mathcal{L}_s\{\mathcal{I}_{V2V}\}\right]$. Eq.(5.5) gives the outage probability associated with a V-RF system employing DF relaying governed by [116, Eq.34].

At receiver, a diversity combining technique is implemented to combine all incoming optical and RF signals to collect higher SINR all the time in the hybrid RF/VLC system. Assuming optical and RF links to be statistically independent, the outage probability associated with such hybrid RF-VLC systems[75] as: $\mathcal{P}_{out,Hyb} = \mathcal{P}_{out,VLC}(\zeta)\mathcal{P}_{out,RF}(\zeta)$.

5.3.2 System Goodput Analysis

The system goodput, an application-level throughput metric can be used to characterize the number of successfully delivered information bits from the source to the destination node in a give time instant. Let us assume that S transmits a bit frame of length $b_L = b_T + b_I$ bits comprising of training bits (b_T) and information bits (b_I) in each transmission. The information

coding rate of each transmission frame can be defined as $r = \frac{b_T}{b_L}$. Therefore, for a given targeted coding rate R , we can obtain the expression for goodput (\mathbb{G}) as given in [124, Eq. 19] as: $\mathbb{G} = \left(1 - \frac{b_T}{b_L}\right) R(1 - \mathcal{P}_{out})(e^r - 1)$.

5.3.3 Delay Outage Analysis

For delay sensitive applications, we consider the data-oriented metric of delay outage rate (DOR), which represents the probability that the minimum transmission time (MTT) required for sending a certain amount of data is higher than the tolerable duration, T_{th} . For ultra high reliability and low latency small data transmission, the DOR associated with transmitting data size of H bits over a channel with system bandwidth, B_s within a given coherence time can be given as[125]: $DOR = \mathbb{P}(SINR < 2^{\frac{H}{B_s T_{th}}} - 1)$.

5.4 Results and Discussions

In this section, we discuss salient features of proposed system setup using numerical results and validate our analytical findings using Monte Carlo (MC) simulations. Unless otherwise specified explicitly, in the following figures, we set, $l_m = w_m = 0.01$ m, $L_A = 2$, $A_R = 1$ cm², $\xi = 0.44$ W/A, $\mathcal{R} = 0.54$ A/W, $\rho_M = 0.8$, $d_{SR} = d_{RD} = d_0$, $\zeta = 8$ dB, $T_s = 1$, $y_s = y_d = 0.8$ m, and $B_s = 20$ MHz, analogous to a practical vehicular communication scenario[116]. Fig. 5.3 shows

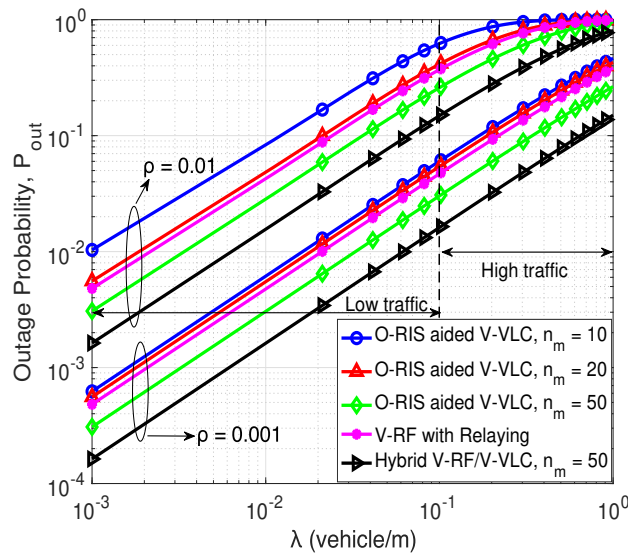


Figure 5.3: Comparison of analytical (solid line) and simulation (markers) results of outage performance for various configuration with varying vehicular density, λ . Here, $d_o = 50m$.

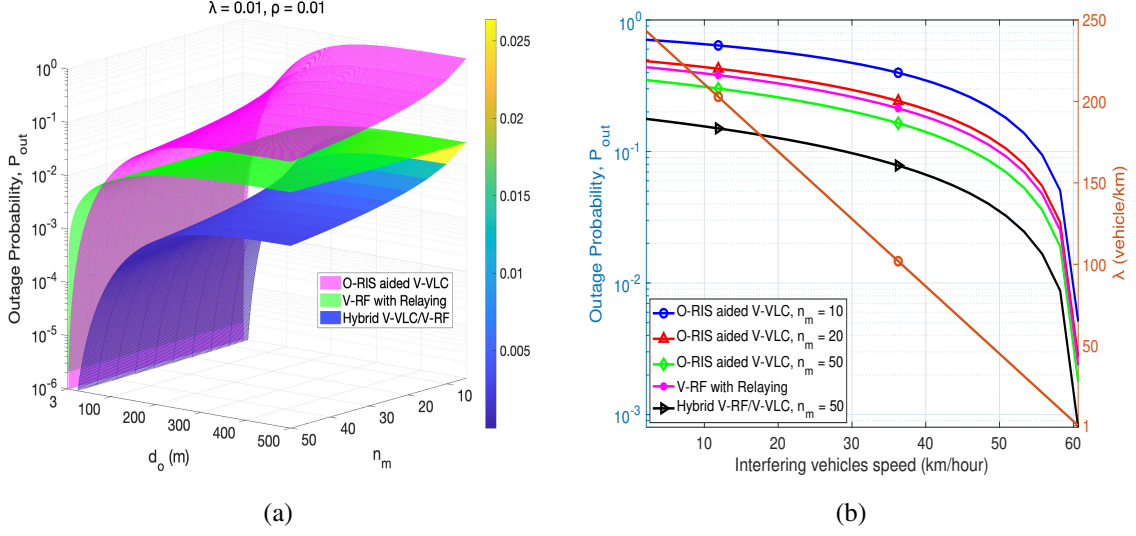


Figure 5.4: (a) 3D outage plots and (b) Impact of vehicle's speed on outage performance. Here, $d_o = 50m$.

the outage performance of O-RIS aided V-VLC with $n_m \in \{10, 20, 50\}$, V-RF with relaying and proposed O-RIS enabled hybrid V-VLC/V-RF under low and high traffic regimes. The enhanced performance can be observed for lower values of ρ . The reason is as follows: smaller value of ρ implies probability of medium access by interfering vehicles is lower, resulting in less interference, and thereby increasing the SINR and hence reduce the outage. However, irrespective of traffic scenario and ρ , the proposed hybrid V-VLC/V-RF exhibits better performance compared to the stand-alone O-RIS aided V-VLC as well as V-RF with relaying.

To gain more useful insights, we also plot a 3D curve illustrating the cumulative impact of d_{SR} and n_m on the outage of the O-RIS aided V-VLC, V-RF with relaying and the proposed hybrid V-VLC/V-RF schemes in Fig. 5.4(a). Interestingly, irrespective of d_{SR} and n_m , the proposed system always outperforms the other configuration in terms of outage performance. From a scheme design perspective, n_m play a key role in deciding the performance of O-RIS aided V-VLC schemes.

Next, we employ traffic flow theory to reveal the impact of interfering vehicles' speed (v_i) on the outage performance of proposed system assuming stationary traffic conditions¹. Given the traffic flow $q = v_i \times \lambda$, we utilize speed-density flow model to show the impact of v_i on the outage performance [119]. Fig. 5.4(b) illustrates the behaviour of outage and λ (veh/km) as a function of v_i . Under such traffic condition, the outage of the system improves with increase in

¹Under non-stationary traffic conditions, the time varying effects of V2X channels and Doppler shift are beyond the scope of this study and has been left as a subject of future investigation.

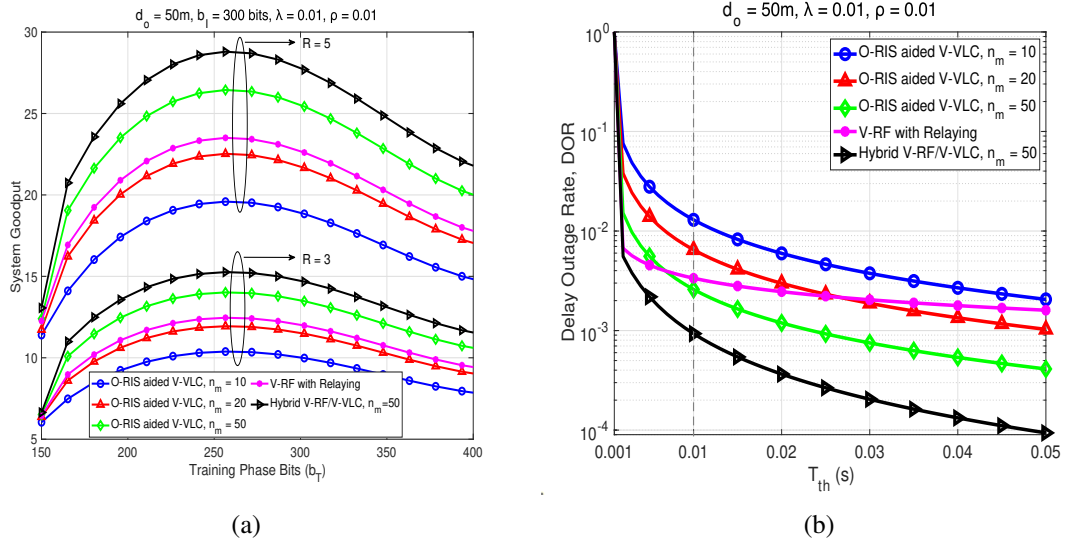


Figure 5.5: (a) System goodput versus number of training bits (b_T) for $R \in \{3, 5\}$ and (b) Impact of delay threshold (t_{th}) on DOR.

vehicular speed. This is due to fact that light traffic (low λ) supports high vehicular speed and vice versa obeying speed-density flow model.

Fig. 5.5(a), shows the variations of system goodput versus training phase bits (b_T) for various configurations. Notice that for given b_I transmission and arbitrary b_T bits, O-RIS enabled hybrid RF-VLC V2X always offers highest \mathbb{G} . Note that \mathbb{G} is a function of r and probability of successful transmission, $P_s (= 1 - P_{out})$. For sending given b_I , with increase in b_T , r decreases, which in turn increase P_s . This demonstrates that there exists an optimal value of b_T which must be carefully set in order to maximize \mathbb{G} under given traffic conditions. Fig. 5.5(b) compares DOR performance for various V2X schemes ensuring different delay threshold requirement for sending data amount, $H=50$ KB. Interestingly, for data traffic with stringent delay constraint, say $T_{th}=10$ ms, the proposed O-RIS enabled hybrid V-VLC/V-RF supports minimum delay in transmitting H bits from S to D as compared to standalone V-RF with relaying and O-RIS aided V-VLC schemes.

5.5 Concluding Remarks

In this chapter, we unlocked the potential benefit of employing O-RIS enabled hybrid RF-VLC V2X communication for enhanced vehicular message dissemination at road intersection. Numerical results demonstrated that the proposed framework offers considerable improvement in outage performance, higher system goodput and low latency compared to standalone V-RF and V-VLC counterparts, making it a promising candidate for 6G-ITS applications.

Impact of Weather Conditions and Interference

6.1 Introduction

V-RF communication in the 5.9 GHz frequency band has virtually no atmospheric or weather effects¹; the main contributors are thermal noise at the antenna receiver and the interference caused from other simultaneous transmissions [126]. Unlike V-RF communication, the performance of V-VLC is considerably affected under various environmental deterrents such as rain, light fog, dense fog, dry snow, wet snow etc.[127]. Apart from the impact of various environmental deterrents, interference from neighboring vehicles is also a major source of degradation for V-VLC channel. Most of the previous studies have not considered the impact of interference from multiple interferers as well as various environmental deterrents on performance of V-VLC based on illumination intensity (power) pattern for a typical vehicle headlamp module. In this work, we compare and model the statistical behaviour of interference experienced by conventional V-RF and V-VLC by utilizing various analytical tools of stochastic geometry. Further, the impact of interference from multiple interferers on performance of V-VLC based on illumination intensity (power) pattern for a typical vehicle headlamp has also been demonstrated for various environmental conditions.

6.1.1 Contribution

The key contribution of the proposed work can be summarized as follows:

¹Recommendation ITU-R P.525-2, 1994

- This article gives an analytic framework for estimating the average signal-to-interference-plus noise ratio (SINR) and thus provides the expected performance for both conventional V-RF as well as V-VLC using various analytical tools of stochastic geometry. The developed framework is also precise in terms of capturing the impact of field-of-view (FOV) of the photo-detector (PD) receiver on the number of interferers and distribution of the aggregate interference for a V-VLC communication system.
- The impact of mean interference as well as various environmental deterrents viz. light fog, dense fog and dry snow conditions on received illumination power (intensity) pattern for original equipment manufacturer (OEM) LED headlamp has also been demonstrated.
- The performance of conventional RF based V2V and VLC based V2V under the above environmental deterrents has been evaluated and compared in terms of probability of successful transmission as a performance metric.

6.2 System Model

A typical V2V communication scenario has been shown in Fig. 6.1. For sake of analysis, we consider one-way double lane highway road wherein communication link either RF or VLC exists between vehicle A and B, whereas vehicles in another lane acts as interferers (say, for instance vehicle C and D are acting as interferers). Vehicle B is the transmitter which is trying to communicate information (for instance, speed of vehicle, traffic direction or warning messages) with vehicle A which acts as receiver. The location of photodetector may be chosen nearby vehicle headlamp/taillight. It is assumed that vehicle B has low beam OEM LED headlamps of a Toyota Corolla Altis (Taiwan model, 2015) whose received illumination pattern has been shown in Fig. 6.2 based on empirical measurements obtained from [128]. All the vehicles use the same frequency (f_c), bandwidth (B) and transmit with same power (P_t) concurrently.

We capture the randomness in geometrical distribution when the locations of interfering vehicles on a certain lane are completely independent of each other. We represent this set of vehicles as Ψ_{PPP} . We assume that the interfering vehicles are nearly aligned on same lane and thus encounters constant lane spacing, L . Since the interfering vehicles are on same lane and their locations are Poisson distributed, the proposed scenario resembles a uni-dimensional Poisson point process (PPP) in \mathbb{R}^1 with a homogeneous congestion parameter, λ measured in number of vehicles per unit length. A more generalized and simplified geometrical layout of proposed scenario has been shown in Fig. 6.3. It is assumed that vehicle A is located at the origin O . Here, L , x and d_n denote the inter-lane spacing, the horizontal distance of interferer from origin O and the distance of n^{th} interferer to vehicle A respectively.

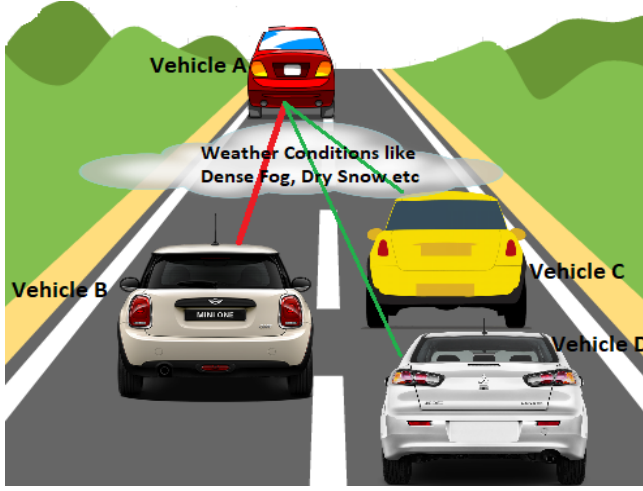


Figure 6.1: System model. Here, vehicle C and vehicle D act as interferers (denoted by green solid line) for the dedicated communication link (denoted by red solid line) between vehicle A and vehicle B.

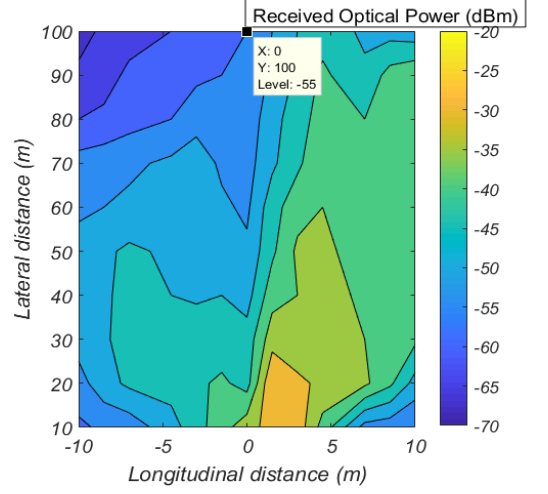


Figure 6.2: OEM headlamp optical illumination pattern with receiver height of 0.7 m. The values in the plots represent the received optical power and are in dBm.

In order to show the reduced effect of interference and increase the communication range from desired vehicle, we introduced the correction function, $C(\theta_R)$ at the receiver, which implies that the interferers that are located within PD's FOV will only be considered. Correction function $C(\theta_R)$ can be expressed in terms of PD's FoV as:

$$C(\theta_R) = \begin{cases} 1; & \text{if } 0 \leq \theta_R \leq \Psi_{FOV}, \\ 0; & \text{if } \theta_R > \Psi_{FOV}, \end{cases} \quad (6.1)$$

The above scenario can be best visualized in the form of Fig. 6.4 which clearly depicts that reducing PD's FOV can significantly reduce the effect of interference caused by interferers from other lane. Like small cell concept for indoor RF scenario, the VLC attocell concept can be applied for outdoor scenarios as well [129], [130]. In fact, the critical radius² (r) of VLC attocell for desired vehicle with communication range (D) can be defined as the radius beyond which the effect of interference is less pronounced (i.e., $P_r > \bar{I}_{VLC}$). The critical radius can be computed as:

$$\frac{C(\theta_R)(m+1)A_R}{2\pi D^\gamma} \frac{D^{(m+1)}}{(D^2 + r^2)^{\frac{(m+1)}{2}}} P_t > C(\theta_R)\lambda k' \quad (6.2)$$

²The notion of critical radius in general contains the effect of PD's FOV variation.

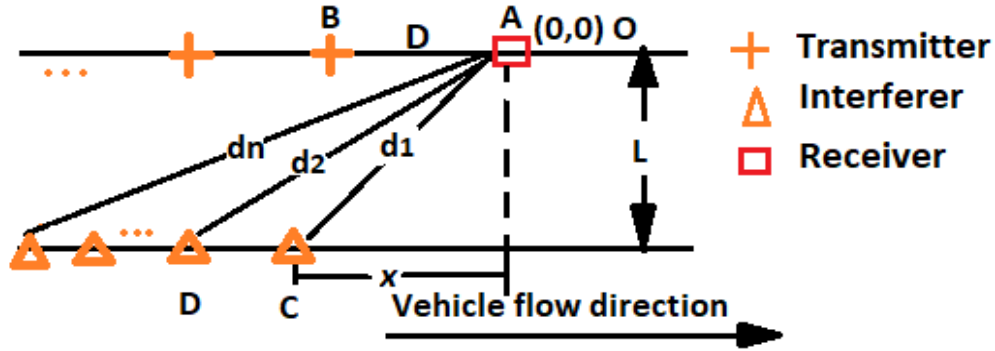


Figure 6.3: Simplified geometrical layout. Vehicle A is assumed to be located at the origin O . Here, D denotes distance between legitimate vehicle and receiver.

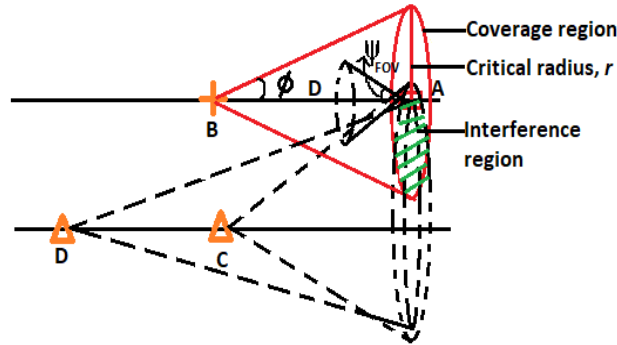


Figure 6.4: Reference scenario illustrating coverage and interference region using VLC attocells. Here, r and D denotes radius of VLC attocell under coverage region of desired vehicle and communication-range respectively.

(6.2) can be rewritten as:

$$r < \left\{ \left[\frac{(m+1)A_R P_t}{\lambda k' D^\gamma} - 1 \right] \frac{2D^2}{(m+1)} \right\}^{\frac{1}{2}} ; \quad D \gg r \quad (6.3)$$

6.2.1 Cumulative distribution function (CDF) of Interference

The cumulative distribution function of interference ($F_{\mathcal{I}}(x)$) is defined as the probability that interference power is below than a certain minimum threshold level. At the receiver, it is indeed important that interference power should be as minimum as possible for a signal to be decoded correctly.

In order to evaluate the statistical behaviour of the interference, we first obtain its characteristics function (CF) denoted as $\varphi_{\mathcal{I}}$ and then evaluate its cumulative distribution function (CDF) denoted as $\mathcal{F}_{\mathcal{I}}(x)$. The CF of a random variable X is defined as $\mathbb{E}[e^{j\omega X}]$. For proposed scenario, the characteristic function can be expressed as

$$\begin{aligned}\varphi_{\mathcal{I}}(\omega) &= \mathbb{E}[e^{j\omega I}] = \mathbb{E}_{x \in \Psi_{PPP}} \left[\exp(j\omega \sum_{x \in \Psi_{PPP}} \mu_1 P_t \frac{x^{m+1}}{(L^2 + x^2)^{\frac{m+\gamma+1}{2}}}) \right], \\ &= \mathbb{E}_{x \in \Psi_{PPP}} \left[\prod_{x \in \Psi_{PPP}} \exp(j\omega \mu_1 P_t \frac{x^{m+1}}{(L^2 + x^2)^{\frac{m+\gamma+1}{2}}}) \right],\end{aligned}\quad (6.4)$$

The probability generating functional (PGFL)³ for function $f(x)$ for homogeneous PPP over region of interest, \mathcal{R} can be given as [103][Th 4.9]:

$$\mathbb{E} \left[\prod_{x \in \Psi_{PPP}} f(x) \right] = \exp \left(-\lambda \int_{\mathcal{R}} [1 - f(x)] dx \right), \quad (6.5)$$

Using (6.5), (6.4) can be rewritten as:

$$\varphi_{\mathcal{I}}(\omega) = \exp \left(-\int_0^\infty \left[1 - \exp \left(\frac{j\omega \mu_1 P_t x^{m+1}}{(L^2 + x^2)^{\frac{m+\gamma+1}{2}}} \right) \right] \lambda dx \right), \quad (6.6)$$

The above integral can be numerically evaluated in order to obtain the CDF using Gil-Peleaz's inversion theorem [131].

$$F_{\mathcal{I}}(x) = \frac{1}{2} - \frac{1}{\pi} \int_0^\infty \frac{1}{\omega} \Im [\varphi_{\mathcal{I}}(\omega) e^{-j\omega x}] d\omega, \quad (6.7)$$

For sake of simplicity, the inter-lane distance, L with respect to the longitudinal stretch of the road is ignored. Without loss of generality, we further simplify the above characteristic function by setting the value of path loss exponent ($\gamma = 2$), thus (6.7) reduces to a more simplified and closed form as:

³The PGFL can be visualized as an equivalent for point process of the moment generating function or characteristic function (that provide an alternative description of random variables). It enables to compute the Laplace transform (LT) of random variables of the form $F = \sum_{X_i \in \Psi_{PPP}} g(X_i)$. Mathematically, LT of such function can be given as:

$$\mathcal{L}(s) = \mathbb{E} \left[\exp(-s \sum_{X_i \in \Psi} g(X_i)) \right] = \mathbb{E} \left[\prod_{X_i \in \Psi} e^{-sg(X_i)} \right]$$

$$\begin{aligned}\varphi_{\mathcal{J}}(\omega) &= \exp\left(-\left[\lambda\Gamma\left(1-\frac{1}{\gamma}\right)(-j\mu_1 P_t \omega)^{\frac{1}{\gamma}}\right]\right), \\ &= \exp\left(-\sqrt{-j\pi\mu_1 P_t \omega \lambda^2}\right),\end{aligned}\tag{6.8}$$

Eq.(6.8) can be compared with a tractable Levy-distribution having a CF and a CDF of the form:

Using similar steps (6.4-6.8) and assumptions as before, the expression for interference cumulative distribution function for V-RF can be given as:

$$F_{\mathcal{J}_{RF}}(x) = \xi_c \left(\sqrt{\frac{\pi\lambda^2\gamma_2 P_t}{4x}} \right).\tag{6.10}$$

The performance of proposed scenario has been evaluated in terms of probability of successful transmission, P_s as performance metric for three different traffic scenarios viz. dense, medium and sparse traffic scenario.

6.3 Probability of successful transmission

For a given modulation and coding scheme (MCS), treating interference as noise, say for instance, by using a simple linear receiver, a well-accepted model for packetized transmissions is considered successful if the SINR exceeds a certain threshold (ζ). The probability of successful transmission (\mathcal{P}_s) is formally defined as the probability that SINR is greater than a certain minimum threshold level. Its complement is outage probability. The SINR can be given as:

$$SINR = \frac{S}{\mathcal{J}_{\{VLC,RF\}} + \sigma_i^2},\tag{6.11}$$

where S , $\mathcal{J}_{\{VLC,RF\}}$ and σ_i^2 denote the desired optical signal power, the interference associated with V-VLC or V-RF and the noise variance respectively. Accordingly, we formulate the

probability of successful packet transmission as:

$$\begin{aligned}
P_s &= \mathbb{P}(SINR \geq \zeta) \\
&= \mathbb{P}\left(\mathcal{I}_{\{VLC,RF\}} \leq \frac{S}{\zeta} - \sigma_t^2\right), \\
&= \mathcal{F}_{\mathcal{I}}\left(\frac{S}{\zeta} - \sigma_t^2\right).
\end{aligned} \tag{6.12}$$

Thus, the probability of successful packet transmission for V-VLC can be given as:

$$\mathcal{P}_s = \xi_c \left(\sqrt{\frac{\pi\lambda^2\mu_1 P_t}{4\left(\frac{S}{\zeta} - \sigma_t^2\right)}} \right). \tag{6.13}$$

For dense traffic scenario, interference becomes the limiting performance factor rather the noise variance and hence, noise variance may be ignored. Hence, (6.13) reduces to:

$$\mathcal{P}_s = \xi_c \left(\sqrt{\frac{\pi\lambda^2\mu_1 P_t \zeta}{4S}} \right). \tag{6.14}$$

We investigate the probability of successful packet transmission for V-RF communication on free space propagation model with no channel fading as well as Rayleigh-fading cases.

6.3.1 No channel fading with path loss exponent, $\alpha=2$

In case of no-channel fading, the presented framework offers a closed-form expression of probability of successful transmission⁴ which is given as:

$$\mathcal{P}_s = \xi_c \left(\sqrt{\frac{\pi\lambda^2\gamma_2 P_t \zeta}{4S}} \right). \tag{6.15}$$

6.3.2 Rayleigh fading case

In this case, we consider a higher path-loss exponent and Rayleigh fading on the interfering signals as worst-case scenario of the multipath-induced random fluctuations in the received power. The probability of successful transmission for V-RF communication with Rayleigh

⁴The expression has been derived in same way as discussed before for V-VLC scenario.

fading can be computed as:

$$\begin{aligned}
P_s &= \mathbb{P}(SINR \geq \zeta) \\
&= \mathbb{P}\left(\frac{P_t G_t G_r \ell h_x D^{-\alpha}}{I_{RF} + \sigma_t^2} > \zeta\right) \\
&= \mathbb{E}_{I_{RF}} \left[\mathcal{P}\left(h_x > \frac{\zeta}{P_t G_t G_r \ell D^{-\alpha}} (I_{RF} + \sigma_t^2)\right) \right] \\
&= \exp\left(-\frac{\zeta \sigma_t^2}{P_t G_t G_r \ell D^{-\alpha}}\right) \mathbb{E}_{I_{RF}} \left[\exp\left(-\frac{\zeta I_{RF}}{P_t G_t G_r \ell D^{-\alpha}}\right) \right] \\
&= \mathcal{L}_{I_{RF}}\left(\frac{\zeta}{P_t G_t G_r \ell D^{-\alpha}}\right) \exp\left(-\frac{\zeta \sigma_t^2}{P_t G_t G_r \ell D^{-\alpha}}\right)
\end{aligned} \tag{6.16}$$

where, $\mathcal{L}(\cdot)$ stands for Laplace transform which is given as:

$$\begin{aligned}
\mathcal{L}_{I_{RF}}(s) &= \mathbb{E}[\exp(-sI_{RF})] \\
&= \mathbb{E}\left[\prod_x \exp(-sP_t G_t G_r \ell h_x ||x||^{-\alpha})\right] \\
&\stackrel{(a)}{=} \mathbb{E}_x \left[\prod_x \mathbb{E}_{h_x} \{ \exp(-sP_t G_t G_r \ell h_x ||x||^{-\alpha}) \} \right] \\
&= \mathbb{E}_x \left[\prod_x \frac{1}{1 + sP_t G_t G_r \ell ||x||^{-\alpha}} \right] \\
&\stackrel{(b)}{=} \exp\left(-\lambda \int_0^\infty \frac{1}{1 + ||x||^\alpha / sP_t G_t G_r \ell} dx\right) \\
&\stackrel{(c)}{=} \exp\left(-\lambda (sP_t G_t G_r \ell)^{\frac{1}{\alpha}} \int_0^\infty \frac{1}{1 + v^\alpha} dv\right) \\
&= \exp\left(-\lambda (sP_t G_t G_r \ell)^{\frac{1}{\alpha}} \frac{\pi}{\alpha} \csc\left(\frac{\pi}{\alpha}\right)\right)
\end{aligned} \tag{6.17}$$

here, (a) holds due to independence of fading coefficients h_x and assumes $L \ll x$, (b) uses the definition of PGFL for PPP, and (c) involves the change of variable $||x|| / (sP_t G_t G_r \ell)^{\frac{1}{\alpha}} \rightarrow v$. Substituting $s = \frac{\zeta}{P_t G_t G_r \ell D^{-\alpha}}$ yields the following result.

$$\mathcal{L}_{I_{RF}}\left(\frac{\zeta}{P_t G_t G_r \ell D^{-\alpha}}\right) = \exp\left(-\lambda (\zeta)^{\frac{1}{\alpha}} D \frac{\pi}{\alpha} \csc\left(\frac{\pi}{\alpha}\right)\right). \tag{6.18}$$

6.4 Simulation Results and Discussion

In this section, we present numerical results that substantiate our theoretical findings. The system model parameters are adopted in accordance with practical vehicular scenario as used

in Table I. In order to validate the accuracy of our theoretical findings, Monte Carlo simulations are performed by averaging over 10,000 realizations of PPPs and fading channel parameters. We consider a worst case scenario where interference from interferers arise from infinite road segment. In traffic flow theory, space headway (s) is defined as horizontal distance between vehicles (in metres). The space headway is related to congestion parameter as $s = \frac{1}{\lambda}$ [132]. Hence, space headway can also be referred as inverse congestion parameter. Fig. 6.5 (a)-(c)

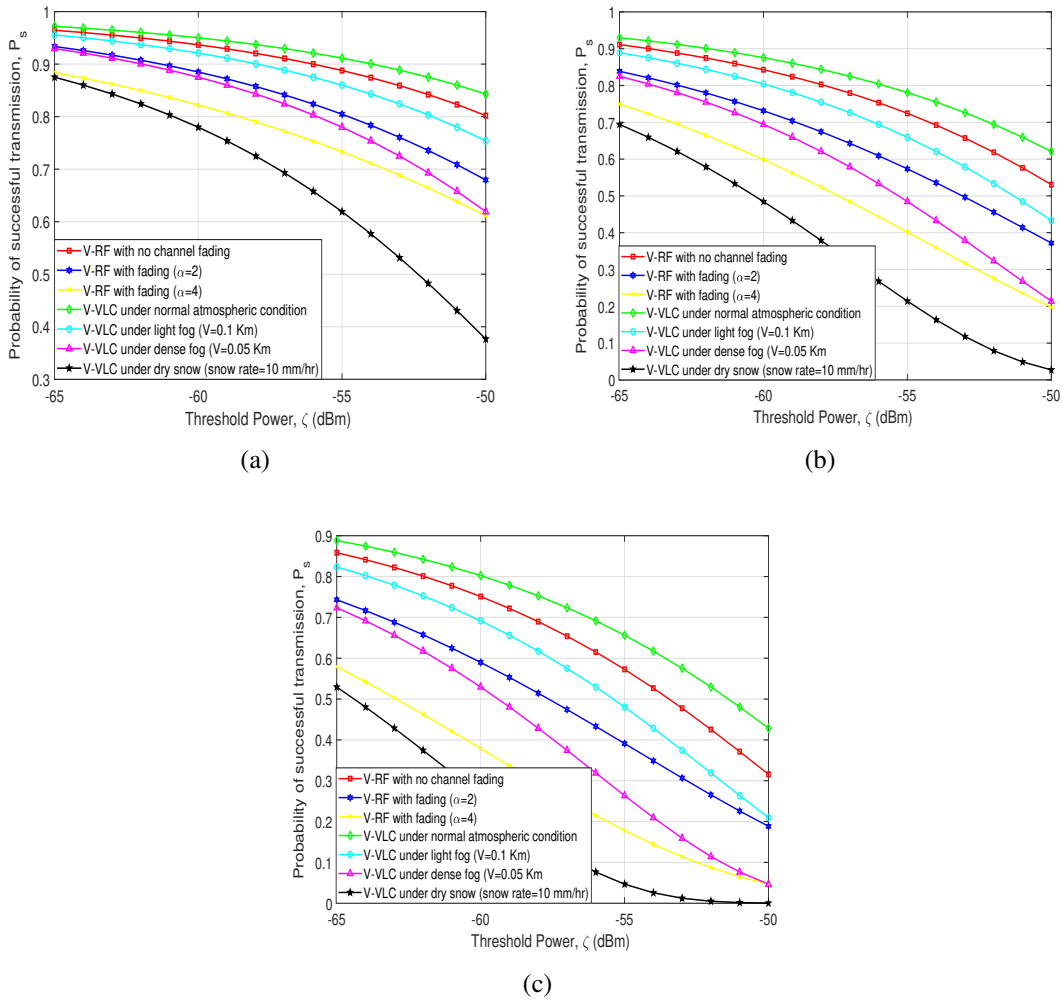


Figure 6.5: Probability of successful transmission over a range of threshold power (a) sparse traffic scenario when $s=50$ m, (b) medium traffic scenario when $s=20$ m, and (c) dense traffic scenario when $s=12.5$ m.

show probability of successful transmission variation over a range of threshold power for V-RF and V-VLC under various environmental deterrents for three different traffic scenarios viz. sparse, medium and dense traffic. It can be observed that irrespective of traffic scenario, the probability of successful transmission for V-VLC communication under normal atmospheric

condition outperforms V-RF communication for a given threshold power. However, it is also worth noting here that for a given threshold power, V-RF communication under no fading conditions outperforms V-VLC when environmental deterrents such as light fog, dense and dry snow conditions are considered. Interestingly, the performance of V-VLC under light fog condition is comparatively better than the performance of V-RF communication under rayleigh fading conditions with path loss exponent, α of 2 or 4. With threshold power of -65 dBm,

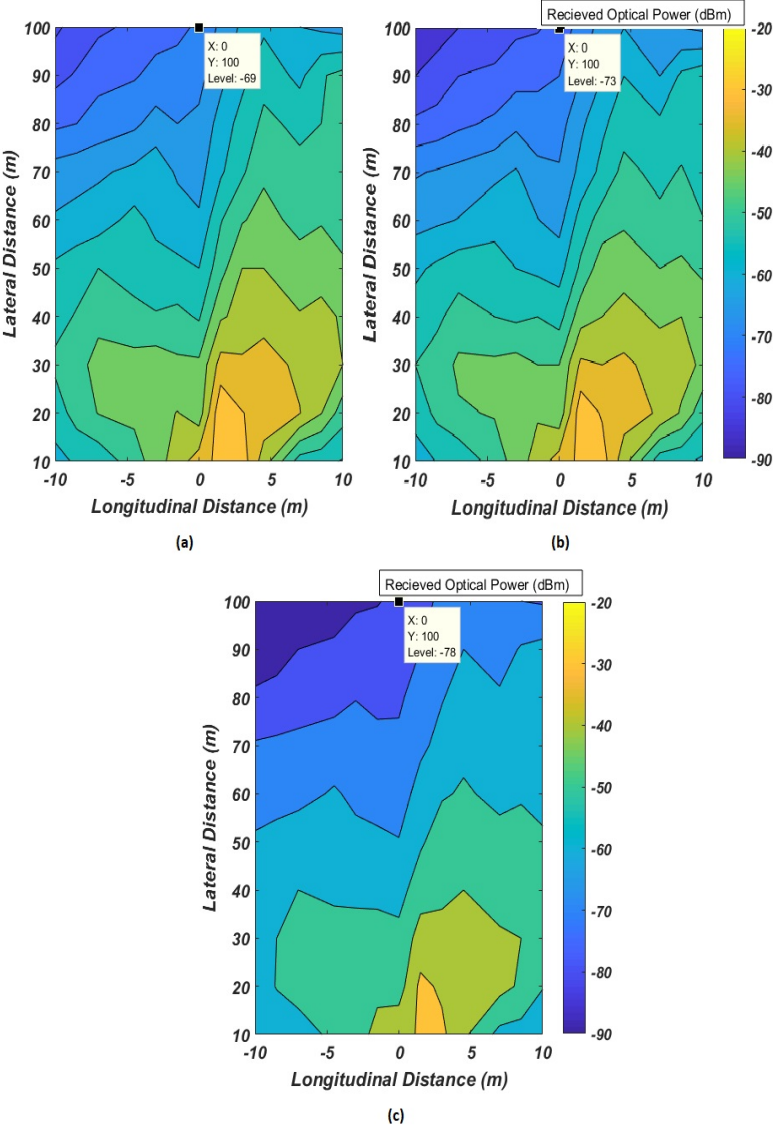


Figure 6.6: OEM headlamp optical radiation pattern with receiver height of 0.7 m with interference when space headway between interferers is 20 m under (a) light fog ($V=0.1$ Km), (b) dense fog ($V=0.05$ Km) and (c) dry snow condition (Snow rate=10 mm/hr).

the performance of V-VLC under dry snow condition falls by 40% as compared to normal weather conditions under dense traffic scenario when inverse congestion parameter is 12.5

m. This is primarily due to high attenuation in the average optical power received under dry snow condition. Kindly note that the proposed work does not take into account scheduling for vehicular transmission, which indeed resulted in lower probability of successful transmission for some curves, especially dense traffic scenario.

Fig. 6.6 shows the impact of various environmental deterrents on OEM headlamp optical radiation pattern based on [133] and [134]. Table 6.1 shows the impact of interference as well as various environmental deterrents on average received optical power with receiver height of 0.7 m at a distance of 100 m from location of headlamp. As compared to normal atmospheric conditions, the optical power loss⁵ at a distance of 100 m from transmitter under dry snow condition reduces by 23 dB taking into consideration the effect of interference as well as the environmental deterrent.

Table 6.1: Average received optical power for V-VLC in presence of interference when space headway between interferer is 20 m under different environmental deterrents at a distance of 100 m from transmitter.

S.No.	V2V Communication	Received power (dBm)	Power loss (dB)
1	V-VLC under normal atmospheric	-65 dBm	10 dB
2	V-VLC under light fog	-69 dBm	14 dB
3	V-VLC under dense fog	-73 dBm	18 dB
4	V-VLC under dry snow	-78 dBm	23 dB

6.5 Concluding Remarks

The proposed work characterized various aspects of stochastic behaviour of interference by modelling location of road vehicles as a spatial Poisson point process. This work is also precise in terms of capturing the impact of reducing FOV of receiver on the level of interference experienced from interferers. The performance of conventional V-RF and V-VLC under various environmental deterrents viz. light fog, dense fog and dry snow conditions has been investigated and evaluated in terms of probability of successful transmission as a performance metric. We have also illustrated OEM headlamp illumination patterns in presence of interference under above environmental deterrents. Irrespective of any traffic scenario, the performance of V-VLC communication under normal atmospheric condition always outperforms V-RF communication. However, the performance of V-RF communication is comparatively better than V-VLC under various environmental deterrents. The proposed result motivates the benefit of employing

⁵Power loss has been calculated with respect to average optical power received at a distance of 100 m from transmitter without taking into consideration the impact of interference and environmental deterrents

RF-based or VLC-based V2V communication which can cater for different environmental deterrents, thus serving as a better alternative option to meet diverse application needs for future intelligent transportation system.

Part II

6.6 Overview of Part II

In this work, we show how the judicious link aggregation (LA) of V-VLC and V-RF improves the network performance as compared to standalone RF or VLC based V2X communication systems under different meteorological factors. Briefly, link aggregation results in more efficient use of physical resources as well as improves reliability and availability.

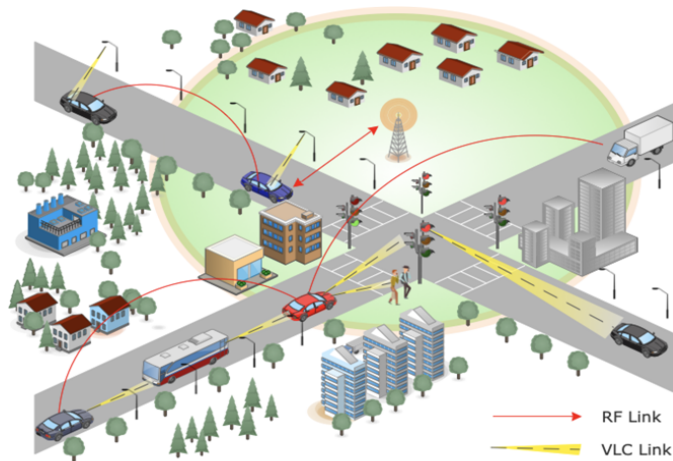


Figure 6.7: Illustration of a generic hybrid RF-VLC communication in a vehicular network.

6.7 Case Study: Hybrid RF-VLC V2X Systems

In hybrid RF-VLC V2X systems, the co-deployment of vehicular-VLC (V-VLC) and V-RF communication systems is capable of improving the safety message dissemination at road intersections. It has been shown in [112] that non LA hybrid RF-VLC V2X networks lead to substantial reduction of outage along with improvements of throughput and latency as compared to pure V-VLC or pure V-RF networks. However, the judicious link aggregation of V-VLC and V-RF can further improve the network performance as compared to standalone RF or VLC based V2X communication systems. For sake of analysis, we consider a typical road

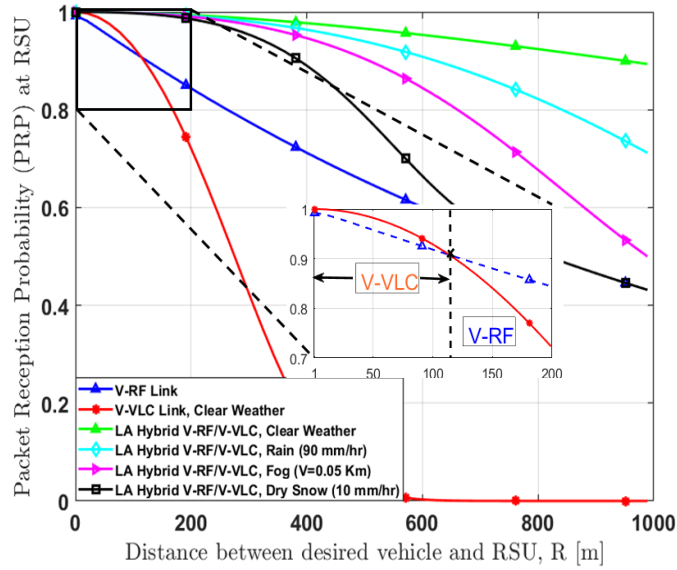


Figure 6.8: PRP at RSU for pure V-RF, pure V-VLC and LA hybrid RF-VLC V2X communication system under rain, fog and dry snow conditions.

intersection scenario as shown in Fig. 6.7, in which vehicles equipped with both VLC and RF transceivers are assumed. For the sake of illustration, we consider a LA hybrid RF-VLC V2X uplink scenario and compare its performance to that of the pure V-VLC and pure V-RF uplink taking into consideration the impact of interference and various meteorological phenomenon such as rain, fog and dry snow conditions with an aid of stochastic geometry tools. The LA technique enhances not only the total available bandwidth, but also leads to more reliable network performance, and reduction in the end-to-end latency. We take into account that the communications between the RSU and desired vehicle are subject to interference from the same lane as well as from vehicles in the perpendicular lanes. The system parameters were chosen in accordance with a practical vehicular communication scenario as in [112]. The attenuation coefficient under rain (rain rate=90 mm/hr), fog ($V=0.05$ Km) and dry snow (snow rate=10 mm/hr) are taken to be 21.9, 78.8 and 131 dB/km respectively as given in [135, Table 2]. Unless otherwise stated, we assume having the vehicular density λ and channel access probability ρ to be 0.01 and 0.01, respectively. Observe from Fig. 6.8 that depending on the transmitter's location, the pure V-VLC and V-RF systems exhibit complementary roles in terms of packet reception probability (PRP). In particular, the PRP for standalone V-VLC links is better as compared to V-RF links, when the distance between the RSU and desired vehicle is not higher than 120 m. However, pure V-RF is a more reliable option for longer-range communication. Interestingly, regardless of the distance between the desired vehicle and the RSU and any prevailing weather conditions, the LA hybrid RF-VLC V2X systems outperform the pure

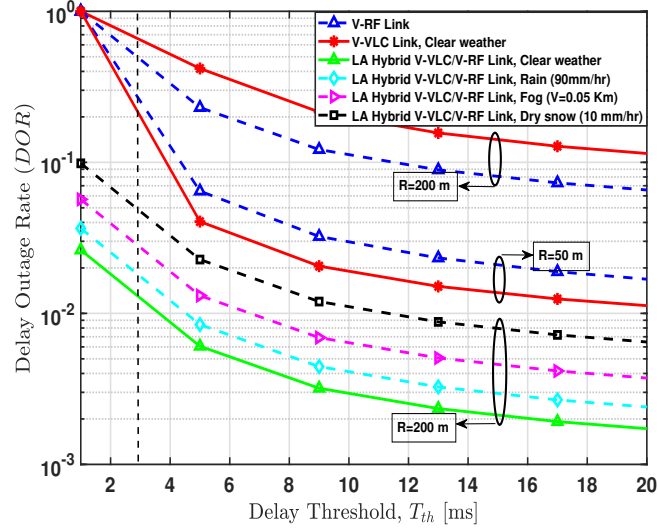


Figure 6.9: Delay outage performance for pure V-RF, pure V-VLC and LA hybrid RF-VLC V2X communication system as a function of delay threshold, T_{th} .

V-VLC or V-RF links. Notice that the performance of LA systems are mainly influenced under dry snow condition. This is primarily due to high attenuation in the pure V-VLC link under dry snow condition.

Many warning/safety specific messages are life-critical, hence a high latency is unacceptable, especially in accident-prone situations. It is anticipated that the hybrid RF-VLC V2X systems can offer ultra-reliable low latency communication (URLLC) among vehicles, while meeting 6G key performance indicators (KPIs) vehicular network requirements. According to [112, Eq.(28)], we consider the metric of delay outage rate (DOR), which represents the probability that the minimum transmission time (MTT) required for sending a certain amount of data is higher than the tolerable duration. We plot the DOR of standalone V-RF, LA hybrid RF-VLC V2X, and pure V-VLC ensuring different maximum delay requirements for both 50m and 200m distances in Fig. 6.9. Here, we assume that the system bandwidth for pure RF and VLC system to be 20 MHz⁶. Again, depending on the transmitter's location, pure V-VLC and V-RF exhibit complementary roles, as evidenced by Fig. 6.9. Additionally, for data traffic having stringent delay requirements of < 3 ms, the LA-aided hybrid RF-VLC V2X under any weather condition ensures having the minimum delay in transmitting data size, $H=50$ KB from the desired vehicle to the RSU as compared to pure V-VLC or V-RF systems. In light of the above results, it can be inferred that irrespective of any meteorological phenomenon, the LA-aided hybrid RF-VLC V2X system achieves ultra high reliability ($\sim 99.999\%$) and ultra-low latency (< 3 ms) up to

⁶RF spectrum is generally licensed and expensive, whereas VLC spectrum is free, hence it more cost effective.

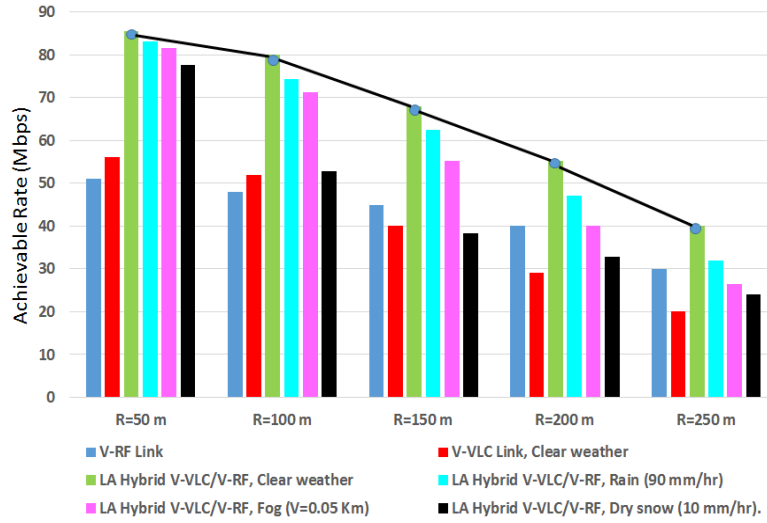


Figure 6.10: Achievable data rate for different network configuration for different values of distance between RSU and desired vehicle.

$R=200\text{m}$. For an interference-limited scenario, the LA-aided hybrid RF-VLC V2X system meets stringent reliability and latency requirements for advanced vehicular scenarios [3].

Fig. 6.10 shows the achievable data rate for different network configurations for various R values. In an interference-limited scenario, the maximum achievable data rate associated with LA-aided hybrid RF-VLC V2X can be as high as 83.2 Mbps at $R=50\text{m}$, which reduces to 39.8 Mbps at $R=250\text{m}$ under clear weather conditions. Note that the achievable rate of a non-LA hybrid RF-VLC V2X system depends on the maximum throughput offered by either pure V-VLC or pure V-RF systems. Here, we assume that the desired vehicle accesses the channel at a transmission probability of $p_A=0.9$ and link aggregation overload of $\beta_{ov}=0.8$ [136]. The results presented meet the data rate requirements of advanced vehicular scenarios that have been investigated in [3]. Note that advanced driving scenario covers the cases of semi-automated or fully-automated driving for longer inter-vehicle distance, supporting data rates ranging from 10-53 Mbps among vehicles or RSUs in the proximity.

6.8 Concluding Remarks

In this work, we have shown that the potential benefits of hybrid RF-VLC based vehicular communication systems by exploiting the complementary advantages of both technologies. In particular, Figures 6.8-6.10 have demonstrated that regardless of any meteorological phenomenon, link aggregation aided hybrid RF-VLC V2X systems are capable of achieving considerable performance improvement in successful packet reception probability, data rate

and latency compared to pure RF and VLC counterparts, making it a promising technology for various 6G-V2X applications.

Conclusion and Future Work

In this chapter, we summarize the key contributions of this dissertation and discuss a few promising future directions of research.

7.1 Summary

We are witnessing a transition to a new era where driverless cars are pervasively connected to deliver significantly improved safety, traffic efficiency, and travel experiences. A diverse range of advanced vehicular use cases including connected autonomous vehicles will be made possible with the 6G wireless networks. Among many 6G wireless technologies, the mission of this research work is to introduce the potential benefits of the hybrid integration (and co-existence) of V-VLC and V-RF communication systems for various use-case scenarios.

In this thesis, we advocated the use of V-VLC for basic safety messages (BSMs) dissemination in lieu of conventional V-RF communication in road intersection applications, where the reception performance is affected by interference from the concurrent transmissions of other vehicles. Numerical results illustrate that the implementation of MAC protocol based hybrid V-VLC/V-RF network leads to considerable improvement in outage performance, throughput and low latency as compared to stand-alone V-VLC or stand-alone V-RF network. Additionally, we proposed to use practical deployment strategies namely hybrid V-VLC/VRF with relaying and RIS aided V-RF solutions to improve the communication range for urban V2V communication. Numerical results illustrate that the proposed solutions can achieve considerable performance improvement in outage, throughput while ensuring low latency as compared to conventional V-RF with relaying.

In Chapter 4, we explored the potential benefits and practical challenges associated with implementation of optical power domain non-orthogonal multiple access (OPD-NOMA) scheme

for visible light communications (VLC) based vehicle-to-everything (V2X) networks with a major aim of providing vehicles with reliable, ubiquitous, and massive connectivity. Through the obtained results, it has been shown that the downlink OPD NOMA based V2X network offers improved performance in terms of outage performance and average achievable rate as compared to the conventional RF based V2X communication. Further, we investigated the performance of a novel cooperative NOMA assisted hybrid VVLC and V-RF solution to the V2X communication at road intersections. It has been shown through simulation results that the performance of the hybrid V-VLC/V-RF network is better than a conventional V-RF system in terms of outage probability and average achievable rate.

We also highlighted the benefit of employing optical reconfigurable intelligent surfaces (O-RIS) for hybrid RF-VLC V2X communication network for enhanced traffic safety message dissemination particularly at the road intersections in Chapter 5. Numerical results indicate that compared to existing classical RF with relaying solution, a significant improvement in outage performance, system goodput, and delay outage rate (DOR) performance can be achieved for proposed system setup.

In chapter 6, we analyzed the impact of interference and meteorological phenomenon on the performance of hybrid V-VLC/V-RF system. In particular, we show that regardless of any meteorological impact, a properly configured link-aggregated hybrid V-VLC/V-RF system is capable of meeting stringent ultra high reliability ($\geq 99.999\%$) and ultra-low latency (< 3 ms) requirements, making it a promising candidate for 6G Vehicle-to-Everything (V2X) Communications.

7.2 Future Directions

There are numerous ways in which this dissertation's work can be extended. The following are some potential future research directions:

7.2.1 Reconfigurable Intelligent Surfaces (RIS) Enabled Hybrid RF-VLC V2X Systems

Recently, RIS has attracted much research attention owing to its salient feature of transforming hostile wireless channels into benign ones. It has emerged as a disruptive communication technology for enhancing signal quality and transmission coverage in wireless vehicular networks. Significant gains may be gleaned by incorporating RISs into hybrid RF-VLC V2X systems, thanks to the enhanced resilience to LoS blockages, especially, when striking a flexible tradeoff between lighting and communications, quality-of-service, interference mitigation,

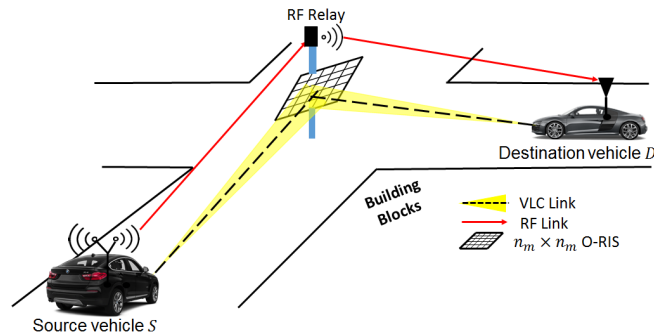


Figure 7.1: O-RIS/metasurface can be deployed on RSU/buildings at road intersection to relax the LOS requirement between source and destination vehicles in hybrid RF-VLC V2X systems.

enhanced localization services, and improved energy harvesting. In particular, 6G-V2X can take advantage of RISs in coverage-limited scenarios. For instance, in urban areas, road intersections constitute an ideal use case for deploying RIS-aided RF-VLC V2X systems, where the exchange of safety messages between vehicle lights may be blocked by buildings, walls, surrounding vehicles and other obstructions, as shown in Fig. 7.1. By enabling an RIS controller to actively relay the information from the source to the destination vehicle, the RIS can not only potentially help improve the transmission rate for standalone V-VLC systems, but also provide wide coverage range using RIS controller. As soon as the quality of VLC link degrades (eg. long range communication case), the communication between source and destination vehicles can still be accomplished using conventional V-RF systems employing relaying [116]. Nonetheless, several distinctive research challenges such as channel estimation in highly dynamic scenarios, optimal RIS deployment, reliable energy management schemes, optimal resource allocation and reflection optimization have to be carefully addressed before the practical integration of RIS into hybrid RF and VLC vehicular communication systems.

7.2.2 ML-assisted System Design

Machine learning (ML) assisted 6G is expected to unlock the promise of future ITS[4]. These features are desirable in vehicular networks to accommodate diverse and advanced use cases and their technical requirements. Due to the inherent heterogeneity and mobility of vehicular networks, communication environments are highly complex resulting in varying wireless or optical channels. On the other hand, different layers of the current RF and VLC communication systems are optimized independently. Such a design paradigm may not be ideal when dealing with diverse quality of service (QoS) requirements (e.g., throughput, delay, reliability, and spectrum efficiency), particularly when dealing with complex and dynamic vehicular environments. There is a need to configure different functional blocks of VLC/RF communication

systems in a joint and adaptive manner according to the dynamically varying vehicular network. For example, ML-assisted adaptive coding and modulation (ACM) is expected to improve the robustness whilst reducing the communication latency. ML can also be applied to optimize multiple configurations simultaneously. An end-to-end hybrid communication architecture needs to be considered when an ML-based joint optimization is developed. A hybrid RF-VLC V2X system would also face resource allocation issues such as bandwidth allocations and access point selection based on the requirements of the network, availability of resources, and mobility of the vehicles. In addition, dynamic decision making on whether to use LA or non-LA hybrid techniques can be crucial for effective and energy-efficient V2X communications. Using traditional methods of resource allocation would mean re-running the simulation for every small change, resulting in significantly large overhead [137]. In this case, ML-based approaches can be an efficient tool for making data-driven decisions to enhance the resource allocation performance in RF/VLC vehicular networks. In particular, a reinforcement learning solution for hybrid RF-VLC V2X systems can be helpful to tackle the challenge arising due to dynamic environments and shortage of relevant datasets for vehicular networks. Future research may be devoted to developing ML-based resource allocation algorithms for RF/VLC V2X network with the goal of ensuring maximum network performance and decrease in control overhead and handover latency.

7.2.3 Deployment Issues

Despite the huge potential of hybrid RF-VLC V2X systems, their widespread deployment can be hampered by availability of VLC links under meteorological phenomena such as rain, fog, snow and hazy conditions [138]. In addition, solar irradiance and artificial light sources (e.g roadside illumination, sign boards, fluorescent lamps) also impose challenges for such hybrid systems in the real world. Further, the received signal strength in VLC may dramatically vary due to the vehicles' mobility. Hence, mobility induced channel variations and ambient lighting induced interference need to be carefully addressed before deploying VLC in 6G-V2X ecosystems. Compared with V-RF, V-VLC are subject to light-path blockages, which can drastically reduce the data rate in such hybrid vehicular applications. The authors of [139] overcome this challenge by proposing omnidirectional and ubiquitous coverage in VLC. Furthermore, the specific bandwidth aggregation in LA-aided hybrid RF-VLC V2X systems constitutes an open research challenge, given for example 1Hz RF bandwidth in the sub-6GHz band and 1Hz VLC bandwidth in the 800 THz band. In light of the above discussions, it is clear that these challenges have to be tackled before the practical deployment of such hybrid systems.

7.2.4 Coexistence of mmWave, THz and VLC

Both VLC and TeraHertz (THz) techniques constitute promising candidates for realizing the vision of 6G V2X. It is anticipated that operation of 6G V2X will rely on usage of a wide range of transmission frequencies including RF, VLC, THz, and mm-wave frequencies. There exists a trade-off among coverage area, ergodic rate, mobility and latency when dealing with variety of spectrum. There can be two ways to realize the presence of multiple frequencies namely; flexible spectrum coexistence and hybrid deployment. In the flexible spectrum coexistence approach, the base stations (BSs) with different frequencies are deployed separately and each BS at a certain time can operate on only one of RF, VLC, and THz frequency bands. For flexible multi-band utilization, the multi-band C-V2X system needs advanced front-end hardware. In addition, the coexistence of different network spectrum leads to new interference problems[140]. In the hybrid approach, each BS leverages on more than one frequency band. Optimizing the opportunistic spectrum selection at the users' end, traffic-load aware network activation mechanisms, deployment of BSs, and multi-connectivity solutions will be primary challenges for such multiband vehicular networks (MBVNs).

7.2.5 NOMA and its variants

Multiple access plays a pivotal role in vehicular communication and networking. In DSRC, carrier sense multiple access (CSMA) is adopted, whereby all vehicles that have messages to send must constantly sense the availability of the channel. CSMA is simple, however may lead to large communication overhead and high collision rates in dense vehicular networks. LTE-V2X and 5G-NR-V2X, on the other hand, use OFDMA for multiple access, but they could suffer the same problem due to its orthogonal nature. In view of the explosive growth of communication sensors and connected vehicles, tremendous research activities have been carried out in recent years on non-orthogonal multiple access (NOMA) for supporting a massive number of concurrent communication links. Both power-domain NOMA and code-domain NOMA may be applied to hybrid RF-VLC based V2X communication systems. In this line of research, it is interesting to optimize the user pairing, power allocation, codebook design, and multiuser detection algorithms in order to meet the diverse QoS requirements in future vehicular networks [141]. Further, it is of practical interest to carry out user grouping such that some are supported by NOMA and some by orthogonal multiple access (e.g., OFDMA).

7.2.6 Standardization Activities

The protocols compatible interoperability between V-VLC and IEEE 802.11p is critical in designing a standard compliant outdoor aggregated RF-VLC systems. The IEEE has introduced IEEE 802.15.7 standard which comprises of PHY and MAC layer specifications designed for indoor VLC systems. It proposes three specific PHYs including one for outdoor environment, therefore, suitable to automotive applications. The authors in [142] provided a comprehensive analysis of the IEEE 802.15.7 standard in vehicular networking applications. Till now, there is only one task group (TG) in the scope of IEEE 802.15 working on the revision of the standard [143] capable of delivering data rates sufficient to support audio and video multimedia services. However there are no dedicated efforts potentially applicable for V-VLC applications. In addition to the standard mentioned above, there are two ongoing standardization activities within the IEEE, viz. TG 13 within IEEE 802.15 working group and TG "bb" within IEEE 802.11 Working Group. IEEE 802.15.13 is a revision of IEEE 802.15.7, focusing on high-speed PD-based VLC. It specifies the PHY and MAC capable of supporting data rates of up to 10 Gbps in LOS communications over distances of up to 200 meters. V-VLC systems compatible with the standard are described in [143], [144]. Against above, the IEEE 802.11 TG "bd" project was formed to develop the standard that complements the next generation of V2X wireless technology, while maintaining compatibility with the IEEE 802.11p standard.

Recently, a new TG focusing on light communications, named as IEEE 802.11bb has started working on VLC related standard. The primary motivation of this TG is to define the appropriate scope for a potential IEEE amendment on Light Communications. Amjad *et al.*[144] proposed a V-VLC system compatible with the IEEE 802.11 standard, which could be adapted to the IEEE 802.11bb standard. By integrating the PHY and MAC layer changes, the basic idea is to use the protocol already created for IEEE 802.11 and provide interoperability with IEEE 802.11 compliant devices. This strategy may have many benefits for indoor VLC manufacturers, operators and end customers, but its impact on outdoor VLC is still a subject of further investigation.

Author's Publications

Journals (Published)

1. **G. Singh**, D. Gupta, A. Srivastava, V. A. Bohara, and Zilong L., "Exploring Cooperative NOMA Assisted Hybrid Visible Light and Radio Frequency for Enhanced Vehicular Message Dissemination at Road Intersections", *Elsevier Physical Communication*, Dec, 2022.
2. **G. Singh**, A. Srivastava and V. A. Bohara, "Visible Light and Reconfigurable Intelligent Surfaces for Beyond 5G V2X Communication Networks at Road Intersections", *IEEE Transactions on Vehicular Technology*, Apr., 2022. doi: 10.1109/TVT.2022.3174131.
3. **G.Singh**, A. Srivastava, V.A.Bohara, Zilong L., M.N. Rahim, and G. Ghatak, "Heterogeneous Visible Light and Radio Communication for Improving Safety Message Dissemination at Road Intersection", *IEEE Transactions on Intelligent Transportation Systems*, Feb, 2022. doi:10.1109/TITS.2022.3156119.
4. **G.Singh**, A. Srivastava, V.A.Bohara, and Zilong L. "Downlink Performance of Optical Power Domain NOMA for Beyond 5G Enabled V2X Networks", *IEEE Open Journal of Vehicular Technology*, vol. 2, pp. 235-248, May 2021, doi:10.1109/OJVT.2021.3083919.
5. **G.Singh**, A. Srivastava, and V.A.Bohara, "Stochastic Geometry Based Interference Characterization for RF and VLC Based Vehicular Communication System", *IEEE System Journal*, vol. 15, no. 2, pp. 2035-2045, Sept. 2020, doi: 10.1109/JSYST.2020.3027883.

Communicated Journal Article

1. **G. Singh**, A. Srivastava, V. A. Bohara, M.N. Rahim, Zilong L., and Pesch D., “Towards 6G-V2X: Aggregated RF-VLC for Ultra-Reliable and Low-Latency Autonomous Driving Under Meteorological Impact”, submitted to *IEEE Communication Standards Magazine*, Jan, 2023. Available online: <https://arxiv.org/abs/2208.06287>

Conferences (Published)

1. T. Pal, **G.Singh**, A. Srivastava, and V.A.Bohara “On Performance of Optical-RIS Aided Vehicular Communication Systems”, *Wireless World Research Forum Meeting 47*, Bristol, UK, June 2022.
2. **G.Singh**, A. Srivastava, V.A.Bohara, and Zilong L. “Comparison of PD-NOMA for RF and VLC based Vehicular Communication Under Various Weather Conditions”, *Wireless World Research Forum Meeting 44*, Copenhagen, Denmark, June, 2020.
3. **G. Singh**, A. Srivastava, and V. Bohara, “On Feasibility of VLC Based Car-to-Car Communication under Solar Irradiance and Fog Conditions,” in Proc. *ACM 1st Int. Workshop Commun. Comput. Connected Veh. Platooning, ACM MobiCom*, Oct. 2018, pp. 1–7.
4. K. Joshi, N. Roy, **G.Singh**, V.A.Bohara and A. Srivastava, “Experimental Observations on the Feasibility of VLC-Based V2X Communications under various Environmental Deterrants”, *IEEE International Conference on Advanced Networks and Telecommunications Systems (ANTS)*, Dec 2019 BITS Goa, India.
5. **G. Singh**, A. Srivastava, and V. A. Bohara, “Impact of Weather Conditions and Interference on the Performance of VLC based V2V Communication,” in Proc. *IEEE 21st International Conference on Transparent Optical Network (ICTON)*, Angers, France, July, 2019, pp. 1–4.
6. T. Pal, **G. Singh**, A. Srivastava and V. A. Bohara, “Optical IRS Aided B5G V2V Solution for Road Safety Applications”, *IEEE International Conference on Advanced Networks and Telecommunications Systems (ANTS)*, Dec, 2022. **Best Paper Award**
7. **G. Singh**, T.Pal, A. Srivastava and V. A. Bohara, “Optical RIS Enabled Hybrid RF-VLC V2X Communication Network: A Promising New Frontier for 6G-ITS”, *IEEE International Conference on Advanced Networks and Telecommunications Systems (ANTS)*, MNIT Jaipur, Dec, 2023. Accepted for publication.

References

- [1] S. Chen, J. Hu, Y. Shi, Y. Peng, J. Fang, R. Zhao, and L. Zhao, "Vehicle-to-everything (V2X) services supported by LTE-based systems and 5G," *IEEE Commun. Standards Mag.*, vol. 1, no. 2, pp. 70–76, 2017.
- [2] M. Noor-A-Rahim, Z. Liu, H. Lee, M. O. Khyam, J. He, D. Pesch, K. Moessner, W. Saad, and H. V. Poor, "6G for vehicle-to-everything (V2X) communications: Enabling technologies, challenges, and opportunities," *Proceedings of the IEEE*, vol. 110, no. 6, pp. 712–734, 2022.
- [3] D. P. Moya Osorio, I. Ahmad, J. D. V. Sánchez, A. Gurtov, J. Scholliers, M. Kutila, and P. Porambage, "Towards 6G-enabled internet of vehicles: Security and privacy," *IEEE Open J. Commun. Soc.*, vol. 3, pp. 82–105, 2022.
- [4] E. Calvanese Strinati, S. Barbarossa, J. L. Gonzalez-Jimenez, D. Ktenas, N. Cassiau, L. Maret, and C. Dehos, "6G: The next frontier: From holographic messaging to artificial intelligence using subterahertz and visible light communication," *IEEE Veh. Tech. Mag.*, vol. 14, no. 3, pp. 42–50, 2019.
- [5] A. Memedi and F. Dressler, "Vehicular visible light communications: A survey," *IEEE Communications Surveys Tutorials*, vol. 23, no. 1, pp. 161–181, 2021.
- [6] H. Abuella, M. Elamassie, M. Uysal, Z. Xu, E. Serpedin, K. A. Qaraqe, and S. Ekin, "Hybrid RF/VLC systems: A comprehensive survey on network topologies, performance analyses, applications, and future directions," *IEEE Access*, vol. 9, pp. 160 402–160 436, 2021.
- [7] S. Aboagye, A. R. Ndjiongue, T. Ngatched, O. Dobre, and H. V. Poor, "RIS-assisted visible light communication systems: A tutorial," *arXiv preprint arXiv:2204.07198*, 2022.
- [8] N. Agrawal, A. Bansal, K. Singh, and C.-P. Li, "Performance evaluation of RIS-assisted UAV-enabled vehicular communication system with multiple non-identical interferers," *IEEE Trans. Intell. Transport. Syst.*, vol. 23, no. 7, pp. 9883–9894, 2022.
- [9] A. Bazzi, B. M. Masini, A. Zanella, and I. Thibault, "On the performance of IEEE 802.11 p and LTE-V2V for the cooperative awareness of connected vehicles," *IEEE Transactions on Vehicular Technology*, vol. 66, no. 11, pp. 10 419–10 432, 2017.

- [10] Y. Hu, H. Li, Z. Chang, and Z. Han, “End-to-end backlog and delay bound analysis for multi-hop vehicular ad hoc networks,” *IEEE Transactions on Wireless Communications*, vol. 16, no. 10, pp. 6808–6821, 2017.
- [11] M. Segata, B. Bloessl, S. Joerer, C. Sommer, M. Gerla, R. L. Cigno, and F. Dressler, “Toward communication strategies for platooning: Simulative and experimental evaluation,” *IEEE Transactions on Vehicular Technology*, vol. 64, no. 12, pp. 5411–5423, 2015.
- [12] Z. Liu, H. Lee, M. O. Khyam, J. He, D. Pesch, K. Moessner, W. Saad, H. V. Poor *et al.*, “6G for vehicle-to-everything (V2X) communications: Enabling technologies, challenges, and opportunities,” *arXiv preprint arXiv:2012.07753*, 2020.
- [13] C. F. Mecklenbrauker, A. F. Molisch, J. Karedal, F. Tufvesson, A. Paier, L. Bernadó, T. Zemen, O. Klemp, and N. Czink, “Vehicular channel characterization and its implications for wireless system design and performance,” *Proc. IEEE*, vol. 99, no. 7, pp. 1189–1212, 2011.
- [14] J. Santa, R. Toledo-Moreo, M. A. Zamora-Izquierdo, B. Úbeda, and A. F. Gomez-Skarmeta, “An analysis of communication and navigation issues in collision avoidance support systems,” *Transportation Research Part C: Emerging Technologies*, vol. 18, no. 3, pp. 351–366, 2010.
- [15] Y. Xie, I. W.-H. Ho, and E. R. Magsino, “The modeling and cross-layer optimization of 802.11p VANET unicast,” *IEEE Access*, vol. 6, pp. 171–186, 2017.
- [16] E. Torres-Zapata, V. Guerra, J. Rabadan, R. Perez-Jimenez, and J. M. Luna-Rivera, “Vehicular communications in tunnels using vlc,” in *Proc. 15th International Conference on Telecommunications (ConTEL)*, 2019, pp. 1–6.
- [17] A. Memedi and F. Dressler, “Vehicular visible light communications: A survey,” *IEEE Communications Surveys & Tutorials*, vol. 23, no. 1, pp. 161–181, 2020.
- [18] H. Elgala, R. Mesleh, H. Haas, and B. Pricope, “Ofdm visible light wireless communication based on white leds,” in *Proc. IEEE 65th Vehicular Technology Conference-VTC2007-Spring*, 2007, pp. 2185–2189.
- [19] M. Z. Afgani, H. Haas, H. Elgala, and D. Knipp, “Visible light communication using ofdm,” in *Proc. IEEE 2nd International Conference on Testbeds and Research Infrastructures for the Development of Networks and Communities, 2006*, 2006, pp. 6–10.
- [20] F. Dong, R. Singh, and D. O’Brien, “Adaptive mimo-vlc system for high data rate communications,” in *Proc. IEEE Globecom Workshops (GC Wkshps)*, 2020, pp. 1–6.
- [21] G. Singh, A. Srivastava, V. A. Bohara, and Z. Liu, “Downlink performance of optical power domain noma for beyond 5G enabled v2x networks,” *IEEE Open Journal of Vehicular Technology*, 2021.
- [22] G. Singh, A. Srivastava, and V. A. Bohara, “Stochastic geometry-based interference characterization for rf and vlc-based vehicular communication system,” *IEEE Systems Journal*, 2020.

- [23] S. Ishihara, R. V. Rabsatt, and M. Gerla, "Improving reliability of platooning control messages using radio and visible light hybrid communication," in *Proc. IEEE Vehicular Networking Conference (VNC)*, 2015, pp. 96–103.
- [24] S. Ucar, S. C. Ergen, and O. Ozkasap, "IEEE 802.11 p and visible light hybrid communication based secure autonomous platoon," *IEEE Transactions on Vehicular Technology*, vol. 67, no. 9, pp. 8667–8681, 2018.
- [25] B. M. Masini, A. Bazzi, and A. Zanella, "Vehicular visible light networks for urban mobile crowd sensing," *Sensors*, vol. 18, no. 4, p. 1177, 2018.
- [26] D. Marabissi, L. Mucchi, S. Caputo, F. Nizzi, T. Pecorella, R. Fantacci, T. Nawaz, M. Seminara, and J. Catani, "Experimental measurements of a joint 5g-vlc communication for future vehicular networks," *J. Sensor and Actuator Networks*, vol. 9, no. 3, p. 32, 2020.
- [27] M. Liaqat, K. A. Noordin, T. A. Latef, and K. Dimyati, "Power-Domain Non Orthogonal Multiple Access (PD-NOMA) in Cooperative Networks: an Overview," *Wireless Networks*, pp. 1–23, 2018.
- [28] B. Di, L. Song, Y. Li, and Z. Han, "V2X meets NOMA: Non-orthogonal multiple access for 5G-enabled vehicular networks," *IEEE Wireless Commun.*, vol. 24, no. 6, pp. 14–21, 2017.
- [29] İ. Coşandal, M. Koca, E. Biglieri, and H. Sari, "NOMA-2000 versus PD-NOMA: An outage probability comparison," *IEEE Commun. Lett.*, vol. 25, no. 2, pp. 427–431, 2020.
- [30] R. C. Kizilirmak, C. R. Rowell, and M. Uysal, "Non-orthogonal multiple access (NOMA) for indoor visible light communications," in *Proc. IEEE 4th Int. Workshop Opt. Wireless Commun.*, 2015, pp. 98–101.
- [31] L. Yin, W. O. Popoola, X. Wu, and H. Haas, "Performance evaluation of non-orthogonal multiple access in visible light communication," *IEEE Trans. on Commun.*, vol. 64, no. 12, pp. 5162–5175, 2016.
- [32] X. Guan, Q. Yang, Y. Hong, and C. C.-K. Chan, "Non-orthogonal multiple access with phase pre-distortion in visible light communication," *Opt. Exp.*, vol. 24, no. 22, pp. 25 816–25 823, 2016.
- [33] Y. Fu, Y. Hong, L.-K. Chen, and C. W. Sung, "Enhanced power allocation for sum rate maximization in OFDM-NOMA VLC systems," *IEEE Photon. Technol. Lett.*, vol. 30, no. 13, pp. 1218–1221, 2018.
- [34] C. Chen, W.-D. Zhong, H. Yang, and P. Du, "On the performance of MIMO-NOMA-based visible light communication systems," *IEEE Photon. Technol. Lett.*, vol. 30, no. 4, pp. 307–310, 2017.
- [35] H. Marshoud, P. C. Sofotasios, S. Muhaidat, G. K. Karagiannidis, and B. S. Sharif, "Error performance of NOMA VLC systems," in *Proc. IEEE Int. Conf. on Commun.*, 2017, pp. 1–6.

- [36] G. Singh, A. Srivastava, V. A. Bohara, and Z. Liu, "Downlink performance of optical power domain noma for beyond 5G enabled V2X networks," *IEEE Open J. Veh. Technol.*, 2021.
- [37] G. Li and D. Mishra, "Cooperative noma networks: User cooperation or relay cooperation?" in *Proc. IEEE International Conference on Communications (ICC)*, 2020, pp. 1–6.
- [38] L. Dai, B. Wang, Z. Ding, Z. Wang, S. Chen, and L. Hanzo, "A survey of non-orthogonal multiple access for 5G," *IEEE Commun. Surveys Tutorials*, vol. 20, no. 3, pp. 2294–2323, 2018.
- [39] Z. Ding, M. Peng, and H. V. Poor, "Cooperative non-orthogonal multiple access in 5G systems," *IEEE Commun. Lett.*, vol. 19, no. 8, pp. 1462–1465, 2015.
- [40] X. Liu, Y. Wang, and Z. Na, "Cooperative noma-based DCO-OFDM VLC system," in *International Conference on Green Communications and Networking*. Springer, 2019, pp. 14–24.
- [41] Y. Xiao, P. D. Diamantoulakis, Z. Fang, Z. Ma, L. Hao, and G. K. Karagiannidis, "Hybrid lightwave/RF cooperative NOMA networks," *IEEE Trans. Wireless Commun.*, vol. 19, no. 2, pp. 1154–1166, 2020.
- [42] M. Latva-aho, K. Leppänen, F. Clazzer, and A. Munari, "Key drivers and research challenges for 6G ubiquitous wireless intelligence," 2020.
- [43] E. Basar, M. Di Renzo, J. De Rosny, M. Debbah, M.-S. Alouini, and R. Zhang, "Wireless communications through reconfigurable intelligent surfaces," *IEEE access*, vol. 7, pp. 116 753–116 773, 2019.
- [44] A. M. Abdelhady, A. K. S. Salem, O. Amin, B. Shihada, and M.-S. Alouini, "Visible light communications via intelligent reflecting surfaces: Metasurfaces vs mirror arrays," *IEEE Open J. of the Commun. Soc.*, vol. 2, pp. 1–20, 2021.
- [45] Y. Chen, Y. Wang, J. Zhang, and Z. Li, "Resource allocation for intelligent reflecting surface aided vehicular communications," *IEEE Trans. on Veh. Technol.*, vol. 69, no. 10, pp. 12 321–12 326, 2020.
- [46] J. Wang, W. Zhang, X. Bao, T. Song, and C. Pan, "Outage analysis for intelligent reflecting surface assisted vehicular communication networks," *arXiv preprint arXiv:2004.08063*, 2020.
- [47] A. U. Makarfi, K. M. Rabie, O. Kaiwartya, K. Adhikari, X. Li, M. Quiroz-Castellanos, and R. Kharel, "Reconfigurable intelligent surfaces-enabled vehicular networks: A physical layer security perspective," *arXiv preprint arXiv:2004.11288*, 2020.
- [48] B. M. Masini, C. M. Silva, and A. Balador, "The use of meta-surfaces in vehicular networks," *J. Networks*, vol. 9, no. 1, p. 15, 2020.
- [49] S. Aboagye, T. M. N. Ngatched, O. A. Dobre, and A. R. Ndjiongue, "Intelligent reflecting surface-aided indoor visible light communication systems," *IEEE Communications Letters*, vol. 25, no. 12, pp. 3913–3917, 2021.

- [50] B. Cao, M. Chen, Z. Yang, M. Zhang, J. Zhao, and M. Chen, "Reflecting the light: Energy efficient visible light communication with reconfigurable intelligent surface," in *2020 IEEE 92nd Vehicular Technology Conference (VTC2020-Fall)*, 2020, pp. 1–5.
- [51] L. Qian, X. Chi, L. Zhao, and A. Chaaban, "Secure visible light communications via intelligent reflecting surfaces," in *ICC 2021 - IEEE International Conference on Communications*, 2021, pp. 1–6.
- [52] S. Sun, F. Yang, and J. Song, "Sum rate maximization for intelligent reflecting surface-aided visible light communications," *IEEE Communications Letters*, vol. 25, no. 11, pp. 3619–3623, 2021.
- [53] S. Sun, F. Yang, J. Song, and Z. Han, "Joint resource management for intelligent reflecting surface-aided visible light communications," *IEEE Transactions on Wireless Communications*, vol. 21, no. 8, pp. 6508–6522, 2022.
- [54] S. Ibne Mushfique, A. Alsharoa, and M. Yuksel, "Mirrorvlc: Optimal mirror placement for multielement vlc networks," *IEEE Transactions on Wireless Communications*, vol. 21, no. 11, pp. 10 050–10 064, 2022.
- [55] L. Zhan, H. Zhao, W. Zhang, J. Lin, X. Zhao *et al.*, "Performance analysis and node selection of intelligent reflecting surface-aided visible light communication for parallel vehicles," *Wireless Communications and Mobile Computing*, vol. 2022, 2022.
- [56] T. Komine and M. Nakagawa, "Fundamental Analysis for Visible-Light Communication System using LED lights," *IEEE Trans. on Consumer Electronics*, vol. 50, no. 1, pp. 100–107, 2004.
- [57] R. B. Chiaramonte and K. R. L. J. C. Branco, "Collision detection using received signal strength in FANETs," in *Proc. IEEE International Conference on Unmanned Aircraft Systems (ICUAS)*. IEEE, 2014, pp. 1274–1283.
- [58] R. C. Kizilirmak and M. Torkamani-Azar, "Reducing collision probability with multihop diversity for vehicle-to-roadside networks," in *Proc. IEEE Symposium on Wireless Technology & Applications (ISWTA)*. IEEE, 2013, pp. 17–22.
- [59] S.-w. Chang, J. Cha, and S.-s. Lee, "Adaptive EDCA mechanism for vehicular ad-hoc network," in *Proc. IEEE International Conference on Information Network*. IEEE, 2012, pp. 379–383.
- [60] N. Boulila and L. A. Saidane, "Medium access control in vanet," in *Proc. IEEE 6th International Conference on Communications and Networking (ComNet)*, 2017, pp. 1–6.
- [61] E. Steinmetz, M. Wildemeersch, T. Q. S. Quek, and H. Wymeersch, "Packet reception probabilities in vehicular communications close to intersections," *IEEE Transactions on Intelligent Transportation Systems*, vol. 22, no. 5, pp. 2823–2833, 2021.
- [62] B. E. Y. Belmekki, A. Hamza, and B. Escrig, "Performance analysis of cooperative communications at road intersections using stochastic geometry tools," *Digital Signal Processing*, p. 103112, 2021.

- [63] M. Haenggi, *Stochastic geometry for wireless networks*. Cambridge University Press, 2012.
- [64] C. A. O’cinneide, “Euler Summation for Fourier series and Laplace Transform Inversion,” *Stochastic Models*, vol. 13, no. 2, pp. 315–337, 1997.
- [65] J. Abate and W. Whitt, “Numerical Inversion of Laplace Transforms of Probability Distributions,” *ORSA Journal on computing*, vol. 7, no. 1, pp. 36–43, 1995.
- [66] A. Goldsmith, *Wireless Communications*. Cambridge university press, 2005.
- [67] H.-C. Yang and M.-S. Alouini, “Wireless transmission of big data: Data-oriented performance limits and their applications,” *arXiv preprint arXiv:1805.09923*, 2018.
- [68] G. Singh, A. Srivastava, and V. A. Bohara, “Stochastic geometry-based interference characterization for RF and VLC-based vehicular communication system,” *IEEE Syst. J.*, pp. 1–11, 2020.
- [69] J. Choi, V. Marojevic, R. Nealy, J. H. Reed, and C. B. Dietrich, “Dsrc and iee 802.11 ac adjacent channel interference assessment for the 5.9 ghz band,” in *Proc. IEEE 89th Vehicular Technology Conference (VTC2019-Spring)*, 2019, pp. 1–5.
- [70] E. Steinmetz, M. Wildemeersch, and H. Wymeersch, “Wip abstract: Reception probability model for vehicular ad-hoc networks in the vicinity of intersections,” in *Proc. IEEE International Conference on Cyber-Physical Systems (ICCPs)*, 2014, pp. 223–223.
- [71] E. Steinmetz, M. Wildemeersch, T. Q. Quek, and H. Wymeersch, “A Stochastic Geometry Model for Vehicular Communication near Intersections,” in *Proc. IEEE Globecom Workshops (GC Wkshps)*, 2015, pp. 1–6.
- [72] I. Trigui, W. Ajib, and W.-P. Zhu, “A comprehensive study of reconfigurable intelligent surfaces in generalized fading,” *arXiv preprint arXiv:2004.02922*, 2020.
- [73] M. Noor-A-Rahim, G. M. N. Ali, H. Nguyen, and Y. L. Guan, “Performance analysis of IEEE 802.11 p safety message broadcast with and without relaying at road intersection,” *IEEE Access*, vol. 6, pp. 23 786–23 799, 2018.
- [74] Z. Xu, L. Bernadó, M. Gan, M. Hofer, T. Abbas, V. Shivaldova, K. Mahler, D. Smely, and T. Zemen, “Relaying for IEEE 802.11 p at road intersection using a vehicular non-stationary channel model,” in *Proc. IEEE 6th International Symposium on Wireless Vehicular Communications (WiVeC 2014)*, 2014, pp. 1–6.
- [75] B. Bag, A. Das, I. S. Ansari, A. Prokeš, C. Bose, and A. Chandra, “Performance analysis of hybrid FSO systems using FSO/RF-FSO link adaptation,” *IEEE Photonics Journal*, vol. 10, no. 3, pp. 1–17, 2018.
- [76] W. M. R. Shakir, “Performance evaluation of a selection combining scheme for the hybrid FSO/RF system,” *IEEE Photonics Journal*, vol. 10, no. 1, pp. 1–10, 2017.
- [77] M. Di Renzo, F. H. Danufane, X. Xi, J. De Rosny, and S. Tretyakov, “Analytical modeling of the path-loss for reconfigurable intelligent surfaces—anomalous mirror or scatterer?” in *Proc. IEEE 21st International Workshop on Signal Processing Advances in Wireless Communications (SPAWC)*, 2020, pp. 1–5.

- [78] C. Zhang, W. Yi, Y. Liu, Z. Qin, and K. K. Chai, "Downlink analysis for reconfigurable intelligent surfaces aided noma networks," *arXiv preprint arXiv:2006.13260*, 2020.
- [79] D. Dampahalage, K. S. Manosha, N. Rajatheva, and M. Latva-aho, "Intelligent reflecting surface aided vehicular communications," in *Proc. IEEE Globecom Workshops (GC Wkshps)*, 2020, pp. 1–6.
- [80] H. Zhang, L. Song, Z. Han, and H. V. Poor, "Spatial equalization before reception: reconfigurable intelligent surfaces for multi-path mitigation," in *Proc. IEEE International Conference on Acoustics, Speech and Signal Processing (ICASSP)*, 2021, pp. 8062–8066.
- [81] N. Kapucu, M. Bilim, and I. Develi, "Outage probability analysis of dual-hop decode-and-forward relaying over mixed rayleigh and generalized gamma fading channels," *Wireless personal communications*, vol. 71, no. 2, pp. 947–954, 2013.
- [82] T. V. Nguyen, F. Baccelli, K. Zhu, S. Subramanian, and X. Wu, "A performance analysis of csma based broadcast protocol in vanets," in *Proc. IEEE INFOCOM*, 2013, pp. 2805–2813.
- [83] S. Subramanian, M. Werner, S. Liu, J. Jose, R. Lupoai, and X. Wu, "Congestion control for vehicular safety: synchronous and asynchronous mac algorithms," in *Proc. ACM 9th international workshop on Vehicular inter-networking, systems, and applications*, 2012, pp. 63–72.
- [84] M. Haenggi, "Outage, local throughput, and capacity of random wireless networks," *IEEE Transactions on Wireless Communications*, vol. 8, no. 8, pp. 4350–4359, 2009.
- [85] Y.-C. Ko, M.-S. Alouini, and M. Simon, "An mgf-based numerical technique for the outage probability evaluation of diversity systems," in *Proc. IEEE International Symposium on Information Theory (Cat. No. 00CH37060)*, 2000, p. 304.
- [86] Y.-C. Ko, M.-S. Alouini, and M. K. Simon, "Outage probability of diversity systems over generalized fading channels," *IEEE Transactions on Communications*, vol. 48, no. 11, pp. 1783–1787, 2000.
- [87] M. Di Renzo, K. Ntontin, J. Song, F. H. Danufane, X. Qian, F. Lazarakis, J. De Rosny, D.-T. Phan-Huy, O. Simeone, R. Zhang *et al.*, "Reconfigurable intelligent surfaces vs. relaying: Differences, similarities, and performance comparison," *IEEE Open Journal of the Communications Society*, vol. 1, pp. 798–807, 2020.
- [88] C. Zhang, W. Yi, and Y. Liu, "Reconfigurable intelligent surfaces aided multi-cell noma networks: A stochastic geometry model," *arXiv preprint arXiv:2008.08457*, 2020.
- [89] A.-A. A. Boulogeorgos and A. Alexiou, "Performance analysis of reconfigurable intelligent surface-assisted wireless systems and comparison with relaying," *IEEE Access*, vol. 8, pp. 94 463–94 483, 2020.
- [90] A. U. Makarfi, R. Kharel, K. M. Rabie, O. Kaiwartya, and G. Nauryzbayev, "Physical layer security in vehicular communication networks in the presence of interference," in *Proc. IEEE Global Communications Conference (GLOBECOM)*, 2019, pp. 1–6.

- [91] A. S. Akki and F. Haber, "A statistical model of mobile-to-mobile land communication channel," *IEEE transactions on vehicular technology*, vol. 35, no. 1, pp. 2–7, 1986.
- [92] V. Erceg, S. J. Fortune, J. Ling, A. Rustako, and R. A. Valenzuela, "Comparisons of a computer-based propagation prediction tool with experimental data collected in urban microcellular environments," *IEEE Journal on Selected Areas in Communications*, vol. 15, no. 4, pp. 677–684, 1997.
- [93] Z. Cui, K. Guan, J. Zhang, and Z. Zhong, "Coverage probability analysis of irs-aided communication systems," *arXiv preprint arXiv:2012.03171*, 2020.
- [94] C. Zhang, W. Yi, Y. Liu, and Q. Wang, "Multi-cell noma: Coherent reconfigurable intelligent surfaces model with stochastic geometry," *arXiv preprint arXiv:2103.02450*, 2021.
- [95] E. Steinmetz, M. Wildemeersch, T. Q. Quek, and H. Wymeersch, "Packet reception probabilities in vehicular communications close to intersections," *IEEE Transactions on Intelligent Transportation Systems*, 2020.
- [96] B. E. Y. Belmekki, A. Hamza, and B. Escrig, "Performance analysis of cooperative communications at road intersections using stochastic geometry tools," *arXiv preprint arXiv:1807.08532*, 2018.
- [97] C.-S. Choi and F. Baccelli, "An analytical framework for coverage in cellular networks leveraging vehicles," *IEEE Transactions on Communications*, vol. 66, no. 10, pp. 4950–4964, 2018.
- [98] Z. Tong, H. Lu, M. Haenggi, and C. Poellabauer, "A stochastic geometry approach to the modeling of DSRC for vehicular safety communication," *IEEE Trans. Intell. Transport. Syst.*, vol. 17, no. 5, pp. 1448–1458, 2016.
- [99] A. Costanzo and V. Loscri, "Adaptive energy saving technique with saturation avoidance for outdoor vlc," in *2022 IEEE 95th Vehicular Technology Conference: (VTC2022-Spring)*, 2022, pp. 1–5.
- [100] Z. Ding, H. Dai, and H. V. Poor, "Relay selection for cooperative NOMA," *IEEE Wireless Commun. Lett.*, vol. 5, no. 4, pp. 416–419, 2016.
- [101] Z. Ding, L. Dai, and H. V. Poor, "MIMO-NOMA design for small packet transmission in the internet of things," *IEEE access*, vol. 4, pp. 1393–1405, 2016.
- [102] Y. Saito, Y. Kishiyama, A. Benjebbour, T. Nakamura, A. Li, and K. Higuchi, "Non-Orthogonal Multiple Access (NOMA) for Cellular Future Radio Access," in *Proc. IEEE 77th vehicular technology conference (VTC Spring)*, 2013, pp. 1–5.
- [103] A. Al-Hourani, S. Kandeepan, and A. Jamalipour, "Stochastic geometry study on device-to-device communication as a disaster relief solution," *IEEE Trans. Veh. Technol.*, vol. 65, no. 5, pp. 3005–3017, May. 2016.
- [104] P. Luo, Z. Ghassemlooy, H. Le Minh, E. Bentley, A. Burton, and X. Tang, "Fundamental analysis of a car to car visible light communication system," in *Proc. IEEE 9th International Symposium on Communication Systems, Networks & Digital Sign (CSNDSP)*, 2014, pp. 1011–1016.

- [105] K. Janghel and S. Prakriya, "Performance of adaptive OMA/cooperative-NOMA scheme with user selection," *IEEE Communications Letters*, vol. 22, no. 10, pp. 2092–2095, 2018.
- [106] M. Noor-A-Rahim, G. G. M. N. Ali, Y. L. Guan, B. Ayalew, P. H. J. Chong, and D. Pesch, "Broadcast performance analysis and improvements of the LTE-V2V autonomous mode at road intersection," *IEEE Trans. Veh. Tech.*, vol. 68, no. 10, pp. 9359–9369, 2019.
- [107] Y. Yao, Z. Ni, W. Hu, and M. Motani, "Optimizing energy harvesting decode-and-forward relays with decoding energy costs and energy storage," *IEEE Access*, vol. 9, pp. 96 613–96 628, 2021.
- [108] Z. Ding, Z. Yang, P. Fan, and H. V. Poor, "On the performance of non-orthogonal multiple access in 5G systems with randomly deployed users," *IEEE Signal Proc. Lett.*, vol. 21, no. 12, pp. 1501–1505, 2014.
- [109] Z. Ding, H. Dai, and H. V. Poor, "Relay selection for cooperative NOMA," *IEEE Wireless Commun. Lett.*, vol. 5, no. 4, pp. 416–419, 2016.
- [110] Z. Ding, L. Dai, and H. V. Poor, "MIMO-NOMA design for small packet transmission in the internet of things," *IEEE Access*, vol. 4, pp. 1393–1405, 2016.
- [111] B. E. Y. Belmekki, A. Hamza, and B. Escrig, "Performance evaluation of adaptive cooperative NOMA protocol at road junctions," in *Proc. IEEE 91st veh. tech. conf. (VTC2020-spring)*. IEEE, 2020, pp. 1–6.
- [112] G. Singh, A. Srivastava, V. A. Bohara, Z. Liu, M. Noor-A-Rahim, and G. Ghatak, "Heterogeneous visible light and radio communication for improving safety message dissemination at road intersection," *IEEE Trans. Intell. Transport. Syst.*, pp. 1–13, 2022.
- [113] M. Karbalayghareh, F. Miramirkhani, H. B. Eldeeb, R. C. Kizilirmak, S. M. Sait, and M. Uysal, "Channel modelling and performance limits of vehicular visible light communication systems," *IEEE Trans. on Veh. Technol.*, vol. 69, no. 7, pp. 6891–6901, 2020.
- [114] E. Steinmetz, M. Wildemeersch, T. Q. Quek, and H. Wymeersch, "Packet reception probabilities in vehicular communications close to intersections," *IEEE Trans. on Intell. Transp. Syst.*, vol. 22, no. 5, pp. 2823–2833, 2020.
- [115] B. E. Y. Belmekki, A. Hamza, and B. Escrig, "Outage analysis of cooperative NOMA Using maximum ratio combining at intersections," in *Proc. IEEE Int. Conf. on Wireless and Mobile Computing, Netw. and Commun.*, 2019, pp. 1–6.
- [116] G. Singh, A. Srivastava, and V. A. Bohara, "Visible light and reconfigurable intelligent surfaces for beyond 5G V2X communication networks at road intersections," *IEEE Trans. Veh. Tech.*, vol. 71, no. 8, pp. 8137–8151, 2022.
- [117] M. Haenggi, *Stochastic geometry for wireless networks*. Cambridge University Press, 2012.

- [118] B. E. Y. Belmekki, A. Hamza, and B. Escrig, "On the performance of 5G non-orthogonal multiple access for vehicular communications at road intersections," *Veh. Commun.*, vol. 22, p. 100202, 2020.
- [119] S. Hoogendoorn and V. Knoop, "Traffic flow theory and modelling," *The transport system and transport policy: an introduction*, pp. 125–159, 2013.
- [120] L. Hua, Y. Zhuang, L. Qi, J. Yang, and L. Shi, "Noise analysis and modeling in visible light communication using allan variance," *IEEE Access*, vol. 6, pp. 74 320–74 327, 2018.
- [121] Y. Chen, Y. Wang, J. Zhang, and Z. Li, "Resource allocation for intelligent reflecting surface aided vehicular communications," *IEEE Trans. Veh. Tech.*, vol. 69, no. 10, pp. 12 321–12 326, 2020.
- [122] G. Singh, A. Srivastava, V. A. Bohara, and Z. Liu, "Downlink performance of optical power domain noma for beyond 5G enabled V2X networks," *IEEE Open J. Veh. Tech.*, vol. 2, pp. 235–248, 2021.
- [123] J. Abate and W. Whitt, "A unified framework for numerically inverting laplace transforms," *INFORMS Journal on Computing*, vol. 18, no. 4, pp. 408–421, 2006.
- [124] N. I. Miridakis, T. A. Tsiftsis, and H.-M. Wang, "Zero forcing detection for short packet transmission under channel estimation errors," *IEEE Trans. Veh. Tech.*, vol. 68, no. 7, pp. 7164–7168, 2019.
- [125] H.-C. Yang, S. Choi, and M.-S. Alouini, "Ultra-reliable low-latency transmission of small data over fading channels: A data-oriented analysis," *IEEE Commun. Lett.*, vol. 24, no. 3, pp. 515–519, 2020.
- [126] L. Cheng, W. Viriyasitavat, M. Boban, and H.-M. Tsai, "Comparison of radio frequency and visible light propagation channels for vehicular communications," *IEEE Access*, vol. 6, pp. 2634–2644, Dec. 2017.
- [127] M. Elamassie, M. Karbalayghareh, F. Miramirkhani, R. C. Kizilirmak, and M. Uysal, "Effect of fog and rain on the performance of vehicular visible light communications," in *Proc. IEEE 87th Veh. Technol. Conf. Spring (VTC)*, Jun. 2018, pp. 1–6.
- [128] H.-Y. Tseng, Y.-L. Wei, A.-L. Chen, H.-P. Wu, H. Hsu, and H.-M. Tsai, "Characterizing link asymmetry in vehicle-to-vehicle visible light communications," in *Proc. IEEE Veh. Netw. Conf. (VNC)*, Dec. 2015, pp. 88–95.
- [129] C. Chen, M. Ijaz, D. Tsonev, and H. Haas, "Analysis of downlink transmission in DCO-OFDM-based optical attocell networks," in *Proc. IEEE Global Commun. Conf.*, Feb. 2015, pp. 2072–2077.
- [130] A. Surampudi and R. K. Ganti, "Interference characterization in downlink Li-Fi optical attocell networks," *IEEE J. Lightw. Technol.*, vol. 36, no. 16, pp. 3211–3228, Aug. 2018.
- [131] J. Gil-Pelaez, "Note on the inversion theorem," *Biometrika*, vol. 38, no. 3-4, pp. 481–482, 1951.

- [132] J. H. Banks, “Two-Capacity Phenomenon at Freeway Bottlenecks: a basis for Ramp Metering?” *Transportation Research Record*, no. 1320, 1991.
- [133] Y. H. Kim, W. A. Cahyadi, and Y. H. Chung, “Experimental demonstration of VLC-based vehicle-to-vehicle communications under fog conditions,” *IEEE Photon. J.*, vol. 7, no. 6, pp. 1–9, Nov. 2015.
- [134] G. Singh, A. Srivastava, and V. Bohara, “On feasibility of VLC based car-to-car communication under solar irradiance and fog conditions,” *Proc. ACM 1st Int. Workshop on Commun. and Comput. in Connected Veh. and Platooning*, pp. 1–7, Oct. 2018.
- [135] G. Singh, A. Srivastava, and V. A. Bohara, “Impact of weather conditions and interference on the performance of VLC based V2V communication,” in *Proc. IEEE Intl. Conf. Transparent Optical Net. (ICTON)*, 2019, pp. 1–4.
- [136] N. M. Karoti, S. Paramita, R. Ahmad, V. A. Bohara, and A. Srivastava, “Improving the performance of heterogeneous LiFi-WiFi network using a novel link aggregation framework,” in *Proc. IEEE Wireless Communications and Networking Conference (WCNC)*, 2022, pp. 2322–2327.
- [137] L. Liang, H. Ye, and G. Y. Li, “Toward intelligent vehicular networks: A machine learning framework,” *IEEE Internet of Things Journal*, vol. 6, no. 1, pp. 124–135, 2019.
- [138] B. Genovés Guzmán, V. P. Gil Jiménez, M. C. Aguayo-Torres, H. Haas, and L. Hanzo, “Downlink performance of optical OFDM in outdoor visible light communication,” *IEEE Access*, vol. 6, pp. 76 854–76 866, 2018.
- [139] H. B. Eldeeb, S. M. Sait, and M. Uysal, “Visible light communication for connected vehicles: How to achieve the omnidirectional coverage?” *IEEE Access*, vol. 9, pp. 103 885–103 905, 2021.
- [140] T. Xu, M. Zhang, Y. Zeng, and H. Hu, “Harmonious coexistence of heterogeneous wireless networks in unlicensed bands: Solutions from the statistical signal transmission technique,” *IEEE Veh. Tech. Mag.*, vol. 14, no. 2, pp. 61–69, 2019.
- [141] Z. Liu and L.-L. Yang, “Sparse or dense: A comparative study of code-domain noma systems,” *IEEE Trans. Wireless Commun.*, vol. 20, no. 8, pp. 4768–4780, 2021.
- [142] A.-M. Cailean and M. Dimian, “Impact of IEEE 802.15.7 standard on visible light communications usage in automotive applications,” *IEEE Commun. Mag.*, vol. 55, no. 4, pp. 169–175, 2017.
- [143] “IEEE standard for local and metropolitan area networks—part 15.7: Short-range optical wireless communications,” *IEEE Std 802.15.7-2018 (Revision of IEEE Std 802.15.7-2011)*, pp. 1–407, 2019.
- [144] M. S. Amjad, C. Tebruegge, A. Memedi, S. Kruse, C. Kress, C. Scheytt, and F. Dressler, “An IEEE 802.11 compliant SDR-based system for vehicular visible light communications,” in *Proc. IEEE Intl. Conf. Commun. (ICC)*, 2019, pp. 1–6.